Sourcebook for Linear Collider Physics

Chapter 3 Higgs Bosons at the Linear Collider

1 Introduction

This chapter shows how a linear collider (LC) can contribute to our understanding of the Higgs sector through detailed studies of the physical Higgs boson state(s). Although this subject has been reviewed several times in the past [1–5], there are at least two reasons to revisit the subject. First, the completion of the LEP2 Higgs search, together with earlier precise measurements from SLC, LEP, and the Tevatron, gives us a clearer idea of what to expect. The simplest explanations of these results point to a light Higgs boson with (nearly) standard couplings to W and Z. The key properties of such a particle can be investigated with a 500 GeV LC. Second, the luminosity expected from the LC is now higher: 200–300 $\mathrm{fb}^{-1}\mathrm{yr}^{-1}$ at $\sqrt{s} = 500$ GeV, and 300–500 $\mathrm{fb}^{-1}\mathrm{yr}^{-1}$ at $\sqrt{s} = 800$ GeV. Consequently, several tens of thousands of Higgs bosons should be produced in each year of operation. With such samples, several measurements become more feasible, and the precision of the whole body of expected results becomes such as to lend insight not only into the nature of the Higgs boson(s), but also into the dynamics of higher scales.

There is an enormous literature on the Higgs boson and, more generally, on possible mechanisms of electroweak symmetry breaking. It is impossible to discuss all of it here. To provide a manageable, but nevertheless illustrative, survey of LC capabilities, we focus mostly on the Higgs boson of the Standard Model (SM), and on the Higgs bosons of the minimal supersymmetric extension of the SM (MSSM). Although this choice is partly motivated by simplicity, a stronger impetus comes from the precision data collected over the past few years, and some other related considerations.

The SM, which adds to the observed particles a single complex doublet of scalar fields, is economical. It provides an impressive fit to the precision data. Many extended models of electroweak symmetry breaking possess a limit, called the decoupling limit, that is experimentally almost indistinguishable from the SM. These models agree with the data equally well, and even away from the decoupling limit they usually predict a weakly coupled Higgs boson whose mass is at most several hundred GeV. Thus, the SM serves as a basis for discussing the Higgs phenomenology of a wide range of models, all of which are compatible with experimental constraints.

The SM suffers from several theoretical problems, which are either absent or less severe with weak-scale supersymmetry. The Higgs sector of the MSSM is a constrained two Higgs doublet model, consisting of two CP-even Higgs bosons, h^0 and H^0, a CP-odd Higgs boson, A^0, and a charged Higgs pair, $H^\pm$. The MSSM is especially attractive because the superpartners modify the running of the strong, weak, and

electromagnetic gauge couplings in just the right way as to yield unification at about 10^{16} GeV [6]. For this reason, the MSSM is arguably the most compelling extension of the SM. This is directly relevant to Higgs phenomenology, because in the MSSM a theoretical bound requires that the lightest CP-even Higgs boson h^0 has a mass less than 135 GeV. (In non-minimal supersymmetric models, the bound can be relaxed to around 200 GeV.) Furthermore, the MSSM offers, in some regions of parameter space, very non-standard Higgs phenomenology, so the full range of possibilities in the MSSM can be used to indicate how well the LC performs in non-standard scenarios. Thus, we use the SM to show how the LC fares when there is only one observable Higgs boson, and the MSSM to illustrate how extra fields can complicate the phenomenology. We also use various other models to illustrate important exceptions to conclusions that would be drawn from these two models alone.

The rest of this chapter is organized as follows. Section 2 gives, in some detail, the argument that one should expect a weakly coupled Higgs boson with a mass that is probably below about 200 GeV. In Section 3, we summarize the theory of the Standard Model Higgs boson. In Section 4, we review the expectations for Higgs discovery and the determination of Higgs boson properties at the Tevatron and LHC. In Section 5, we introduce the Higgs sector of the minimal supersymmetric extension of the Standard Model (MSSM) and discuss its theoretical properties. The present direct search limits are reviewed, and expectations for discovery at the Tevatron and LHC are described in Section 6. In Section 7, we treat the theory of the non-minimal Higgs sector more generally. In particular, we focus on the decoupling limit, in which the properties of the lightest Higgs scalar are nearly identical to those of the Standard Model Higgs boson, and discuss how to distinguish the two. We also discuss some non-decoupling exceptions to the usual decoupling scenario.

Finally, we turn to the program of Higgs measurements that can be carried out at the LC, focusing on e^+e^- collisions at higher energy, but also including material on the impact of Giga-Z operation and $\gamma\gamma$ collisions. The measurement of Higgs boson properties in e^+e^- collisions is outlined in Section 8. This includes a survey of the measurements that can be made for a SM-like Higgs boson for all masses up to 500 GeV. We also discuss measurements of the extra Higgs bosons that appear in the MSSM. Because the phenomenology of decoupling limit mimics, by definition, the SM Higgs boson, we emphasize how the precision that stems from high luminosity helps to diagnose the underlying dynamics. In Section 9, we outline the impact of Giga-Z operation on constraining and exploring various scenarios. In Section 10, the most important gains from $\gamma\gamma$ collisions are reviewed. Finally, in Section 11, we briefly discuss the case of a Higgs sector containing triplet Higgs representations and also consider the Higgs-like particles that can arise if the underlying assumption of a weakly coupled elementary Higgs sector is *not* realized in Nature.

2 Expectations for electroweak symmetry breaking

With the recent completion of experimentation at the LEP collider, the Standard Model of particle physics appears close to final experimental verification. After more than ten years of precision measurements of electroweak observables at LEP, SLC and the Tevatron, no definitive departures from Standard Model predictions have been found [7]. In some cases, theoretical predictions have been checked with an accuracy of one part in a thousand or better. However, the dynamics responsible for electroweak symmetry breaking has not yet been directly identified. Nevertheless, this dynamics affects predictions for currently observed electroweak processes at the one-loop quantum level. Consequently, the analysis of precision electroweak data can already provide some useful constraints on the nature of electroweak symmetry breaking dynamics.

In the minimal Standard Model, electroweak symmetry breaking dynamics arises via a self-interacting complex doublet of scalar fields, which consists of four real degrees of freedom. Renormalizable interactions are arranged in such a way that the neutral component of the scalar doublet acquires a vacuum expectation value, $v = 246$ GeV, which sets the scale of electroweak symmetry breaking. Hence, three massless Goldstone bosons are generated that are absorbed by the $W^\pm$ and Z, thereby providing the resulting massive gauge bosons with longitudinal components. The fourth scalar degree of freedom that remains in the physical spectrum is the CP-even neutral Higgs boson of the Standard Model. It is further assumed in the Standard Model that the scalar doublet also couples to fermions through Yukawa interactions. After electroweak symmetry breaking, these interactions are responsible for the generation of quark and charged lepton masses.

The global analysis of electroweak observables provides a superb fit to the Standard Model predictions. Such analyses take the Higgs mass as a free parameter. The electroweak observables depend logarithmically on the Higgs mass through its one-loop effects. The accuracy of the current data (and the reliability of the corresponding theoretical computations) already provides a significant constraint on the value of the Higgs mass. In [8,9], the non-observation of the Higgs boson is combined with the constraints of the global precision electroweak analysis to yield $m_{h_{\rm SM}} \lesssim 205$–$230$ GeV at 95% CL (the quoted range reflects various theoretical choices in the analysis). Meanwhile, direct searches for the Higgs mass at LEP achieved a 95% CL limit of $m_{h_{\rm SM}} > 113.5$ GeV.[1]

One can question the significance of these results. After all, the self-interacting scalar field is only one model of electroweak symmetry breaking; other approaches, based on very different dynamics, are also possible. For example, one can introduce

[1]The LEP experiments presented evidence for a Higgs mass signal at a mass of $m_{h_{\rm SM}} = 115.0^{+1.3}_{-0.9}$ GeV, with an assigned significance of 2.9σ [10]. Although suggestive, the data are not significant enough to warrant a claim of a Higgs discovery.

new fermions and new forces, in which the Goldstone bosons are a consequence of the strong binding of the new fermion fields [11]. Present experimental data are not sufficient to identify with certainty the nature of the dynamics responsible for electroweak symmetry breaking. Nevertheless, one can attempt to classify alternative scenarios and study the constraints of the global precision electroweak fits and the implications for phenomenology at future colliders. Since electroweak symmetry dynamics must affect the one-loop corrections to electroweak observables, the constraints on alternative approaches can be obtained by generalizing the global precision electroweak fits to allow for new contributions at one-loop. These enter primarily through corrections to the self-energies of the gauge bosons (the so-called "oblique" corrections). Under the assumption that any new physics is characterized by a new mass scale $M \gg m_Z$, one can parameterize the leading oblique corrections by three constants, S, T, and U, first introduced by Peskin and Takeuchi [12]. In almost all theories of electroweak symmetry breaking dynamics, $U \ll S$, T, so it is sufficient to consider a global electroweak fit in which $m_{h_{\rm SM}}$, S and T are free parameters. (The zero of the S–T plane must be defined relative to some fixed value of the Higgs mass, usually taken to be 100 GeV.) New electroweak symmetry breaking dynamics could generate non-zero values of S and T, while allowing for a much heavier Higgs mass (or equivalent). Various possibilities have been recently classified by Peskin and Wells [13], who argue that any dynamics that results in a significantly heavier Higgs boson should also generate new experimental signatures at the TeV scale that can be studied at the LC, either directly by producing new particles or indirectly by improving precision measurements of electroweak observables.

In this chapter, we mainly consider the simplest possible interpretation of the precision electroweak data, namely, that there exists a light weakly coupled Higgs boson. Nevertheless, this still does not fix the theory of electroweak symmetry breaking. It is easy to construct extensions of the scalar boson dynamics and generate non-minimal Higgs sectors. Such theories can contain charged Higgs bosons and neutral Higgs bosons of opposite (or indefinite) CP-quantum numbers. Although some theoretical constraints exist, there is still considerable freedom in constructing models which satisfy all known experimental constraints. Moreover, in most extensions of the Standard Model, there exists a large range of parameter space in which the properties of the lightest Higgs scalar are virtually indistinguishable from those of the Standard Model Higgs boson. One of the challenges of experiments at future colliders, once the Higgs boson is discovered, is to see whether there are any deviations from the properties expected for the Standard Model Higgs boson.

Although the Standard Model provides a remarkably successful description of the properties of the quarks, leptons and spin-1 gauge bosons at energy scales of $\mathcal{O}(100)$ GeV and below, the Standard Model is not the ultimate theory of the fundamental particles and their interactions. At an energy scale above the Planck scale, $M_{\rm PL} \simeq 10^{19}$ GeV, quantum gravitational effects become significant and the Standard

Model must be replaced by a more fundamental theory that incorporates gravity. It is also possible that the Standard Model breaks down at some energy scale, Λ, below the Planck scale. In this case, the Standard Model degrees of freedom are no longer adequate for describing the physics above Λ and new physics must enter. Thus, the Standard Model is not a *fundamental* theory; at best, it is an *effective field theory* [14]. At an energy scale below Λ, the Standard Model (with higher-dimension operators to parameterize the new physics at the scale Λ) provides an extremely good description of all observable phenomena.

An essential question that future experiments must address is: what is the minimum scale Λ at which new physics beyond the Standard Model must enter? The answer to this question depends on the value of the Higgs mass, $m_{h_{\rm SM}}$. If $m_{h_{\rm SM}}$ is too large, then the Higgs self-coupling blows up at some scale Λ below the Planck scale [15]. If $m_{h_{\rm SM}}$ is too small, then the Higgs potential develops a second (global) minimum at a large value of the scalar field of order Λ [16]. Thus, new physics must enter at a scale Λ or below in order that the true minimum of the theory correspond to the observed SU(2)×U(1) broken vacuum with $v = 246$ GeV for scales above Λ. Thus, given a value of Λ, one can compute the minimum and maximum Higgs mass allowed. Although the arguments just given are based on perturbation theory, it is possible to repeat the analysis of the Higgs-Yukawa sector non-perturbatively [17]. These results are in agreement with the perturbative estimates. The results of this analysis (with shaded bands indicating the theoretical uncertainty of the result) are illustrated in Fig. 3.1.

Although the Higgs mass range $130\ {\rm GeV} \lesssim m_{h_{\rm SM}} \lesssim 180\ {\rm GeV}$ appears to permit an effective Standard Model that survives all the way to the Planck scale, most theorists consider such a possibility unlikely. This conclusion is based on the "naturalness" [19] argument as follows. In an effective field theory, all parameters of the low-energy theory (*i.e.*, masses and couplings) are calculable in terms of parameters of a more fundamental theory that describes physics at the energy scale Λ. All low-energy couplings and fermion masses are logarithmically sensitive to Λ. In contrast, scalar squared-masses are *quadratically* sensitive to Λ. The Higgs mass (at one-loop) has the following heuristic form:

$$m_h^2 = (m_h^2)_0 + \frac{cg^2}{16\pi^2}\Lambda^2\,, \tag{3.1}$$

where $(m_h^2)_0$ is a parameter of the fundamental theory and c is a constant, presumably of $\mathcal{O}(1)$, that depends on the physics of the low-energy effective theory. The "natural" value for the scalar squared-mass is $g^2\Lambda^2/16\pi^2$. Thus, the expectation for Λ is

$$\Lambda \simeq \frac{4\pi m_h}{g} \sim \mathcal{O}(1\ {\rm TeV})\,. \tag{3.2}$$

If Λ is significantly larger than 1 TeV then the only way for the Higgs mass to be of order the scale of electroweak symmetry breaking is to have an "unnatural"

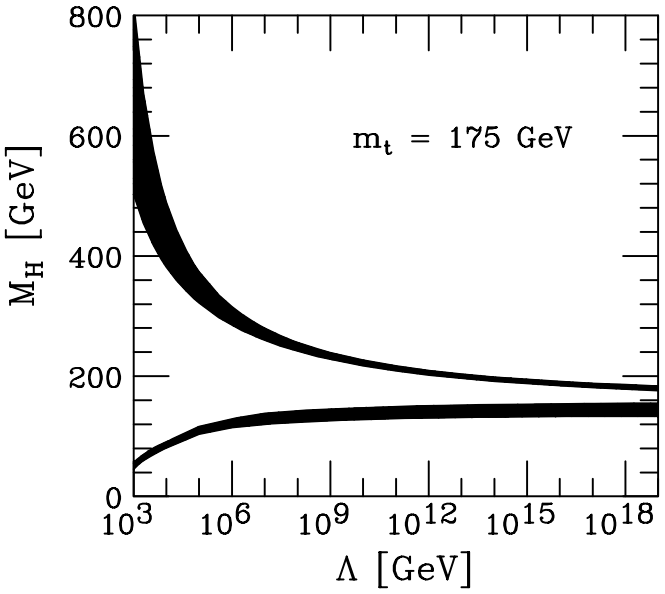

Figure 3.1: The upper [15] and the lower [16] Higgs mass bounds as a function of the energy scale Λ at which the Standard Model breaks down, assuming $m_t = 175$ GeV and $\alpha_s(m_Z) = 0.118$. The shaded areas above reflect the theoretical uncertainties in the calculations of the Higgs mass bounds. This figure is taken from [18].

cancellation between the two terms of Eq. (3.1). This seems highly unlikely given that the two terms of Eq. (3.1) have completely different origins.

An attractive theoretical framework that incorporates weakly coupled Higgs bosons and satisfies the constraint of Eq. (3.2) is that of "low-energy" or "weak-scale" supersymmetry [20,21]. In this framework, supersymmetry is used to relate fermion and boson masses and interaction strengths. Since fermion masses are only logarithmically sensitive to Λ, boson masses will exhibit the same logarithmic sensitivity if supersymmetry is exact. Since no supersymmetric partners of Standard Model particles have yet been found, supersymmetry cannot be an exact symmetry of nature. Thus, Λ should be identified with the supersymmetry breaking scale. The naturalness constraint of Eq. (3.2) is still relevant. It implies that the scale of supersymmetry breaking should not be much larger than 1 TeV, to preserve the naturalness of scalar masses. The supersymmetric extension of the Standard Model would then replace the Standard Model as the effective field theory of the TeV scale. One advantage of the supersymmetric approach is that the effective low-energy supersymmetric theory *can* be valid all the way up to the Planck scale, while still being natural! The unification of the three gauge couplings at an energy scale close to the Planck scale, which does not occur in the Standard Model, is seen to occur in the minimal supersymmetric extension of the Standard Model, and provides an additional motivation

for seriously considering the low-energy supersymmetric framework [6]. However, the fundamental origin of supersymmetry breaking is not known at present. Without a fundamental theory of supersymmetry breaking, one ends up with an effective low-energy theory characterized by over 100 unknown parameters that in principle would have to be measured by experiment. This remains one of the main stumbling blocks for creating a truly predictive model of fundamental particles and their interactions. Nevertheless, the Higgs sectors of the simplest supersymmetric models are quite strongly constrained, and exhibit very specific phenomenological profiles.

3 The Standard Model Higgs boson—theory

In the Standard Model, the Higgs mass is given by $m^2_{h_{\rm SM}} = \lambda v^2$, where λ is the Higgs self-coupling. Since λ is unknown at present, the value of the Standard Model Higgs mass is not predicted (although other theoretical considerations, discussed in Section 2, place constraints on the Higgs mass, as exhibited in Fig. 3.1). The Higgs couplings to fermions and gauge bosons are proportional to the corresponding particle masses. As a result, Higgs phenomenology is governed primarily by the couplings of the Higgs boson to the $W^\pm$ and Z and the third generation quarks and leptons. It should be noted that a $h_{\rm SM}gg$ coupling, where g is the gluon, is induced by the one-loop graph in which the Higgs boson couples to a virtual $t\overline{t}$ pair. Likewise, a $h_{\rm SM}\gamma\gamma$ coupling is generated, although in this case the one-loop graph in which the Higgs boson couples to a virtual W^+W^- pair is the dominant contribution. Further details of Standard Higgs boson properties are given in [1].

3.1 Standard Model Higgs boson decay modes

The Higgs boson mass is the only unknown parameter in the Standard Model. Thus, one can compute Higgs boson branching ratios and production cross sections as a function of $m_{h_{\rm SM}}$. The branching ratios for the dominant decay modes of a Standard Model Higgs boson are shown as a function of Higgs boson mass in Fig. 3.2. Note that subdominant channels are important to establish a complete phenomenological profile of the Higgs boson, and to check consistency (or look for departures from) Standard Model predictions. For 115 GeV $\sim m_{h_{\rm SM}} \lesssim 2m_W$ many decays modes are large enough to measure, as discussed in Section 8.

For $m_{h_{\rm SM}} \lesssim 135$ GeV, the main Higgs decay mode is $h_{\rm SM} \to b\overline{b}$, while the decays $h_{\rm SM} \to \tau^+\tau^-$ and $c\overline{c}$ can also be phenomenologically relevant. In addition, although one–loop suppressed, the decay $h_{\rm SM} \to gg$ is competitive with other decays for $m_{h_{\rm SM}} \lesssim 2m_W$ because of the large top Yukawa coupling and the color factor. As the Higgs mass increases above 135 GeV, the branching ratio to vector boson pairs becomes dominant. In particular, the main Higgs decay mode is $h_{\rm SM} \to WW^{(*)}$, where one of the W's must be off-shell (indicated by the star superscript) if $m_{h_{\rm SM}} < 2m_W$. For

Higgs bosons with $m_{h_{\rm SM}} \gtrsim 2m_t$, the decay $h_{\rm SM} \to t\bar{t}$ begins to increase until it reaches its maximal value of about 20%.

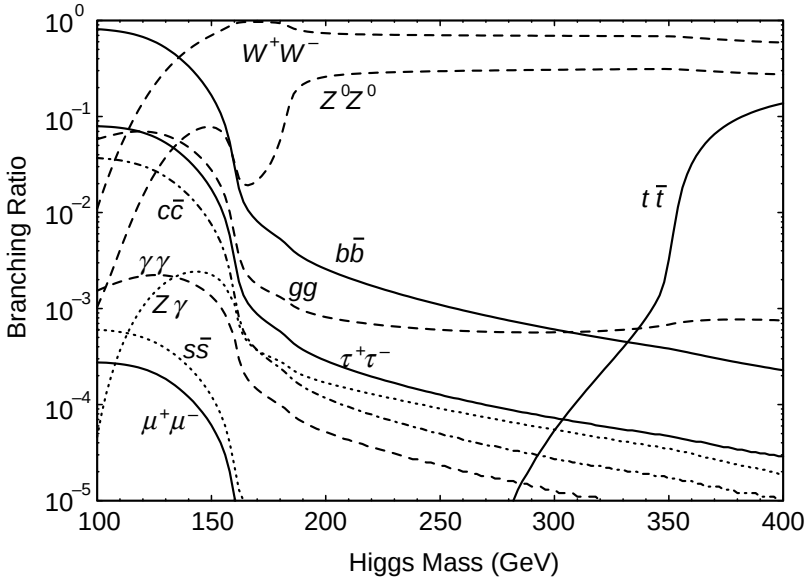

Figure 3.2: Branching ratios of the dominant decay modes of the Standard Model Higgs boson. These results have been obtained with the program HDECAY [22], and include QCD corrections beyond the leading order.

Rare Higgs decay modes can also play an important role. The one-loop decay $h_{\rm SM} \to \gamma\gamma$ is a suppressed mode. For $m_W \lesssim m_{h_{\rm SM}} \lesssim 2m_W$, BR($h_{\rm SM} \to \gamma\gamma$) is above 10^{-3}. This decay channel provides an important Higgs discovery mode at the LHC for 100 GeV $\lesssim m_{h_{\rm SM}} \lesssim$ 150 GeV. At the LC, the direct observation of $h_{\rm SM} \to \gamma\gamma$ is difficult because of its suppressed branching ratio. Perhaps more relevant is the partial width $\Gamma(h^0 \to \gamma\gamma)$, which controls the Higgs production rate at a $\gamma\gamma$ collider.

3.2 Standard Model Higgs boson production at the LC

In the Standard Model there are two main processes to produce the Higgs boson in e^+e^- annihilation. These processes are also relevant in many extensions of the Standard Model, particularly in nearly-decoupled extensions, in which the lightest CP-even Higgs boson possesses properties nearly identical to those of the SM Higgs boson. In the "Higgsstrahlung" process, a virtual Z boson decays to an on-shell Z and the $h_{\rm SM}$, depicted in Fig. 3.3(a). The cross section for Higgsstrahlung rises sharply at threshold to a maximum a few tens of GeV above $m_h + m_Z$, and then falls off as s^{-1}, as shown in Fig. 3.4. The associated production of the Z provides an important trigger for Higgsstrahlung events. In particular, in some theories beyond the Standard Model, in which the Higgs boson decays into invisible modes, the Higgs

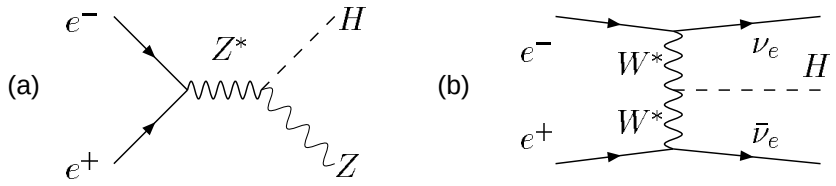

Figure 3.3: Main production processes for Higgs production in e^+e^- annihilation. (a) Higgsstrahlung. (b) WW fusion.

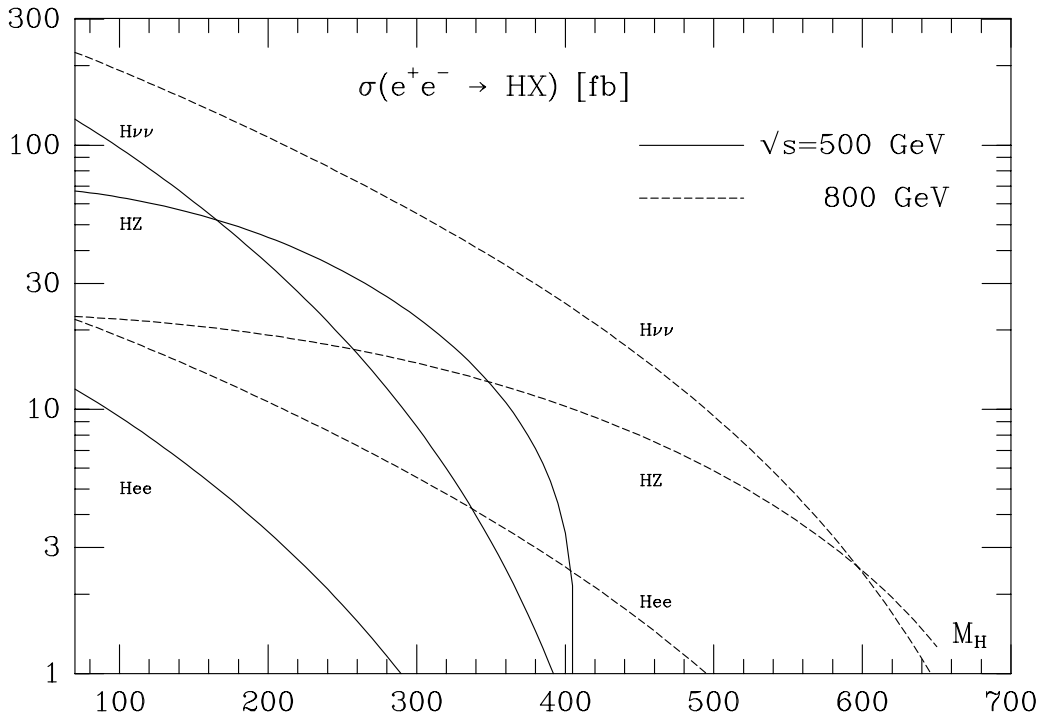

Figure 3.4: Cross sections for Higgsstrahlung ($e^+e^- \to Zh_{\rm SM}$) and Higgs production via W^+W^- fusion ($e^+e^- \to \nu\overline{\nu}h_{\rm SM}$) and ZZ fusion ($e^+e^- \to e^+e^-h_{\rm SM}$) as a function of $m_{h_{\rm SM}}$ for two center-of-mass energies, $\sqrt{s} = 500$ and 800 GeV [5].

boson mass peak can be reconstructed in the spectrum of the missing mass recoiling against the Z. The other production process is called "vector boson fusion", where the incoming e^+ and e^- each emit a virtual vector boson, followed by vector boson fusion to the $h_{\rm SM}$. Figure 3.3(b) depicts the W^+W^- fusion process. Similarly, the ZZ fusion process corresponds to $e^+e^- \to e^+e^-h_{\rm SM}$. In contrast to Higgsstrahlung, the vector boson fusion cross section grows as $\ln s$, and thus is the dominant Higgs production mechanism for $\sqrt{s} \gg m_{h_{\rm SM}}$. The cross section for WW fusion is about ten times larger than that for ZZ fusion. Nevertheless, the latter provides complementary

information on the $ZZh_{\rm SM}$ vertex. Note that at an e^-e^- collider, the Higgsstrahlung and W^+W^- fusion processes are absent, so that ZZ fusion is the dominant Higgs production process.

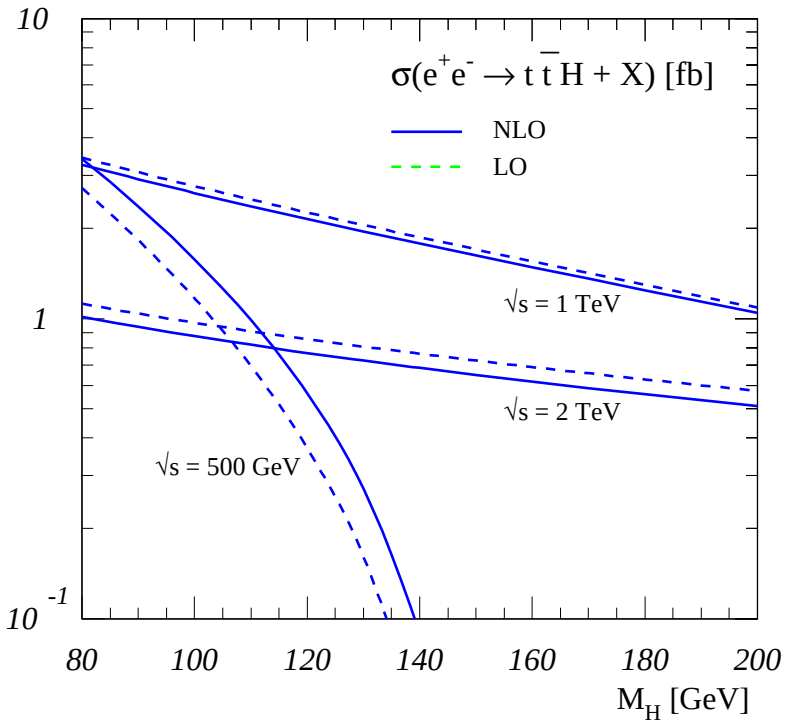

Figure 3.5: Cross-sections for $e^+e^- \to t\bar{t}h_{\rm SM}$ in fb for three choices of center-of-mass energy. The dashed lines correspond to the tree-level result [23], and the solid lines include the next-to-leading order QCD corrections [24].

Other relevant processes for producing Higgs bosons are associated production with a fermion-antifermion pair, and multi-Higgs production. For the former class, only $e^+e^- \to t\bar{t}h_{\rm SM}$ has a significant cross section, around the femtobarn level in the Standard Model, as depicted in Fig. 3.5. As a result, if $m_{h_{\rm SM}}$ is small enough (or $\sqrt{s}$ is large enough), this process can be used for determining the Higgs–top quark Yukawa coupling. The cross section for double Higgs production ($e^+e^- \to Zh_{\rm SM}h_{\rm SM}$) are even smaller, of order 0.1 fb for 100 GeV $\lesssim m_{h_{\rm SM}} \lesssim$ 150 GeV and $\sqrt{s}$ ranging between 500 GeV and 1 TeV. With sufficient luminosity, the latter can be used for extracting the triple Higgs self-coupling.

At the $\gamma\gamma$ collider, a Higgs boson is produced as an s-channel resonance via the one-loop triangle diagram. Every charged particle whose mass is generated by the Higgs boson contributes to this process. In the Standard Model, the main contributors are the $W^\pm$ and the t-quark loops. See Section 10 for further discussion.

4 SM Higgs searches before the linear collider

4.1 Direct search limits from LEP

The LEP collider completed its final run in 2000, and presented tantalizing hints for the possible observation of the Higgs boson. Combining data from all four LEP collaborations [10], one could interpret their observations as corresponding to the production of a Higgs boson with a mass of $m_{h^0} = 115.0^{+1.3}_{-0.9}$ GeV with a significance of 2.9σ. This is clearly not sufficient to announce a discovery or even an "observation". A more conservative interpretation of the data then places a 95% CL lower limit of $m_{h_{\rm SM}} > 113.5$ GeV.

4.2 Implications of precision electroweak measurements

Indirect constraints on the Higgs boson mass within the SM can be obtained from confronting the SM predictions with results of electroweak precision measurements. In the case of the top quark mass, the indirect determination turned out to be in remarkable agreement with the actual experimental value. In comparison, to obtain constraints on $m_{h_{\rm SM}}$ of similar precision, much higher accuracy is required for both the experimental results and the theory predictions. This is due to the fact that the leading dependence of the precision observables on $m_{h_{\rm SM}}$ is only logarithmic, while the dominant effects of the top-quark mass enter quadratically.

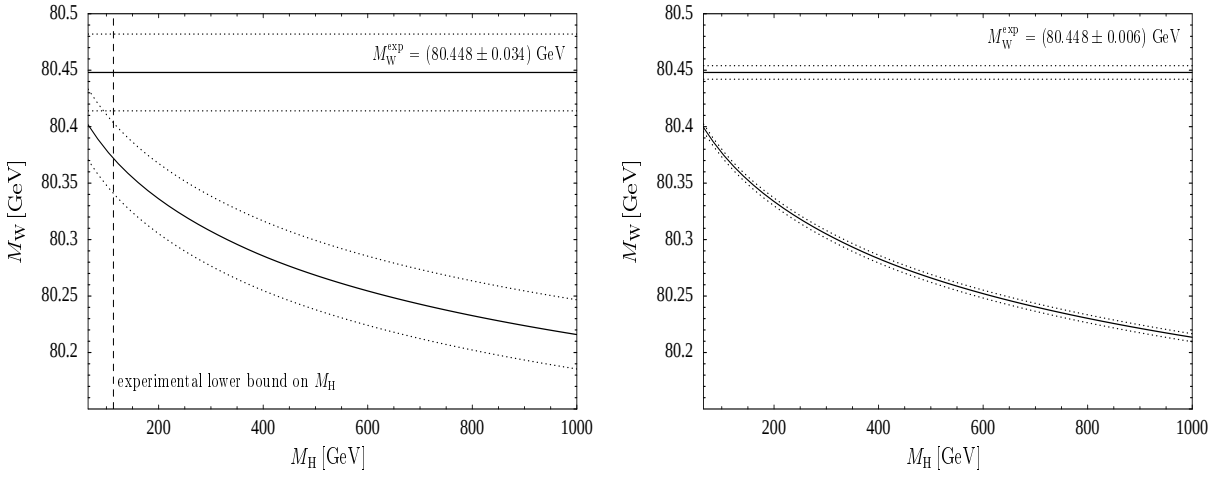

Figure 3.6: The prediction for m_W as a function of $m_{h_{\rm SM}}$ is compared with the experimental value of m_W for the current experimental accuracies of m_W and m_t (left plot) and for the prospective future accuracies at a LC with Giga-Z option (right plot, the present experimental central values are assumed) [25]. In the left plot also the present experimental 95% CL lower bound on the Higgs-boson mass, $m_{h_{\rm SM}} = 113.5$ GeV, is indicated.

The left plot of Fig. 3.6 shows the currently most precise result for m_W as function of $m_{h_{\rm SM}}$ in the SM, and compares it with the present experimental value of m_W. The calculation incorporates the complete electroweak fermion-loop contributions at $\mathcal{O}(\alpha^2)$ [25]. Based on this result, the remaining theoretical uncertainty from unknown higher-order corrections has been estimated to be about 6 MeV [25]. It is about a factor five smaller than the uncertainty induced by the current experimental error on the top-quark mass, $\Delta m_t^{\rm exp} = \pm 5.1\,\text{GeV}$, which presently dominates the theoretical uncertainty. The right plot of Fig. 3.6 shows the prospective situation at a future e^+e^- linear collider after Giga-Z operation and a threshold measurement of the W mass (keeping the present experimental central values for simplicity), which are expected to reduce the experimental errors to $\Delta m_W^{\rm exp} = 6$ MeV and $\Delta m_t^{\rm exp} = 200$ MeV. This program is described in Chapter 8. The plot clearly shows the considerable improvement in the sensitivity to $m_{h_{\rm SM}}$ achievable at the LC via very precise measurements of m_W and m_t. Since furthermore the experimental error of $\sin^2\theta_w^{\rm eff}$ is expected to be reduced by almost a factor of 20 at Giga-Z, the accuracy in the indirect determination of the Higgs-boson mass from all data will improve by about a factor of 10 compared to the present situation [26].

4.3 Expectations for Tevatron searches

The upgraded Tevatron began taking data in the spring of 2001. This is the only collider at which the Higgs boson can be produced for the next five years, until the LHC begins operation in 2006. The Tevatron Higgs working group presented a detailed analysis of the Higgs discovery reach at the upgraded Tevatron [27]. Here, we summarize the main results. Two Higgs mass ranges were considered separately: (i) 100 GeV$\lesssim m_{h_{\rm SM}} \lesssim$ 135 GeV and (ii) 135 GeV$\lesssim m_{h_{\rm SM}} \lesssim$ 190 GeV, corresponding to the two different dominant Higgs decay modes: $h_{\rm SM} \to b\overline{b}$ for the lighter mass range and $h_{\rm SM} \to WW^{(*)}$ for the heavier mass range.

In mass range (i), the relevant production mechanisms are $q_i\overline{q}_j \to Vh_{\rm SM}$, where $V = W$ or Z. In all cases, the dominant $h_{\rm SM} \to b\overline{b}$ decay was employed. The most relevant final-state signatures correspond to events in which the vector boson decays leptonically ($W \to \ell\nu$, $Z \to \ell^+\ell^-$ and $Z \to \nu\overline{\nu}$, where $\ell = e$ or μ), resulting in $\ell\nu b\overline{b}$, $\nu\overline{\nu}b\overline{b}$ and $\ell^+\ell^-b\overline{b}$ final states. In mass range (ii), the relevant production mechanisms include $gg \to h_{\rm SM}$, $V^*V^* \to h_{\rm SM}$ and $q_i\overline{q}_j \to Vh_{\rm SM}$, with decays $h_{\rm SM} \to WW^{(*)}$, $ZZ^{(*)}$. The most relevant phenomenological signals are those in which two of the final-state vector bosons decay leptonically, resulting in $\ell^+\ell^-\nu\overline{\nu}$ or $\ell^\pm\ell^\pm jjX$, where j is a hadronic jet and X consists of two additional leptons (either charged or neutral). For example, the latter can arise from $Wh_{\rm SM}$ production followed by $h_{\rm SM} \to WW^{(*)}$, where the two like-sign W bosons decay leptonically, and the third W decays into hadronic jets. In this case X is a pair of neutrinos.

Figure 3.7 summarizes the Higgs discovery reach versus the total integrated lu-

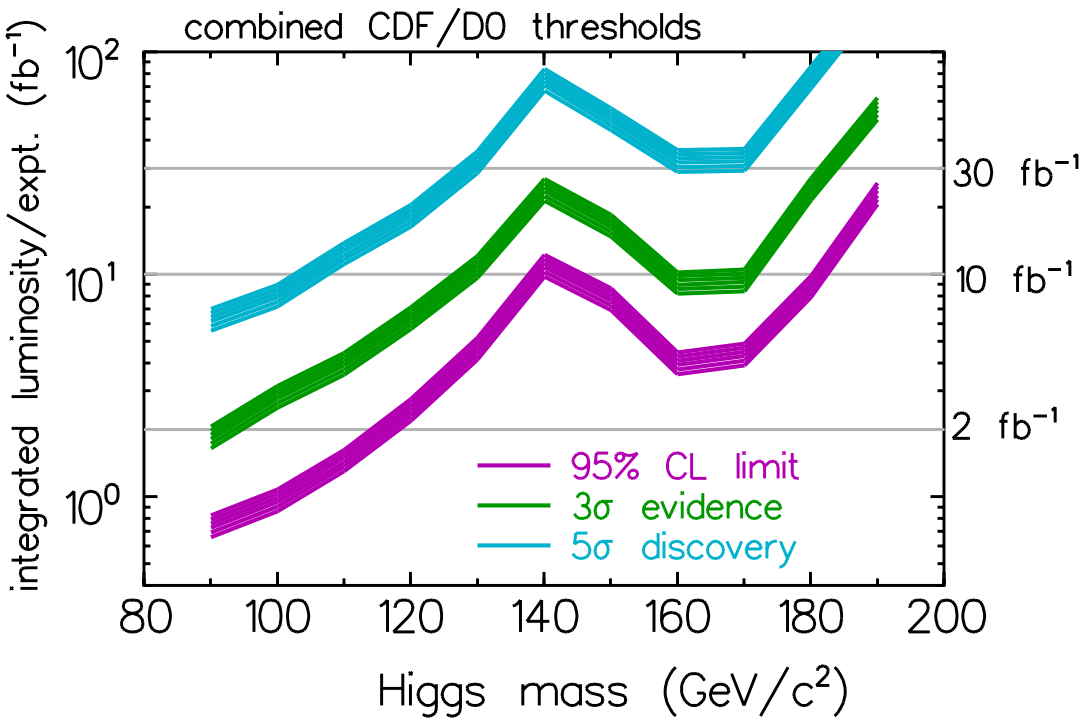

Figure 3.7: The integrated luminosity required per experiment, to either exclude a SM Higgs boson at 95% CL or discover it at the 3σ or 5σ level, as a function of the Higgs mass. These results are based on the combined statistical power of both experiments. The curves shown are obtained by combining the $\ell\nu b\bar{b}$, $\nu\bar{\nu}b\bar{b}$ and $\ell^+\ell^- b\bar{b}$ channels using the neural network selection in the low-mass Higgs region (90 GeV $\lesssim m_{h_{\rm SM}} \lesssim$ 130 GeV), and the $\ell^\pm\ell^\pm jjX$ and $\ell^+\ell^-\nu\bar{\nu}$ channels in the high-mass Higgs region (130 GeV $\lesssim m_{h_{\rm SM}} \lesssim$ 190 GeV). The lower edge of the bands is the calculated threshold; the bands extend upward from these nominal thresholds by 30% as an indication of the uncertainties in b-tagging efficiency, background rate, mass resolution, and other effects.

minosity delivered to the Tevatron (and by assumption, delivered to each detector). As the plot shows, the required integrated luminosity increases rapidly with Higgs mass to 140 GeV, beyond which the high-mass channels play the dominant role. With 2 fb^{-1} per detector (which is expected after one year of running at design luminosity), the 95% CL limits will barely extend the expected LEP2 limits, but with 10 fb^{-1}, the SM Higgs boson can be excluded up to 180 GeV if the Higgs boson does not exist in that mass range.

Current projections envision that the Tevatron, with further machine improvements, will provide an integrated luminosity of 15 fb^{-1} after six years of running. If $m_{h_{\rm SM}} \simeq 115$ GeV, as suggested by LEP data, then the Tevatron experiments will be

able to achieve a 5σ discovery of the Higgs boson. If no Higgs events are detected, the LEP limits will be significantly extended, with a 95% CL exclusion possible up to about $m_{h_{\rm SM}} \simeq 185$ GeV. Moreover, evidence for a Higgs boson at the 3σ level could be achieved up to about $m_{h_{\rm SM}} \simeq 175$ GeV. (The Higgs mass region around 140 GeV might require more luminosity, depending on the magnitude of systematic errors due to uncertainties in b-tagging efficiency, background rate, the $b\overline{b}$ mass resolution, *etc.*) Evidence for or discovery of a Higgs boson at the Tevatron would be a landmark in high energy physics. However, even if a Higgs boson is seen, the Tevatron data would only provide a very rough phenomenological profile. In contrast, the LC, and to a lesser extent, the LHC could measure enough of its properties with sufficient precision to verify that the observed Higgs is truly SM-like. The LHC is also certain to yield $> 5\sigma$ discovery of a SM Higgs boson over the full range of possible masses, up to 1 TeV.

4.4 Expectations for LHC searches

At the LHC, the ATLAS and CMS detectors have been specifically designed so as to guarantee discovery of a SM Higgs boson, regardless of mass. The most important production processes for the $h_{\rm SM}$ are the gluon fusion process, $gg \to h_{\rm SM}$, and the vector boson fusion process, $WW \to h_{\rm SM}$. In particular, for $m_{h_{\rm SM}} \lesssim 130\,{\rm GeV}$ the important discovery modes are $gg, WW \to h_{\rm SM} \to \gamma\gamma$, $\tau^+\tau^-$. At high luminosity, $q_i\overline{q}_j \to W^\pm h_{\rm SM}$ and $gg \to t\overline{t}h_{\rm SM}$ with $h_{\rm SM} \to \gamma\gamma$ and $h_{\rm SM} \to b\overline{b}$ should also be visible. Once $m_{h_{\rm SM}} > 130\,{\rm GeV}$, $gg \to h_{\rm SM} \to ZZ^{(*)} \to 4\ell$ is extremely robust except for the small mass region with $m_{h_{\rm SM}}$ just above $2m_W$ in which $h_{\rm SM} \to WW$ is allowed and $B(h_{\rm SM} \to ZZ^*)$ drops sharply. In this region, $gg, WW \to h_{\rm SM} \to WW \to \ell\nu\ell\nu$ provides a strong Higgs signal. Once $m_{h_{\rm SM}} > 300\,{\rm GeV}$ (400 GeV), the final states $h_{\rm SM} \to WW \to \ell\nu jj$ and $h_{\rm SM} \to ZZ \to \ell\ell\nu\nu$, where the $h_{\rm SM}$ is produced by a combination of gg and WW fusion, provide excellent discovery channels. These latter allow discovery even for $m_{h_{\rm SM}} \gtrsim 1\,{\rm TeV}$, *i.e.*, well beyond the $m_{h_{\rm SM}} \sim 800\,{\rm GeV}$ limit of viability for the $h_{\rm SM} \to 4\ell$ mode. These results are summarized in Fig. 3.8, from which we observe that the net statistical significance for the $h_{\rm SM}$, after combining channels, exceeds 10σ for all $m_{h_{\rm SM}} > 80\,{\rm GeV}$, assuming accumulated luminosity of $L = 100$ fb^{-1} at the ATLAS detector [29]. Similar results are obtained by the CMS group [30], the $\gamma\gamma$ mode being even stronger in the lower mass region.

Precision measurements for a certain number of quantities will be possible, depending upon the exact value of $m_{h_{\rm SM}}$. For instance, in [29] it is estimated that $m_{h_{\rm SM}}$ can be measured to $< 0.1\%$ for $m_{h_{\rm SM}} < 400\,{\rm GeV}$ and to 0.1–1% for $400 < m_{h_{\rm SM}} < 700\,{\rm GeV}$. Using the 4ℓ final state, $\Gamma^T_{h_{\rm SM}}$ can determined for $m_{h_{\rm SM}} > 250\,{\rm GeV}$ from the shape of the 4ℓ mass peak. Various ratios of branching ratios and a selection of partial widths times branching ratios can be measured in any given mass region. Some early estimates of possibilities and achievable accuracies appear in [2]. A more recent, but probably rather optimistic parton-level theoretical study [31] finds that

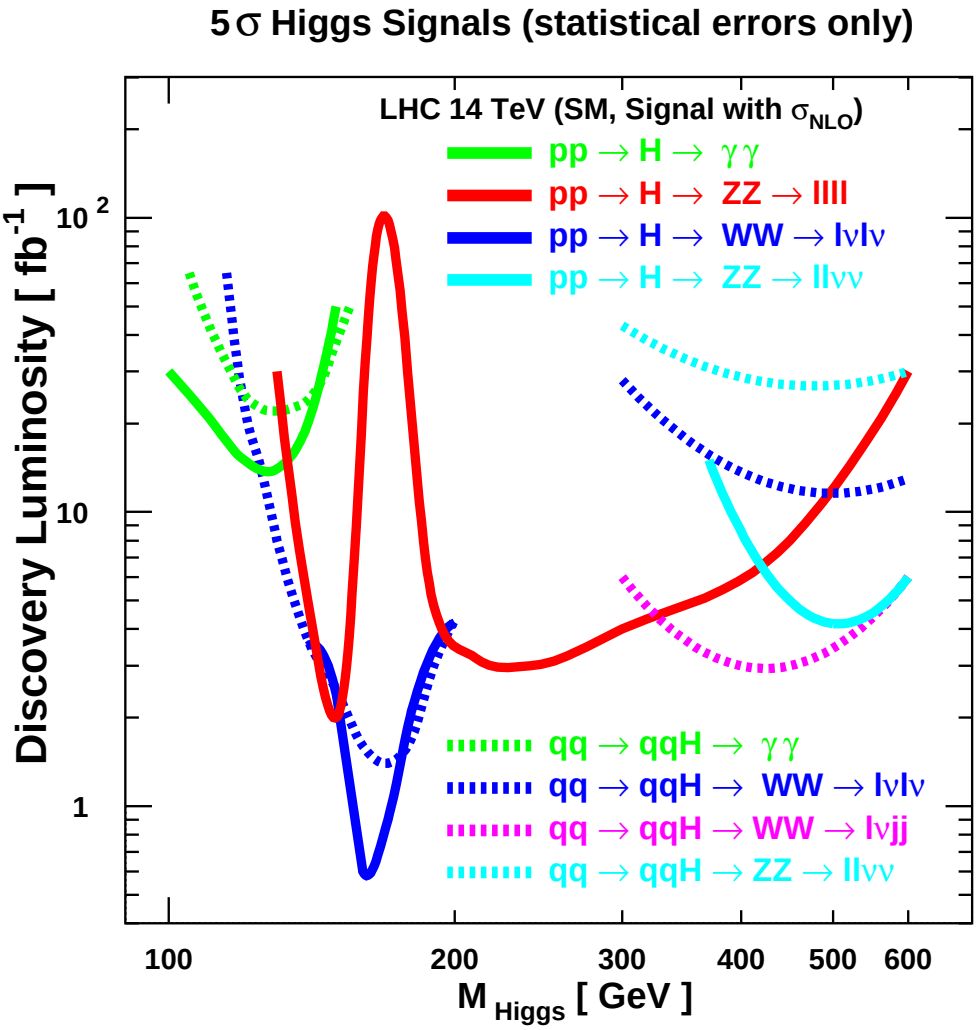

Figure 3.8: Expected 5σ SM Higgs discovery luminosity requirements at the LHC, for one experiment, statistical errors only [28]. The study was performed with CMS fast detector simulation.

if $m_{h_{\rm SM}} \lesssim 200\,\text{GeV}$ then good accuracies can be achieved for many absolute partial widths and for the total width provided: (a) WW fusion production can be reliably separated from gg fusion; (b) the WW/ZZ coupling ratio is as expected in the SM from the SU(2)×U(1) symmetry; (c) the WW^* final state can be observed in both gg and WW fusion; and (d) there are no unexpected decays of the $h_{\rm SM}$. Invisible Higgs decays may also be addressed by this technique [32]; CMS simulations show some promise for this channel. The resulting errors estimated for $L = 200$ fb^{-1} of accumulated data are given in Fig. 3.9.

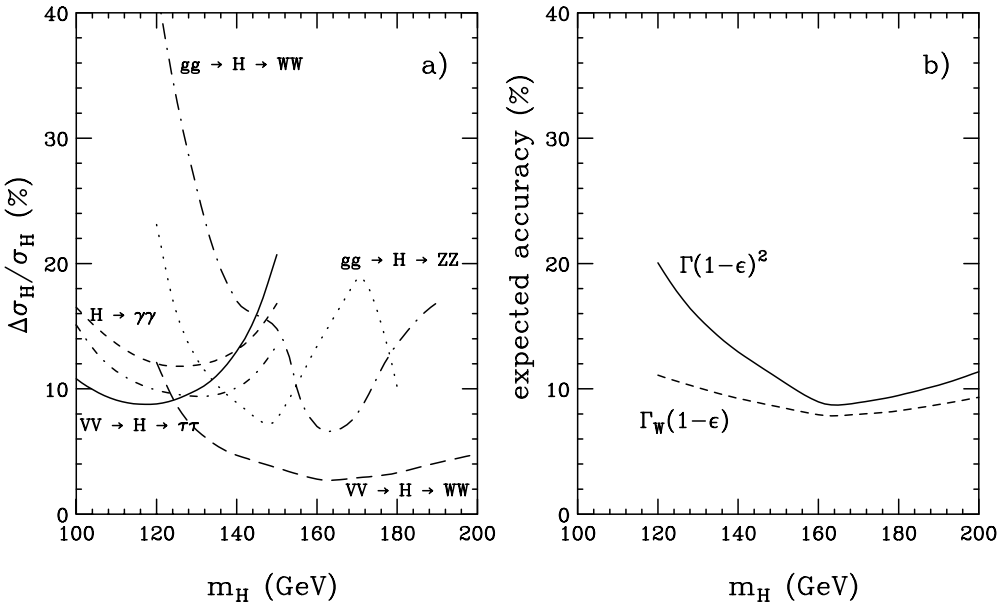

Figure 3.9: Relative accuracy expected at the LHC with 200 fb^{-1} of data. (a) Cross section times branching fraction for several inclusive modes (dotted and dash-dotted lines) and vector boson fusion channels (dashed and solid lines). (b) Extracted total width (solid line) and $H \to WW$ partial width (dashed line). In the latter, $\epsilon = 1 - [B(H \to b\overline{b}) + B(H \to \tau\tau) + B(H \to WW^{(*)}) + B(H \to ZZ^{(*)}) + B(H \to gg) + B(H \to \gamma\gamma)]$. To the extent that ϵ is small, the indicated accuracies can be achieved.

5 Higgs bosons in low-energy supersymmetry

The simplest realistic model of low-energy supersymmetry is the minimal supersymmetric Standard Model (MSSM), which consists of the two-Higgs-doublet extension of the Standard Model plus the corresponding superpartners [21]. Two Higgs doublets, one with $Y = +1$ and one with $Y = -1$, are needed in order that gauge anomalies due to the higgsino superpartners are exactly canceled. The supersymmetric structure also constrains the Higgs-fermion interactions. In particular, it is the $Y = -1$ Higgs doublet that generates mass for "up"-type quarks and the $Y = +1$ Higgs doublet that generates mass for "down"-type quarks (and charged leptons) [33,34].

After electroweak symmetry breaking, one finds five physical Higgs particles: a charged Higgs pair ($H^{\pm}$), two CP-even neutral Higgs bosons (denoted by h^0 and H^0 where $m_{h^0} \leq m_{H^0}$) and one CP-odd neutral Higgs boson (A^0).[2] Two other relevant

[2]The tree-level MSSM Higgs sector automatically conserves CP. Hence, the two neutral Higgs vacuum expectation values can be chosen to be real and positive, and the neutral Higgs eigenstates possess definite CP quantum numbers.

parameters are the ratio of neutral Higgs vacuum expectation values, $\tan\beta$, and an angle α that measures the component of the original $Y = \pm 1$ Higgs doublet states in the physical CP-even neutral scalars.

5.1 MSSM Higgs sector at tree-level

The supersymmetric structure of the theory imposes constraints on the Higgs sector of the model [35]. As a result, all Higgs sector parameters at tree-level are determined by two free parameters: $\tan\beta$ and one Higgs mass, conveniently chosen to be m_{A^0}. There is an upper bound to the tree-level mass of the light CP-even Higgs boson: $m_{h^0}^2 \leq m_Z^2 \cos 2\beta \leq m_Z^2$. However, radiative corrections can significantly alter this upper bound as described in Section 5.2.

The limit of $m_{A^0} \gg m_Z$ is of particular interest, with two key consequences. First, $m_{A^0} \simeq m_{H^0} \simeq m_{H^\pm}$, up to corrections of $\mathcal{O}(m_Z^2/m_{A^0})$. Second, $\cos(\beta-\alpha) = 0$ up to corrections of $\mathcal{O}(m_Z^2/m_{A^0}^2)$. This limit is known as the *decoupling* limit [36] because when m_{A^0} is large, the effective low-energy theory below the scale of m_{A^0} contains a single CP-even Higgs boson, h^0, whose properties are nearly identical to those of the Standard Model Higgs boson, $h_{\rm SM}$.

The phenomenology of the Higgs sector is determined by the various couplings of the Higgs bosons to gauge bosons, Higgs bosons and fermions. The couplings of the two CP-even Higgs bosons to W and Z pairs are given in terms of the angles α and β by

$$\begin{aligned} g_{h^0VV} &= g_V m_V \sin(\beta-\alpha) \\ g_{H^0VV} &= g_V m_V \cos(\beta-\alpha)\,, \end{aligned} \tag{3.3}$$

where

$$g_V \equiv \begin{array}{ll} g, & V = W, \\ g/\cos\theta_W, & V = Z. \end{array} \tag{3.4}$$

There are no tree-level couplings of A^0 or $H^\pm$ to VV. The couplings of one gauge boson to two neutral Higgs bosons are given by:

$$\begin{aligned} g_{h^0A^0Z} &= \frac{g\cos(\beta-\alpha)}{2\cos\theta_W}\,, \\ g_{H^0A^0Z} &= \frac{-g\sin(\beta-\alpha)}{2\cos\theta_W}\,. \end{aligned} \tag{3.5}$$

In the MSSM, the Higgs tree-level couplings to fermions obey the following property: the neutral member of the $Y = -1$ [$Y = +1$] Higgs doublet couples exclusively to down-type [up-type] fermion pairs. This pattern of Higgs-fermion couplings defines the Type-II two-Higgs-doublet model [37,1]. Consequently, the couplings of the neutral Higgs bosons to $f\overline{f}$ relative to the Standard Model value, $gm_f/2m_W$, are given

by (using third family notation):

$$\begin{aligned}
h^0 b\overline{b} \quad (\text{or } h^0\tau^+\tau^-) \quad &: \quad -\frac{\sin\alpha}{\cos\beta} = \sin(\beta-\alpha) - \tan\beta\cos(\beta-\alpha)\,, \\
h^0 t\overline{t} \quad &: \quad \frac{\cos\alpha}{\sin\beta} = \sin(\beta-\alpha) + \cot\beta\cos(\beta-\alpha)\,, \\
H^0 b\overline{b} \quad (\text{or } H^0\tau^+\tau^-) \quad &: \quad \frac{\cos\alpha}{\cos\beta} = \cos(\beta-\alpha) + \tan\beta\sin(\beta-\alpha)\,, \\
H^0 t\overline{t} \quad &: \quad \frac{\sin\alpha}{\sin\beta} = \cos(\beta-\alpha) - \cot\beta\sin(\beta-\alpha)\,, \\
A^0 b\overline{b} \quad (\text{or } A^0\tau^+\tau^-) \quad &: \quad \gamma_5\tan\beta\,, \\
A^0 t\overline{t} \quad &: \quad \gamma_5\cot\beta\,. \qquad (3.6)
\end{aligned}$$

In these expressions, γ_5 indicates a pseudoscalar coupling.

The neutral Higgs boson couplings to fermion pairs (3.6) have been written in such a way that their behavior can be immediately ascertained in the decoupling limit ($m_{A^0} \gg m_Z$) by setting $\cos(\beta-\alpha) = 0$. In particular, in the decoupling limit, the couplings of h^0 to vector bosons and fermion pairs are equal to the corresponding couplings of the Standard Model Higgs boson.

The region of MSSM Higgs sector parameter space in which the decoupling limit applies is large, because $\sin(\beta-\alpha)$ approaches 1 quite rapidly once m_{A^0} is larger than about 200 GeV, as shown in Fig. 3.10. As a result, over a significant region of the MSSM parameter space, the search for the lightest CP-even Higgs boson of the MSSM is equivalent to the search for the Standard Model Higgs boson. This result is more general; in many theories of non-minimal Higgs sectors, there is a significant portion of the parameter space that approximates the decoupling limit. Consequently, simulations of the Standard Model Higgs signal are also relevant for exploring the more general Higgs sector.

5.2 The radiatively corrected MSSM Higgs sector

When one-loop radiative corrections are incorporated, the Higgs masses and couplings depend on additional parameters of the supersymmetric model that enter via the virtual loops. One of the most striking effects of the radiative corrections to the MSSM Higgs sector is the modification of the upper bound of the light CP-even Higgs mass, as first noted in [38]. When $\tan\beta \gg 1$ and $m_{A^0} \gg m_Z$, the *tree-level* prediction for m_{h^0} corresponds to its theoretical upper bound, $m_h^{\max} = m_Z$. Including radiative corrections, the theoretical upper bound is increased, primarily because of an incomplete cancellation of the top-quark and top-squark (stop) loops. (These contributions would cancel if supersymmetry were exact.) The relevant parameters that govern the stop sector are the average of the two stop squared-masses:

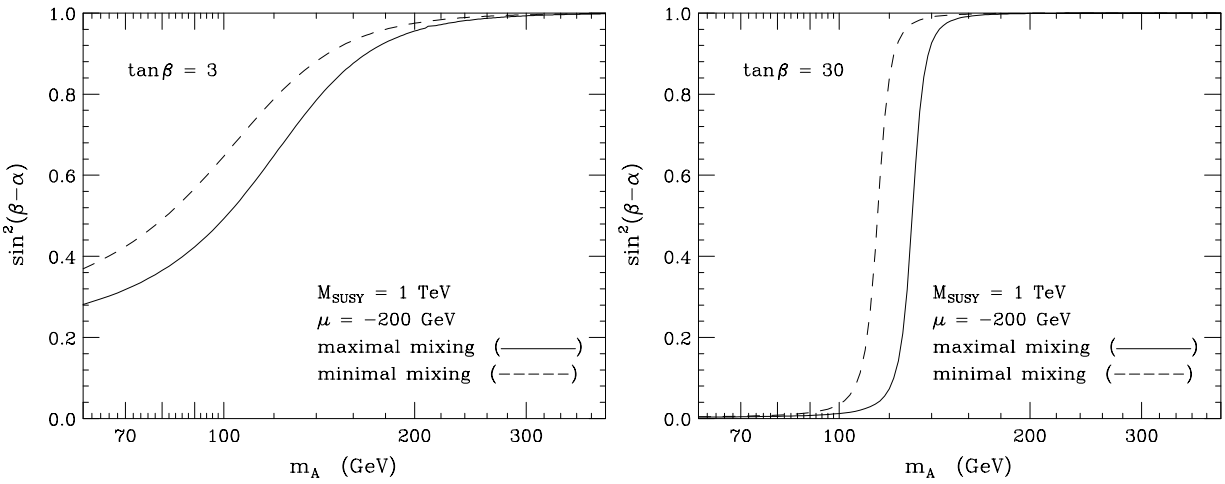

Figure 3.10: The value of $\sin^2(\beta-\alpha)$ is shown as a function of m_{A^0} for two choices of $\tan\beta = 3$ and $\tan\beta = 30$. When radiative corrections are included, one can define an approximate loop-corrected angle α as a function of m_{A^0}, $\tan\beta$ and the MSSM parameters. In the figures above, we have incorporated radiative corrections, assuming that $M_{\rm SUSY} = 1$ TeV. In addition, two extreme cases for the squark mixing parameters are shown (see Section 5.2 for further discussion of the radiative corrections and their dependence on the supersymmetric parameters). The decoupling effect expected when $\sin^2(\beta-\alpha) \simeq 1$ for $m_{A^0} \gg m_Z$, continues to hold even when radiative corrections are included.

$M^2_{\rm SUSY} \equiv \frac{1}{2}(M^2_{\tilde{t}_1} + M^2_{\tilde{t}_2})$, and the off-diagonal element of the stop squared-mass matrix: $m_t X_t \equiv m_t(A_t - \mu\cot\beta)$, where A_t is a soft supersymmetry-breaking trilinear scalar interaction term, and μ is the supersymmetric Higgs mass parameter. The qualitative behavior of the radiative corrections can be most easily seen in the large top squark mass limit, where, in addition, the splitting of the two diagonal entries and the off-diagonal entry of the stop squared-mass matrix are both small in comparison to $M^2_{\rm SUSY}$. In this case, the upper bound on the lightest CP-even Higgs mass is approximately given by

$$m^2_{h^0} \lesssim m^2_Z + \frac{3g^2 m_t^4}{8\pi^2 m_W^2}\left[\ln\left(\frac{M^2_{\rm SUSY}}{m_t^2}\right) + \frac{X_t^2}{M^2_{\rm SUSY}}\left(1 - \frac{X_t^2}{12M^2_{\rm SUSY}}\right)\right]. \qquad (3.7)$$

More complete treatments of the radiative corrections include the effects of stop mixing, renormalization group improvement, and the leading two-loop contributions, and imply that these corrections somewhat overestimate the true upper bound of m_{h^0} (see [39] for the most recent results). Nevertheless, Eq. (3.7) correctly illustrates some noteworthy features of the more precise result. First, the increase of the light CP-even Higgs mass bound beyond m_Z can be significant. This is a consequence of the m_t^4 enhancement of the one-loop radiative correction. Second, the dependence of the light Higgs mass on the stop mixing parameter X_t implies that (for a given value

of $M_{\rm SUSY}$) the upper bound of the light Higgs mass initially increases with X_t and reaches its *maximal* value at $X_t \simeq \sqrt{6} M_{\rm SUSY}$. This point is referred to as the *maximal mixing* case (whereas $X_t = 0$ corresponds to the *minimal mixing* case).

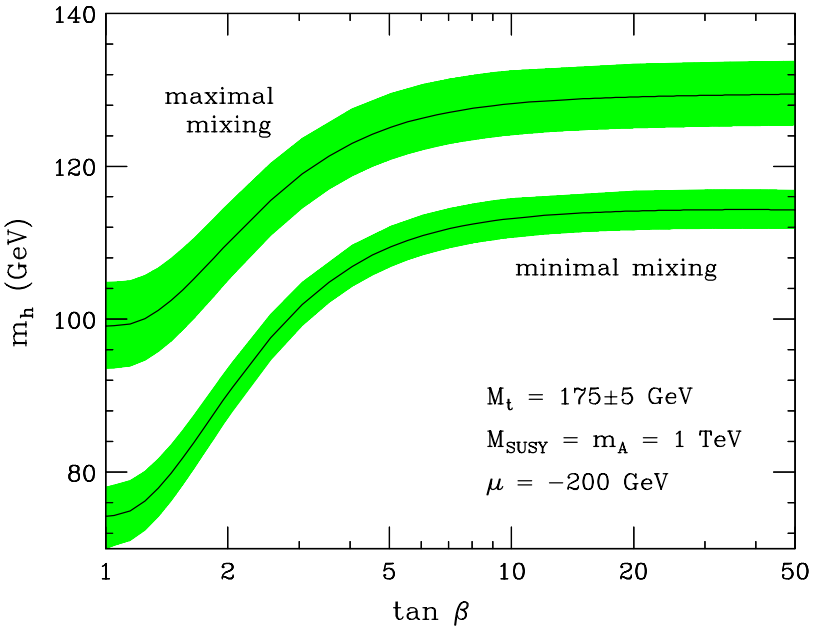

Figure 3.11: The radiatively corrected light CP-even Higgs mass is plotted as a function of $\tan\beta$, for the maximal mixing [upper band] and minimal mixing cases. The impact of the top quark mass is exhibited by the shaded bands; the central value corresponds to $m_t = 175$ GeV, while the upper [lower] edge of the bands correspond to increasing [decreasing] m_t by 5 GeV.

Taking m_{A^0} large, Fig. 3.11 illustrates that the maximal value of the lightest CP-even Higgs mass bound is realized at large $\tan\beta$ in the case of maximal mixing. Allowing for the uncertainty in the measured value of m_t and the uncertainty inherent in the theoretical analysis, one finds for $M_{\rm SUSY} \lesssim 2$ TeV that $m_{h^0} \lesssim m_h^{\rm max}$, where

$$\begin{aligned} m_h^{\rm max} &\simeq 122 \text{ GeV}, \quad \text{minimal stop mixing}, \\ m_h^{\rm max} &\simeq 135 \text{ GeV}, \quad \text{maximal stop mixing}. \end{aligned} \tag{3.8}$$

The h^0 mass bound in the MSSM quoted above does not apply to non-minimal supersymmetric extensions of the Standard Model. If additional Higgs singlet and/or triplet fields are introduced, then new Higgs self-coupling parameters appear, which are not significantly constrained by present data. For example, in the simplest non-minimal supersymmetric extension of the Standard Model (NMSSM), the addition of a complex Higgs singlet field S adds a new Higgs self-coupling parameter, λ_S [40]. The mass of the lightest neutral Higgs boson can be raised arbitrarily by increasing

the value of λ_S, analogous to the behavior of the Higgs mass in the Standard Model. Under the assumption that all couplings stay perturbative up to the Planck scale, one finds in essentially all cases that $m_{h^0} \lesssim 200$ GeV, independent of the details of the low-energy supersymmetric model [41].

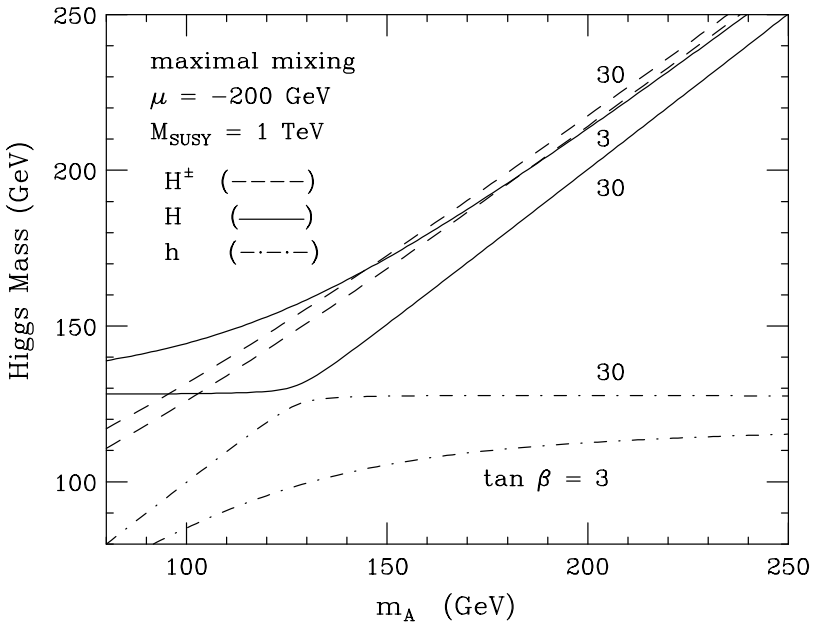

Figure 3.12: Lightest CP-even Higgs mass (m_{h^0}), heaviest CP-even Higgs mass (m_{H^0}) and charged Higgs mass ($m_{H^\pm}$) as a function of m_{A^0} for two choices of $\tan\beta = 3$ and $\tan\beta = 30$. The slight increase in the charged Higgs mass as $\tan\beta$ is increased from 3 to 30 is a consequence of the radiative corrections.

In Fig. 3.12, we exhibit the masses of the CP-even neutral and the charged Higgs masses as a function of m_{A^0}. Note that $m_{H^0} \geq m_h^{\max}$ for all values of m_{A^0} and $\tan\beta$, where $m_h^{\max}$ is to be evaluated depending on the top-squark mixing, as indicated in Eq. (3.8).

Radiative corrections also significantly modify the tree-level values of the Higgs boson couplings to fermion pairs and to vector boson pairs. As discussed above, the tree-level Higgs couplings depend crucially on the value of $\sin(\beta - \alpha)$. In the first approximation, when radiative corrections of the Higgs squared-mass matrix are computed, the diagonalizing angle α is modified. This provides one important source of the radiative corrections of the Higgs couplings. In Fig. 3.10, we show the effect of radiative corrections on the value of $\sin(\beta - \alpha)$ as a function of m_{A^0} for different values of the squark mixing parameters and $\tan\beta$. One can then simply insert the radiatively corrected value of α into eqs. (3.3), (3.5), and (3.6) to obtain radiatively improved couplings of Higgs bosons to vector bosons and to fermions.

At large $\tan\beta$, there is another potentially important class of radiative corrections

in addition to those that enter through the modified α. These corrections arise in the relation between m_b and $\tan\beta$ and depend on the details of the MSSM spectrum (which enter via loop-effects). At tree-level, the Higgs couplings to $b\overline{b}$ are proportional to the Higgs–bottom-quark Yukawa coupling. Deviations from the tree-level relation due to radiative corrections are calculable and finite [42–46]. One of the fascinating properties of such corrections is that in certain cases the corrections do *not* vanish in the limit of large supersymmetric mass parameters. These corrections grow with $\tan\beta$ and therefore can be significant in the large $\tan\beta$ limit. In the supersymmetric limit, $b\overline{b}$ couples only to the neutral component of the $Y=-1$ Higgs doublet. However, when supersymmetry is broken there will be a small coupling of $b\overline{b}$ to the neutral component of the $Y=+1$ Higgs doublet resulting from radiative corrections. From this result, one can compute the couplings of the physical Higgs bosons to $b\overline{b}$ pairs. A useful approximation at large $\tan\beta$ yields the following corrections to Eq. (3.6):

$$\begin{aligned} h^0 b\overline{b} \;&:\quad -\frac{\sin\alpha}{\cos\beta}\frac{1}{1+\Delta_b}\left[1-\frac{\Delta_b\cot\alpha}{\tan\beta}\right], \\ H^0 b\overline{b} \;&:\quad \frac{\cos\alpha}{\cos\beta}\frac{1}{1+\Delta_b}\left[1+\frac{\Delta_b\tan\alpha}{\tan\beta}\right], \\ A^0 b\overline{b} \;&:\quad \gamma_5\,\frac{\tan\beta}{1+\Delta_b}, \end{aligned} \tag{3.9}$$

where $\Delta_b \propto \tan\beta$. The explicit form of Δ_b at one–loop in the limit of $M_{\rm SUSY} \gg m_b$ is given in [43–45]. The correction Δ_b arises from a bottom-squark–gluino loop, which depends on the gluino mass and the supersymmetric Higgs mass parameter μ, and the top-squark–chargino loop, which depends on the top-squark masses and the top-squark mixing parameters μ and A_t. Contributions proportional to the electroweak gauge couplings have been neglected.

Similarly, the neutral Higgs couplings to $\tau^+\tau^-$ are modified by replacing Δ_b in Eq. (3.9) with Δ_τ [44,45]. One can also derive radiatively corrected couplings of the charged Higgs boson to fermion pairs [47,48]. The tree-level couplings of the charged Higgs boson to fermion pairs are modified accordingly by replacing $m_b \to m_b/(1+\Delta_b)$ and $m_\tau \to m_\tau/(1+\Delta_\tau)$, respectively.

One consequence of the above results is that the neutral Higgs coupling to $b\overline{b}$ (which is expected to be the dominant decay mode over nearly all of the MSSM Higgs parameter space), can be significantly suppressed at large $\tan\beta$ [49–51] if $\Delta_b \simeq \mathcal{O}(1)$. Typically $|\Delta_\tau| \ll |\Delta_b|$, since the correction proportional to α_s in the latter is absent in the former. For this reason, the $\tau^+\tau^-$ decay mode can be the dominant Higgs decay channel for the CP-even Higgs boson with SM-like couplings to gauge bosons.

In the decoupling limit, one can show that $\cot\alpha\cot\beta = -1 + \mathcal{O}(m_Z^2/m_{A^0}^2)$. Inserting this result into Eq. (3.9), one can check that the $h^0 b\overline{b}$ coupling does indeed approach its Standard Model value. However, because $\Delta_b \propto \tan\beta$, the deviation of

the $h^0 b\overline{b}$ coupling from the corresponding SM result is of $\mathcal{O}(m_Z^2 \tan\beta/m_{A^0}^2)$. That is, at large $\tan\beta$, the approach to decoupling may be "delayed" [52], depending on the values of other MSSM parameters that enter the radiative corrections.

5.3 MSSM Higgs boson decay modes

In this section, we consider the decay properties of the three neutral Higgs bosons (h^0, H^0 and A^0) and of the charged Higgs pair ($H^\pm$). Let us start with the lightest state, h^0. When $m_{A^0} \gg m_Z$, the decoupling limit applies, and the couplings of h^0 to SM particles are nearly indistinguishable from those of $h_{\rm SM}$. If some superpartners are light, there may be some additional decay modes, and hence the h^0 branching ratios would be different from the corresponding Standard Model values, even though the partial widths to Standard Model particles are the same. Furthermore, loops of light charged or colored superpartners could modify the h^0 coupling to photons and/or gluons, in which case the one-loop gg and $\gamma\gamma$ decay rates would also be different. On the other hand, if all superpartners are heavy, all the decay properties of h^0 are essentially those of the SM Higgs boson, and the discussion of Section 3.1 applies.

The heavier Higgs states, H^0, A^0 and $H^\pm$, are roughly mass-degenerate and have negligible couplings to vector boson pairs. In particular, $\Gamma(H^0 \to VV) \ll \Gamma(h_{\rm SM} \to VV)$, while the couplings of A^0 and $H^\pm$ to the gauge bosons are loop-suppressed. The couplings of H^0, A^0 and $H^\pm$ to down-type (up-type) fermions are significantly enhanced (suppressed) relative to those of $h_{\rm SM}$ if $\tan\beta \gg 1$. Consequently, the decay modes $H^0, A^0 \to b\overline{b}$, $\tau^+\tau^-$ dominate the neutral Higgs decay modes for moderate-to-large values of $\tan\beta$ below the $t\overline{t}$ threshold, while $H^+ \to \tau^+\nu$ dominates the charged Higgs decay below the $t\overline{b}$ threshold.

For values of m_{A^0} of order m_Z, all Higgs boson states lie below 200 GeV in mass, and would all be accessible at the LC. In this parameter regime, there is a significant area of the parameter space in which none of the neutral Higgs boson decay properties approximates those of $h_{\rm SM}$. For example, when $\tan\beta$ is large, supersymmetry-breaking effects can significantly modify the $b\overline{b}$ and/or the $\tau^+\tau^-$ decay rates with respect to those of $h_{\rm SM}$. Additionally, the heavier Higgs bosons can decay into lighter Higgs bosons. Examples of such decay modes are: $H^0 \to h^0h^0$, A^0A^0, and ZA^0, and $H^\pm \to W^\pm h^0$, $W^\pm A^0$ (although in the MSSM, the Higgs branching ratio into vector boson–Higgs boson final states, if kinematically allowed, rarely exceeds a few percent). The decay of the heavier Higgs boson into two lighter Higgs bosons can provide information about Higgs self-couplings. For values of $\tan\beta \lesssim 5$, the branching ratio of $H^0 \to h^0h^0$ is dominant for a Higgs mass range of 200 GeV $\lesssim m_{H^0} \lesssim 2m_t$. The dominant radiative corrections to this decay arise from the corrections to the self-interaction $\lambda_{H^0h^0h^0}$ in the MSSM and are large [53].

The phenomenology of charged Higgs bosons is less model-dependent, and is governed by the values of $\tan\beta$ and $m_{H^\pm}$. Because charged Higgs couplings are proportional to fermion masses, the decays to third-generation quarks and leptons are

dominant. In particular, for $m_{H^\pm} < m_t + m_b$ (so that the channel $H^+ \to t\overline{b}$ is closed), $H^+ \to \tau^+\nu_\tau$ is favored if $\tan\beta \gtrsim 1$, while $H^+ \to c\overline{s}$ is favored only if $\tan\beta$ is small. Indeed, $\mathrm{BR}(H^+ \to \tau^+\nu_\tau) \simeq 1$ if $\tan\beta \gtrsim 5$. These results apply generally to Type-II two-Higgs doublet models. For $m_{H^\pm} \gtrsim 180$ GeV, the decay $H^+ \to t\overline{b} \to W^+ b\overline{b}$ is the dominant decay mode.

In addition to the above decay modes, there exist new Higgs decay channels that involve supersymmetric final states. Higgs decays into charginos, neutralinos and third-generation squarks and sleptons can become important, once they are kinematically allowed [54]. For Higgs masses below 130 GeV, the range of supersymmetric parameter space in which supersymmetric decays are dominant is rather narrow when the current bounds on supersymmetric particle masses are taken into account. One interesting possibility is a significant branching ratio of $h^0 \to \widetilde{\chi}^0\widetilde{\chi}^0$, which could arise for values of m_{h^0} near its upper theoretical limit. Such an invisible decay mode could be detected at the LC by searching for the missing mass recoiling against the Z in $e^+e^- \to h^0 Z$.

5.4 MSSM Higgs boson production at the LC

For $m_{A^0} \gtrsim 150$ GeV, Fig. 3.10 shows that the MSSM Higgs sector quickly approaches the decoupling limit, where the properties of h^0 approximately coincide with those of h_{SM}. Thus, the Higgsstrahlung and vector-boson-fusion cross-sections for h_{SM} production also apply to h^0 production. In contrast, the H^0VV and A^0VV couplings are highly suppressed, since $|\cos(\beta-\alpha)| \ll 1$. Equation (3.3) illustrates this for the H^0W coupling. Thus, these mechanisms are no longer useful for H^0 and A^0 production. The most robust production mechanism is $e^+e^- \to Z^* \to H^0A^0$, which is not suppressed since the ZH^0A^0 coupling is proportional to $\sin(\beta-\alpha)$, as indicated in Eq. (3.5). Radiatively corrected cross-sections for Zh^0, ZH^0, H^0A^0, and h^0A^0 have been recently obtained in [55]. The charged Higgs boson is also produced in pairs via s-channel photon and Z exchange. However, since $m_{H^0} \simeq m_{A^0} \simeq m_{H^\pm}$ in the decoupling limit, H^0A^0 and H^+H^- production are kinematically allowed only when $m_{A^0} \lesssim \sqrt{s}/2$.[3] In $\gamma\gamma$ collisions, one can extend the Higgs mass reach for the neutral Higgs bosons. As described in Section 10, the s-channel resonant production of H^0 and A^0 (due primarily to the top and bottom-quark loops in the one-loop Higgs–$\gamma\gamma$ triangle) can be detected for some choices of m_{A^0} and $\tan\beta$ if the heavy Higgs masses are less than about 80% of the initial $\sqrt{s}$ of the primary e^+e^- system. The corresponding cross sections are a few fb [56,57].

If $m_{A^0} \lesssim 150$ GeV, deviations from the decoupling limit become more apparent, and H^0 can now be produced via Higgsstrahlung and vector boson fusion at an observable rate. In addition, the factor of $\cos(\beta-\alpha)$ in the Zh^0A^0 coupling no longer

[3] The pair production of scalars is P-wave suppressed near threshold, so in practice the corresponding Higgs mass reach is likely to be somewhat lower than $\sqrt{s}/2$.

significantly suppresses h^0A^0 production. Finally, if $m_{H^\pm} \lesssim 170$ GeV, the charged Higgs boson will also be produced in $t \to H^+b$. In the non-decoupling regime, all non-minimal Higgs states can be directly produced and studied at the LC.

The associated production of a single Higgs boson and a fermion-antifermion pair can also be considered. Here, the new feature is the possibility of enhanced Higgs–fermion Yukawa couplings. Consider the behavior of the Higgs couplings at large $\tan\beta$, where some of the Higgs couplings to down type fermion pairs (denoted generically by $b\overline{b}$) can be significantly enhanced.[4] Let us examine two particular large $\tan\beta$ regions of interest. In the decoupling limit (where $m_{A^0} \gg m_Z$ and $|\cos(\beta-\alpha)| \ll 1$), it follows from Eq. (3.6) that the $b\overline{b}H^0$ and $b\overline{b}A^0$ couplings have equal strength and are significantly enhanced by a factor of $\tan\beta$ relative to the $b\overline{b}h_{\rm SM}$ coupling, while the $b\overline{b}h^0$ coupling is given by the corresponding Standard Model value. If $m_{A^0} \lesssim m_Z$ and $\tan\beta \gg 1$, then $|\sin(\beta-\alpha)| \ll 1$, as shown in Fig. 3.10, and $m_{h^0} \simeq m_{A^0}$. In this case, the $b\overline{b}h^0$ and $b\overline{b}A^0$ couplings have equal strength and are significantly enhanced (by a factor of $\tan\beta$) relative to the $b\overline{b}h_{\rm SM}$ coupling.[5] Note that in both cases above, only two of the three neutral Higgs bosons have enhanced couplings to $b\overline{b}$. If ϕ is one of the two neutral Higgs bosons with enhanced $b\overline{b}\phi$ couplings, then the cross-section for $e^+e^- \to f\overline{f}\phi$ ($f = b$ or τ) will be significantly enhanced relative to the corresponding Standard Model cross-section by a factor of $\tan^2\beta$. The phase-space suppression is not as severe as in $e^+e^- \to t\overline{t}\phi$ (see Fig. 3.5), so this process could extend the mass reach of the heavier neutral Higgs states at the LC given sufficient luminosity. The production of the charged Higgs boson via $e^+e^- \to t\overline{b}H^-$ is also enhanced by $\tan^2\beta$, although this process has a more significant phase-space suppression because of the final state top quark. If any of these processes can be observed, it would provide a direct measurement of the corresponding Higgs–fermion Yukawa coupling.

6 MSSM Higgs boson searches before the LC

6.1 Review of direct search limits

Although no direct experimental evidence for the Higgs boson yet exists, there are both experimental as well as theoretical constraints on the parameters of the MSSM

[4] We do not consider the possibility of $\tan\beta \ll 1$, which would lead to enhanced Higgs couplings to up-type fermions. In models of low-energy supersymmetry, there is some theoretical prejudice that suggests that $1 \lesssim \tan\beta \lesssim m_t/m_b$, with the fermion masses evaluated at the electroweak scale. For example, $\tan\beta \lesssim 1$ is disfavored since in this case, the Higgs–top quark Yukawa coupling blows up at an energy scale significantly below the Planck scale. The Higgs-bottom quark Yukawa coupling has a similar problem if $\tan\beta \gtrsim m_t/m_b$. As noted in Section 6.1, some of the low $\tan\beta$ region is already ruled out by the MSSM Higgs search.

[5] However in this case, the value of the $b\overline{b}H^0$ coupling can differ from the corresponding $b\overline{b}h_{\rm SM}$ coupling when $\tan\beta \gg 1$, since in case (ii), where $|\sin(\beta-\alpha)| \ll 1$, the product $\tan\beta\sin(\beta-\alpha)$ need not be particularly small.

Higgs sector. Experimental limits on the charged and neutral Higgs masses have been obtained at LEP. For the charged Higgs boson, $m_{H^\pm} > 78.7$ GeV [58]. This is the most model-independent bound. It is valid for more general non-supersymmetric two-Higgs doublet models and assumes only that the H^+ decays dominantly into $\tau^+\nu_\tau$ and/or $c\overline{s}$. The LEP limits on the masses of h^0 and A^0 are obtained by searching simultaneously for $e^+e^- \to Z \to Zh^0$ and $e^+e^- \to Z \to h^0A^0$. Radiative corrections can be significant, as shown in Section 5.2, so the final limits depend on the choice of MSSM parameters that govern the radiative corrections. The third generation squark parameters are the most important of these. The LEP Higgs working group [59] quotes limits for the case of $M_{\rm SUSY} = 1$ TeV in the maximal-mixing scenario, which corresponds to the choice of third generation squark parameters that yields the largest corrections to m_{h^0}. The present LEP 95% CL lower limits are $m_{A^0} > 91.9$ GeV and $m_{h^0} > 91.0$ GeV. The theoretical upper bound on m_{h^0} as a function of $\tan\beta$, exhibited in Fig. 3.11, can then be used to exclude a region of $\tan\beta$ in which the predicted value of m_{h^0} lies below the experimental bound. Under the same MSSM Higgs parameter assumptions stated above, the LEP Higgs search excludes the region $0.5 < \tan\beta < 2.4$ at 95% CL.

In discussing Higgs discovery prospects at the Tevatron and LHC, we shall quote limits based on the assumption of $M_{\rm SUSY} = 1$ TeV and maximal squark mixing. This tends to be a conservative assumption; that is, other choices give sensitivity to *more* of the m_{A^0} versus $\tan\beta$ plane. However, there are a number of other parameter regimes in which certain Higgs search strategies become more difficult. While these issues are of vital importance to the Tevatron and LHC Higgs searches, they are much less important at the LC.

6.2 MSSM Higgs searches at the Tevatron

At the Tevatron, the SM Higgs search can be reinterpreted in terms of the search for the CP-even Higgs boson of the MSSM. Since the theoretical upper bound was found to be $m_{h^0} \lesssim 135$ GeV (for $M_{\rm SUSY} < 2$ TeV), only the Higgs search of the low-mass region, 100 GeV $\lesssim m_{h^0} \lesssim$ 135 GeV, applies. In the MSSM at large $\tan\beta$, the enhancement of the $A^0b\overline{b}$ coupling (and a similar enhancement of either the $h^0b\overline{b}$ or $H^0b\overline{b}$ coupling) provides a new search channel: $q\overline{q}$, $gg \to b\overline{b}\phi$, where ϕ is a neutral Higgs boson with enhanced couplings to $b\overline{b}$. Combining both sets of analyses, the Tevatron Higgs Working Group obtained the anticipated 95% CL exclusion and 5σ Higgs discovery contours for the maximal mixing scenario as a function of total integrated luminosity per detector (combining both CDF and D0 data sets) shown in Fig. 3.13 [27].

From these results, one sees that 5 fb^{-1} of integrated luminosity per experiment will allow one to test nearly all of the MSSM Higgs parameter space at 95% CL. To assure discovery of a CP-even Higgs boson at the 5σ level, the luminosity requirement becomes very important. Figure 3.13(b) shows that a total integrated luminosity of

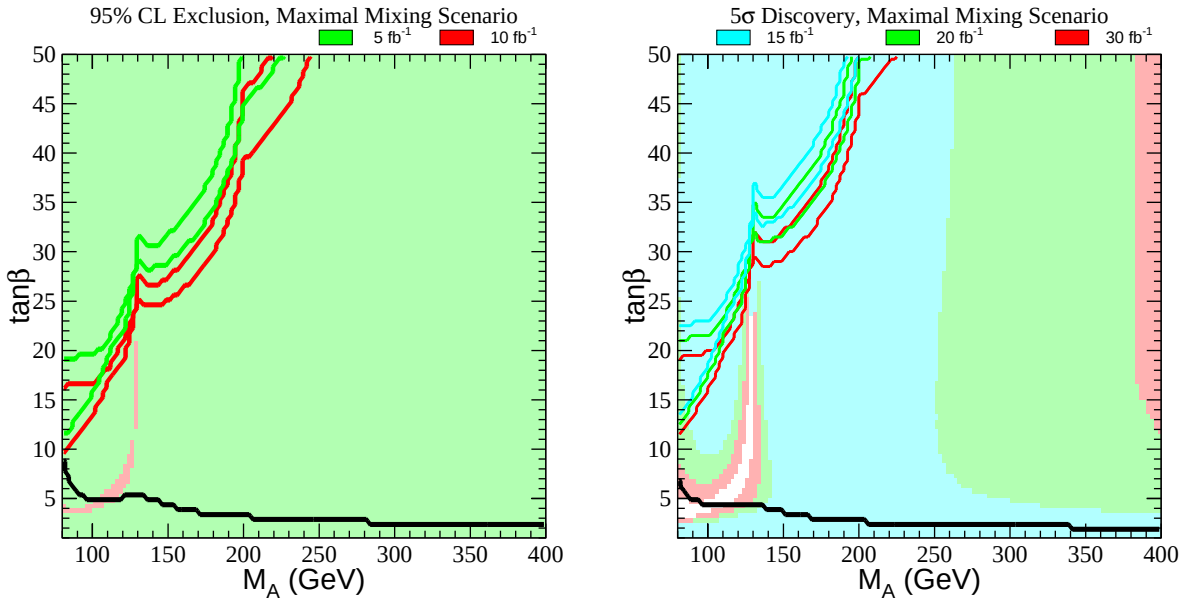

Figure 3.13: (a) 95% CL exclusion region and (b) 5σ discovery region on the m_{A^0}–$\tan\beta$ plane, for the maximal mixing scenario and two different search channels: $q\overline{q} \to V\phi$ ($\phi = h^0$, H^0), $\phi \to b\overline{b}$ (shaded regions) and gg, $q\overline{q} \to b\overline{b}\phi$ ($\phi = h^0$, H^0, A^0), $\phi \to b\overline{b}$ (region in the upper left-hand corner bounded by the solid lines). Different integrated luminosities are explicitly shown by the color coding. The two sets of lines (for a given color) correspond to the CDF and DØ simulations, respectively. The region below the solid black line near the bottom of the plot is excluded by the absence of observed $e^+e^- \to Z\phi$ events at LEP2.

about 20 fb^{-1} per experiment is necessary in order to assure a significant, although not exhaustive, coverage of the MSSM parameter space. If the anticipated 15 fb^{-1} integrated luminosity is achieved, the discovery reach will significantly extend beyond that of LEP. A Higgs discovery would be assured if the Higgs interpretation of the Higgs-like LEP events is correct. Nevertheless, the MSSM Higgs boson could still evade capture at the Tevatron. We would then turn to the LHC to try to obtain a definitive Higgs boson discovery.

6.3 MSSM Higgs searches at the LHC

The potential of the LHC to discover one or more of the MSSM Higgs bosons has been exhaustively studied for the minimal and maximal mixing scenarios described above. One of the primary goals of these studies has been to demonstrate that at least one of the MSSM Higgs bosons will be observed by ATLAS and CMS for any possible choice of $\tan\beta$ and m_{A^0} consistent with bounds coming from current LEP

data. In order to establish such a 'no-lose' theorem, an important issue is whether or not the Higgs bosons have substantial decays to supersymmetric particle pairs. It is reasonable to suppose that these decays will be absent or relatively insignificant for the light h^0. Current mass limits on SUSY particles are such that only $h^0 \to \widetilde{\chi}_1^0\widetilde{\chi}_1^0$ might possibly be kinematically allowed and this possibility arises only in a very limited class of models. For $m_{A^0} \gtrsim 200\,\mathrm{GeV}$, decays of the $A^0, H^0, H^\pm$ to SUSY pair states (especially pairs of light charginos/neutralinos) are certainly a possibility, but the branching ratios are generally not all that large. The discovery limits we discuss below would be weakened, but not dramatically. Further, at high $\tan\beta$ the enhancement of the $b\overline{b}$ and $\tau^+\tau^-$ couplings of the heavy A^0 and H^0 imply that SUSY decay modes will not be important even for quite high $m_{A^0} \sim m_{H^0} \sim m_{H^\pm}$. We will summarize the LHC discovery prospects for the MSSM Higgs bosons assuming that SUSY decays are not significant.

One of the primary Higgs discovery modes is detection of the relatively SM-like h^0 using the same modes as employed for a light $h_{\rm SM}$. Based on Fig. 3.14 (which assumes $L = 300\ \mathrm{fb}^{-1}$) [60], we see that for $m_{A^0} \gtrsim 180\,\mathrm{GeV}$, the h^0 will be detected via $gg, WW \to h^0$ and $Wh^0, t\overline{t}h^0$ with $h^0 \to \gamma\gamma$, while the $t\overline{t}h^0$ with $h^0 \to b\overline{b}$ mode is viable down to $m_{A^0} \gtrsim 100 - 120\,\mathrm{GeV}$, depending on $\tan\beta$. There are also many possibilities for detecting the other MSSM Higgs bosons. We give a descriptive list. First, there is a small domain in which $m_{A^0} \lesssim 130\,\mathrm{GeV}$, but yet m_{A^0} is still large enough for consistency with LEP limits, in which $t \to bH^\pm$ discovery will be possible. However, the most interesting alternative detection modes are based on $gg \to A^0, H^0$ and $gb \to H^\pm t$ production. We focus first on the former. For low-to-moderate $\tan\beta$ values, the channels $H^0 \to ZZ^{(*)} \to 4\ell$, $H^0 \to h^0h^0 \to b\overline{b}\gamma\gamma$ and $A^0 \to Zh^0 \to \ell\ell b\overline{b}$ are viable when $m_{A^0} \lesssim 2m_t$, whereas the $A^0, H^0 \to t\overline{t}$ modes are viable for $m_{A^0} > 2m_t$. For large enough $\tan\beta$ the $gg \to A^0, H^0 \to \tau^+\tau^-, \mu^+\mu^-$ discovery modes become viable. For the $gb \to H^\pm t$ process, the $H^\pm \to tb$ decays provide a 5σ signal both for low-to-moderate $\tan\beta \lesssim$ 2–3 and for high $\tan\beta \gtrsim$ 15–25, depending upon mass. In addition, the $H^\pm \to \tau^\pm\nu$ decay mode yields a viable signal for $\tan\beta \gtrsim$ 7–12. Of course, if the plot were extended to higher m_{A^0}, the minimum $\tan\beta$ value required for H^0, A^0 or $H^\pm$ detection would gradually increase.

It is important to notice that current LEP constraints exclude all of the low-to-moderate $\tan\beta$ regime in the case of maximal mixing (and, of course, even more in the case of minimal mixing). Thus, it is very likely that $\tan\beta$ and m_{A^0} will be in one of two regions: (a) the increasingly large (as m_{A^0} increases) wedge of moderate $\tan\beta > 3$ in which only the h^0 will be detected; or, (b) the high $\tan\beta$ region for which the $gg \to H^0, A^0 \to \tau^+\tau^-, \mu^+\mu^-$ and $gb \to H^\pm t \to \tau^\pm\nu t, tbt$ modes are viable as well. If the $H^0, A^0, H^\pm$ are heavy and cannot be detected either at the LHC (because $\tan\beta$ is not large enough) or at the LC (because they are too heavy to be pair-produced), precision measurements of the h^0 branching ratios and other properties will be particularly crucial. The precision measurements might provide

the only means for constraining or approximately determining the value of m_{A^0} aside from possible direct detection in $\gamma\gamma \to H^0, A^0$ production. Expected LC precisions are such that deviations of h^0 branching ratios from the predicted SM values can be detected for $m_{A^0} \lesssim 700\,\text{GeV}$ [2,61].

At the LHC there is another important possibility for h^0 detection. Provided that the mass of the second-lightest neutralino exceeds that of the lightest neutralino (the LSP) by at least m_{h^0}, gluino and squark production will lead to chain decays in which $\widetilde{\chi}_2^0 \to h^0 \widetilde{\chi}_1^0$ occurs with substantial probability. In this way, an enormous number of h^0's can be produced, and the $h^0 \to b\overline{b}$ decay mode will produce a dramatic signal.

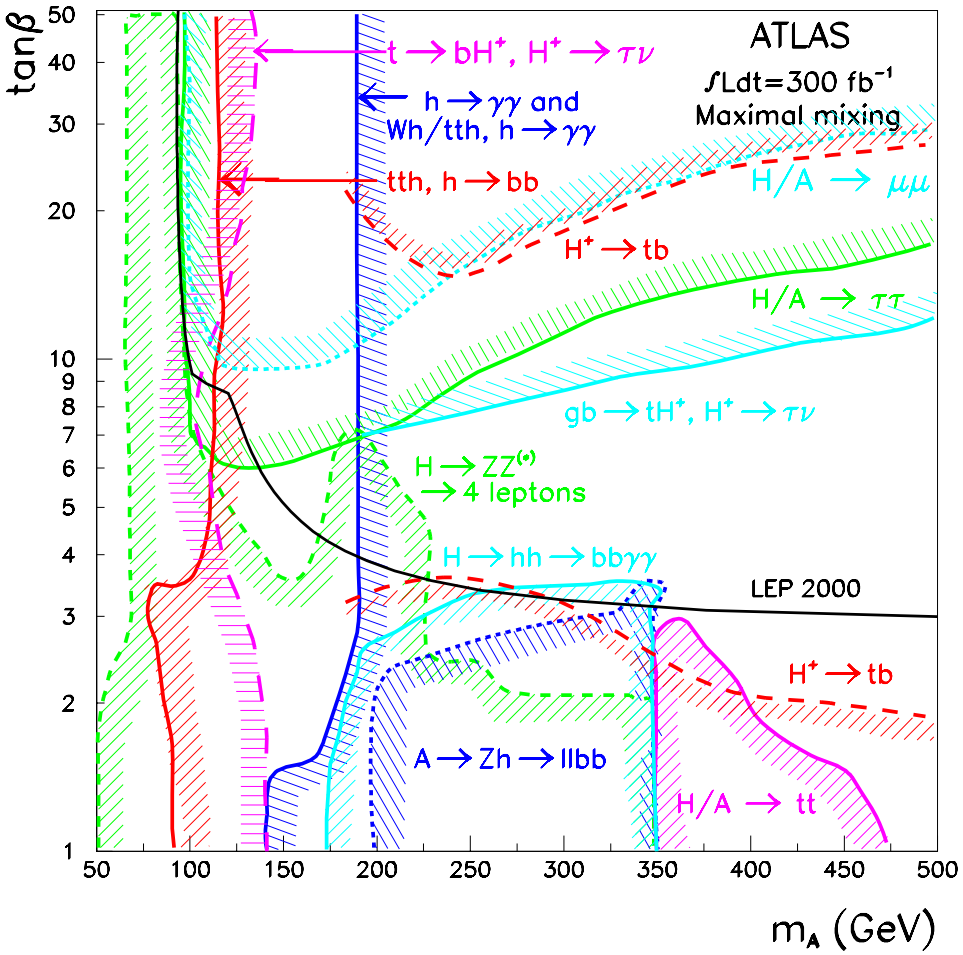

Figure 3.14: 5σ discovery contours for MSSM Higgs boson detection in various channels are shown in the $[m_{A^0}, \tan\beta]$ parameter space, assuming maximal mixing and an integrated luminosity of $L = 300$ fb^{-1} for the ATLAS detector. This figure is preliminary [60].

7 Non-exotic extended Higgs sectors

In this section, we consider the possibility of extending only the Higgs sector of the SM, leaving unchanged the gauge and fermionic sectors of the SM. We will also consider extensions of the two-doublet Higgs sector of the MSSM.

The simplest extensions of the minimal one-doublet Higgs sector of the SM contain additional doublet and/or singlet Higgs fields. Such extended Higgs sectors will be called non-exotic (to distinguish them from exotic Higgs sectors with higher representations, which will be considered briefly in Section 11). Singlet-only extensions have the advantage of not introducing the possibility of charge violation, since there are no charged Higgs bosons. In models with more than one Higgs doublet, tree-level Higgs-mediated flavor-changing neutral currents are present unless additional symmetries (discrete symmetries or supersymmetry) are introduced to restrict the form of the tree-level Higgs-fermion interactions [62]. Extensions containing additional doublet fields allow for spontaneous and explicit CP violation within the Higgs sector. These could be the source of observed CP-violating phenomena. Such models require that the mass-squared of the charged Higgs boson(s) that are introduced be chosen positive in order to avoid spontaneous breaking of electric charge conservation.

Extensions of the SM Higgs sector containing doublets and singlets can certainly be considered on a purely *ad hoc* basis. But there are also many dynamical models in which the effective low-energy sector below some scale Λ of order 1 to 10 TeV, or higher, consists of the SM fermions and gauge bosons plus an extended Higgs sector. Models with an extra doublet of Higgs fields include those related to technicolor, in which the effective Higgs doublet fields are composites containing new heavier fermions. See Chapter 5, Section 3 for further discussion of this case. The heavy fermions should be vector-like to minimize extra contributions to precision electroweak observables. In many of these models, the top quark mixes with the right-handed component of a new vector-like fermion. The top quark could also mix with the right-handed component of a Kaluza-Klein (KK) excitation of a fermion field, so that Higgs bosons would be composites of the top quark and fermionic KK excitations. (For a review and references to the literature, see [63].) Although none of these (non-perturbative) models have been fully developed, they do provide significant motivation for studying the Standard Model with a Higgs sector containing extra doublets and/or singlets if only as the effective low-energy theory below a scale Λ in the TeV range.

When considering Higgs representations in the context of a dynamical model with strong couplings at scale Λ, restrictions on Higgs self-couplings and Yukawa couplings that would arise by requiring perturbativity for such couplings up to some large GUT scale do not apply. At most, one should only demand perturbativity up to the scale Λ at which the new (non-perturbative) dynamics enters and the effective theory breaks down.

The minimal Higgs sector of the MSSM is a Type-II two-doublet model, where one Higgs doublet (H_d) couples at tree-level only to down quarks and leptons while the other (H_u) couples only to up quarks. Non-minimal extended Higgs sectors are also possible in low-energy supersymmetric models. Indeed, string theory realizations of low-energy supersymmetry often contain many extra singlet, doublet and even higher representations, some of which can yield light Higgs bosons (see, *e.g.*, [64]). However, non-singlet Higgs representations spoil gauge coupling unification, unless additional intermediate-scale matter fields are added to restore it. A particularly well-motivated extension is the inclusion of a single extra complex singlet Higgs field, often denoted S. Including S, the superpotential for the theory can contain the term $\lambda_S H_u H_d S$, which can then provide a natural source of a weak scale value for the μ parameter appearing in the bilinear superpotential form $\mu H_u H_d$ required in the MSSM. A weak-scale value for $s \equiv \langle S^0 \rangle$, where S^0 is the scalar component of the superfield S, is natural and yields an effective $\mu = \lambda_S s$. This extension of the MSSM is referred to as the next-to-minimal supersymmetric model, or NMSSM, and has received considerable attention. For an early review and references, see [1].

7.1 The decoupling limit

In many extended Higgs sector models, the most natural parameter possibilities correspond to a decoupling limit in which there is only one light Higgs boson, with Yukawa and vector boson couplings close to those of the SM Higgs boson. In contrast, all the other Higgs bosons are substantially heavier (than the Z) with negligibly small relative mass differences, and with suppressed vector boson couplings (which vanish in the exact limit of decoupling). By assumption, the decoupling limit assumes that all Higgs self-couplings are kept fixed and perturbative in size. [6] In the MSSM, such a decoupling limit arises for large m_{A^0}, and quickly becomes a very good approximation for $m_{A^0} \gtrsim 150$ GeV.

The decoupling limit can be evaded in special cases, in which the scalar potential exhibits a special form (*e.g.*, a discrete symmetry can forbid certain terms). In such models, there could exist regions of parameter space in which all but one Higgs boson are significantly heavier than the Z, but the light scalar state does *not* possess SM-like properties [65]. A complete exposition regarding the decoupling limit in the 2HDM, and special cases that evade the limit can be found in [66].

7.2 Constraints from precision electroweak data and LC implications

In the minimal SM, precision electroweak constraints require $m_{h_{\rm SM}} \lesssim 230\,\text{GeV}$ at 90% CL. This is precisely the mass region preferred in the MSSM and its extensions.

[6] In the decoupling limit, the heavier Higgs bosons may have enhanced couplings to fermions (*e.g.*, at large $\tan\beta$ in the 2HDM). We assume that these couplings also remain perturbative.

However, in the context of general doublets + singlets extensions of the Higgs sector there are many more complicated possibilities. First, it could be that there are several, or even many, Higgs bosons that couple to vector bosons and it is only their average mass weighted by the square of their VV coupling strength (relative to the SM strength) that must obey this limit. Second, there can be weak isospin violations either within the Higgs sector itself or involving extra dynamics (for example related to the composite Higgs approach) that can compensate for the excessive deviations predicted if there is a SM-like Higgs with mass substantially above $\sim 230\,\mathrm{GeV}$.

A particularly simple example of this latter situation arises in the context of the 2HDM [65]. Consider a 2HDM in which one of the CP-even neutral Higgs bosons has SM-like couplings but has mass just above a particular presumed value of $\sqrt{s}$ (500 or 800 GeV) for the linear collider. In addition, focus on cases in which there is a lighter A^0 or h^0 with no VV coupling (for either, we use the notation $\widehat{h}$) and in which all other Higgs bosons have mass larger than $\sqrt{s}$. Next, isolate mass and $\tan\beta$ choices for which detection of the $\widehat{h}$ will also be impossible at the LC. Finally, scan over masses of the heavy Higgs bosons so as to achieve the smallest precision electroweak $\Delta\chi^2$ relative to that found in the minimal SM for $m_{h_{\rm SM}} = 115\,\mathrm{GeV}$. The blobs of overlapping points in Fig. 3.15 indicate the S, T values for the optimal choices and lie well within the current 90% CL ellipse. The heavy Higgs boson with SM couplings gives a large positive contribution to S and large negative contribution to T, and in the absence of the other Higgs bosons would give the S, T location indicated by the star. However, there is an additional positive contribution to T arising from a slight mass non-degeneracy among the heavier Higgs bosons. For instance, for the case of a light $\widehat{h} = A^0$, the h^0 is heavy and SM-like and

$$\Delta\rho \equiv \alpha\Delta T = \frac{\alpha}{16\pi m_W^2 c_W^2}\left\{\frac{c_W^2}{s_W^2}\frac{m_{H^\pm}^2 - m_H^2}{2} - 3m_W^2\left[\log\frac{m_h^2}{m_W^2} + \frac{1}{6} + \frac{1}{s_W^2}\log\frac{m_W^2}{m_Z^2}\right]\right\} \tag{3.10}$$

can be adjusted to place the S, T prediction at the location of the blob in Fig. 3.15 by an appropriate choice of $m_{H^\pm}^2 - m_{H^0}^2$. Indeed, even if the "light" decoupled Higgs boson is not so light, but rather has mass equal to $\sqrt{s}$ (and is therefore unobservable), one can still obtain entirely adequate agreement with current precision electroweak data. Fortunately, one can only push this scenario so far. To avoid moving beyond the current 90% ellipse (and also to maintain perturbativity for the Higgs self-couplings), the Higgs with SM-like VV coupling must have mass $\lesssim 1\,\mathrm{TeV}$.

In composite Higgs models with extra fermions, there are similar non-degeneracies of the fermions that can yield a similar positive contribution to $\Delta\rho$ and thence T. As reviewed in [13], consistency with current precision electroweak data inevitably constrains parameters so that some type of new physics (including a possible heavy scalar sector) would again have to lie below a TeV or so. Future Giga-Z data could provide much stronger constraints on these types of models, as discussed in Section 9.

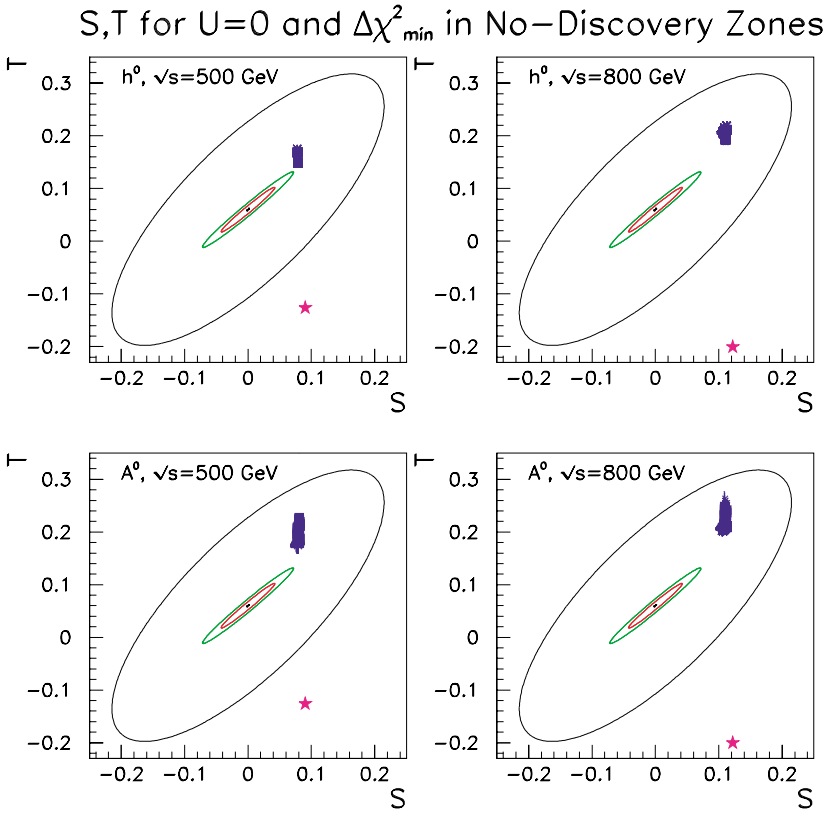

Figure 3.15: The outer ellipse gives the current 90% CL region for $U = 0$ and SM Higgs mass of 115 GeV. The blobs show the S, T predictions for the 2HDM models described in the text that have minimum $\Delta\chi^2$ relative to this SM benchmark and for which no Higgs boson of the 2HDM will be detected at the LC. The innermost (middle) ellipse gives the 90% (99.9%) CL region for $m_{h_{\rm SM}} = 115\,\text{GeV}$ obtained after Giga-Z precision measurements and a $\Delta m_W \lesssim 6$ MeV threshold scan measurement of m_W. The stars indicate the minimal SM S, T prediction if $m_{h_{\rm SM}} = \sqrt{s}$.

7.3 Constraints on Higgs bosons with VV coupling

In the MSSM, we know that the Higgs boson(s) that carry the VV coupling must be light: if m_{A^0} is large (the decoupling limit) then it is the mass-bounded h^0 that has all the VV coupling strength; if $m_{A^0} \lesssim 2m_Z$, then the H^0 can share the VV coupling with the h^0, but then m_{H^0} cannot be larger than about $2m_Z$. In the NMSSM, assuming Higgs-sector CP conservation, there are 3 neutral CP-even Higgs bosons, $h_{1,2,3}$ ($m_1 < m_2 < m_3$), which can share the VV coupling strength. One can show (see [67] for a recent update) that the masses of the h_i with substantial

VV coupling are strongly bounded from above. This result generalizes to the most general supersymmetric Higgs sector as follows. Labeling the neutral Higgs bosons by i with masses m_{h_i} and denoting the ZZ squared-coupling relative to the SM by K_i, it can be shown that

$$\sum_i K_i \geq 1\,, \quad \sum_i K_i m_{h_i}^2 \leq (200\,\mathrm{GeV})^2\,. \tag{3.11}$$

That is, the aggregate strength of the VV coupling-squared of all the neutral Higgs bosons is at least that of the SM, and the masses-squared of the neutral h_i weighted by the coupling-squared must lie below a certain bound. The upper bound of $(200\,\mathrm{GeV})^2$ in Eq. (3.11) is obtained [41] by assuming that the MSSM remains perturbative up to the the GUT scale of order 10^{19} GeV. This bound applies for the most general possible Higgs representations (including triplets) in the supersymmetric Higgs sector and for arbitrary numbers of representations. If only doublet and singlet representations are allowed for, the bound would be lower. The $(200\,\mathrm{GeV})^2$ bound also applies to general Higgs-sector-only extensions of the SM by requiring consistency with precision electroweak constraints *and* assuming the absence of a large contribution to T from the Higgs sector itself or from new physics, such as discussed in Section 7.2.

7.4 Detection of non-exotic extended Higgs sector scalars at the Tevatron and LHC

In the case of extended Higgs sectors, all of the same processes as discussed for the SM and MSSM will again be relevant. However, we can no longer guarantee Higgs discovery at the Tevatron and/or LHC. In particular, if there are many Higgs bosons sharing the WW, ZZ coupling, Higgs boson discovery based on processes that rely on the VV coupling could be much more difficult than in models with just a few light Higgs bosons with substantial VV coupling. This is true even if the sum rule of Eq. (3.11) applies. For example, at the LHC even the NMSSM addition of a single singlet to the minimal two-doublet structure in the perturbative supersymmetric context allows for parameter choices such that no Higgs boson can be discovered [68] using any of the processes considered for SM Higgs and MSSM Higgs detection. The $\gamma\gamma$ decay channel signals are all weak (because of decreased W-loop contribution to the coupling). Further, if a moderate value of $\tan\beta$ is chosen then $t\overline{t}$+Higgs processes are small and $b\overline{b}$+Higgs processes are insufficiently enhanced. In short, the equivalent to the wedge of Fig. 3.14 enlarges. The h^0 signal is divided among the three light neutral CP-even Higgs bosons and diluted to too low a statistical significance.

However, in other cases, the Tevatron and LHC could observe signals not expected in an approximate decoupling limit. For example, in the 2HDM model discussed earlier the light $\widehat{h}$ with no VV couplings decays via $\widehat{h} \to b\overline{b}, \tau^+\tau^-$ and discovery in $t\overline{t}\widehat{h}$, $b\overline{b}\widehat{h}$ and even $gg \to \widehat{h}$ [69] is possible, though certainly not guaranteed. Further, in these models there is a heavy neutral Higgs boson having the bulk of the VV

coupling and (for consistency with current precision electroweak constraints or with perturbativity) mass $\lesssim 1\,\text{TeV}$. This latter Higgs boson would be detected at the LHC using gg, WW fusion production and $ZZ \to 4\ell, WW \to 2j\ell\nu, \ldots$ decay modes, just like a heavy minimal SM Higgs boson.

7.5 LC production mechanisms for non-exotic extended Higgs sector scalars

Any physical Higgs eigenstate with substantial WW and ZZ coupling will be produced in Higgsstrahlung and WW fusion at the LC. Although there could be considerable cross section dilution and/or resonance peak overlap, the LC will nonetheless always detect a signal. This has been discussed for the MSSM in Section 5.4. In the NMSSM, if one of the heavier CP-even h_i has most of the VV coupling, the strong bound on its mass [67] noted earlier implies that it will be detected at any LC with $\sqrt{s} > 350\,\text{GeV}$ within a small fraction of a year when running at planned luminosities. The worst possible case is that in which there are many Higgs bosons with VV coupling with masses spread out over a large interval with separation smaller than the mass resolution. In this case, the Higgs signal becomes a kind of continuum distribution. Still, in [70] it is shown that the sum rule of Eq. (3.11) guarantees that the Higgs continuum signal will still be detectable for sufficient integrated luminosity, $L \gtrsim 200\ \text{fb}^{-1}$, as a broad excess in the recoil mass spectrum of the $e^+e^- \to ZX$ process. (In this case, WW fusion events do *not* allow for the reconstruction of Higgs events independently of the final state Higgs decay channel.) As already noted, the value of 200 GeV appearing in Eq. (3.11) can be derived from perturbative RGE constraints for the most general Higgs sector in supersymmetric theories and is also required by precision electroweak data for general SM Higgs sector extensions, at least in theories that do not have a large positive contribution to T from a non-decoupling structure in the Higgs sector or from new physics not associated with the Higgs sector.

Other production modes of relevance include Higgs pair production, $t\bar{t}$+Higgs, and $b\bar{b}$+Higgs. In multi-doublet models, $t\bar{b}H^-$ and $b\bar{t}H^+$ reactions are present. However, none of these are guaranteed to be either kinematically accessible or, if accessible, to have a sufficiently high event rate to be observed.

Regardless of the production process, relevant decay channels could include cases where heavier Higgs bosons decay to lighter ones. If observed, such decays would provide vital information regarding Higgs self-couplings.

We should particularly consider what production processes are most relevant for those Higgs bosons (denoted $\widehat{h}$) that do not have substantial VV coupling. Such processes have particular relevance in the non-decoupling scenario for the general 2HDM model discussed earlier. There, such a $\widehat{h}$ is the only Higgs boson light enough to be produced at an LC with $\sqrt{s} \lesssim 1\,\text{TeV}$ and it cannot be produced and detected in WW fusion or Higgsstrahlung. Since the other Higgs bosons are heavy, the $\widehat{h}$ also

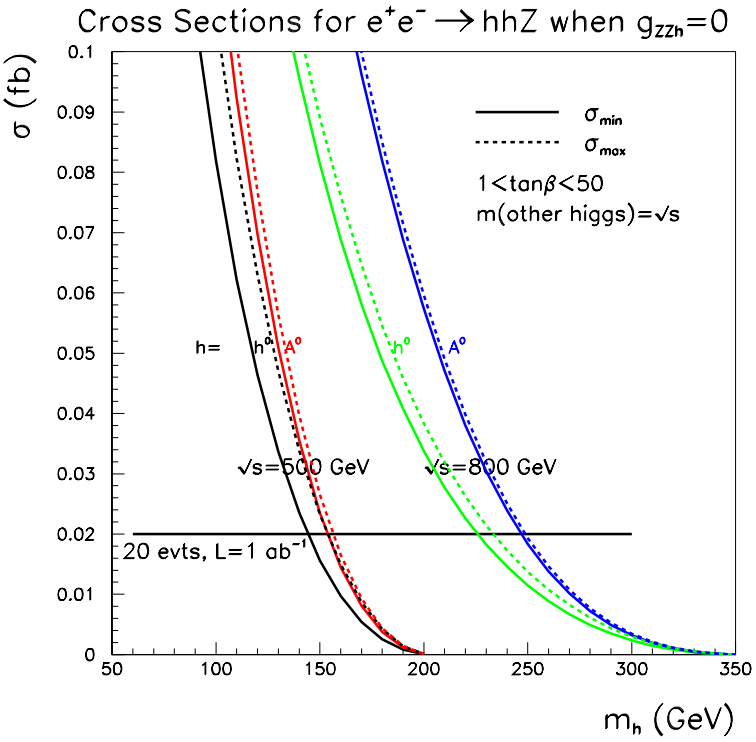

Figure 3.16: For $\sqrt{s} = 500\,\text{GeV}$ and $800\,\text{GeV}$ and for $\widehat{h} = h^0$ and $\widehat{h} = A^0$, we plot as a function of $m_{\widehat{h}}$ the maximum and minimum values of $\sigma(e^+e^- \to \widehat{h}\widehat{h}Z)$ found after scanning $1 < \tan\beta < 50$ taking all other higgs masses equal to $\sqrt{s}$. For $\widehat{h} = h^0$, we require $\sin(\beta-\alpha) = 0$ during the scan. The 20 event level for $L = 1000\ \text{fb}^{-1}$ is indicated.

cannot be produced in association with another Higgs boson. As shown in [71,65], the $b\overline{b}\widehat{h}$ and $t\overline{t}\widehat{h}$ processes will also not be detectable at the LC if $\tan\beta$ is moderate in value. The most interesting tree-level processes are then those based on the quartic couplings $WW\widehat{h}\widehat{h}$ and $ZZ\widehat{h}\widehat{h}$ required by gauge invariance [72,73]. These couplings allow for $WW \to \widehat{h}\widehat{h}$ fusion and $Z^* \to Z\widehat{h}\widehat{h}$ production, respectively. The exact cross sections for these processes are only mildly sensitive to the masses of the other heavier Higgs bosons via 2HDM Higgs self-couplings. Of course, phase space restrictions imply an upper limit on the $\widehat{h}$ masses that can be probed in this way. Cross sections in the case of $Z^* \to Z\widehat{h}\widehat{h}$ are plotted in Fig. 3.16 for both $\widehat{h} = A^0$ and $\widehat{h} = h^0$ taking $\sqrt{s} = 500$ [74]. Assuming optimistically that 20 events in $L = 1000\ \text{fb}^{-1}$ could be detected, $Z^* \to Z\widehat{h}\widehat{h}$ could be detected for $m_{\widehat{h}}$ as large as $150\,\text{GeV}$. At $\sqrt{s} = 800\,\text{GeV}$, this limit increases to $250\,\text{GeV}$. Similar results are obtained for $WW \to \widehat{h}\widehat{h}$ fusion production.

8 Measurements of Higgs boson properties at the LC

The strength of the LC physics program is that it cannot only observe one or more Higgs boson(s), but also precisely determine the Higgs boson mass, width, couplings, and quantum numbers, and parameters of the Higgs potential. These measurements are crucial to establish the nature of the Higgs and thus to illuminate the mechanism of electroweak symmetry breaking. Measurements of the Higgs couplings can demonstrate that a Higgs boson generates the masses of vector bosons, charged leptons, and up- and down-type quarks. If the measured couplings are not simply proportional to mass, this will require a Higgs sector more complex than a single complex Higgs doublet. Accurate measurements are needed to distinguish the SM Higgs and h^0 of the MSSM near the decoupling limit. Couplings are determined through measurements of Higgs branching ratios and cross sections. Higgs bosons are also expected to couple to themselves, and this self-coupling λ can only be explored through the direct production of two or more Higgs bosons. The measurement of *direct* and *model independent* absolute Higgs couplings is a major cornerstone of the LC program.

Details of some of the studies of Higgs coupling measurements can be found in [75]. A comprehensive description of European studies using the simulated TESLA detector can be found in [76]. North American studies consider simulations of detectors with capabilities described in Chapter 15. The program of measurements of Higgs boson properties strongly impacts detector design. Measurement of branching ratios into fermions requires sophisticated vertex detectors to separate b from c (and gluon) jets. Precise recoil mass measurements need excellent momentum resolution (particularly for $\mu^+\mu^-$) from charged particle tracking. The performance of the combined tracking and calorimetry systems needs to result in precise jet-jet invariant masses, missing mass measurements, and the ability to separate hadronic W from hadronic Z decays.

The specific measurements used to determine the Higgs couplings to vector bosons, fermions and scalars are significantly different depending on the mass of the Higgs boson. A generic neutral CP-even Higgs boson will be denoted by h in this section. We treat three cases separately: a light Higgs boson ($m_h < 2m_W$), an intermediate mass Higgs boson ($2m_W \leq m_h < 2m_t$), and a heavy Higgs boson ($m_h \geq 2m_t$).

8.1 Mass

In the Standard Model, the Higgs mass determines all its other properties. Thus, the precision of the mass measurement affects the comparison of theory and experiment, for example, in a global fit of cross sections, branching ratios, and precision electroweak data. Similarly, in the MSSM or other models with extended Higgs sectors, the masses of all the Higgs bosons are an important input in determining the underlying model parameters.

For this fundamental mass measurement, a LC can reconstruct the system recoiling against a Z (independent of Higgs decay). Full event reconstruction, plus

kinematic constraints, can improve resolution and clean up mass tails. For a light or intermediate mass Higgs boson, the optimal running conditions would have a smaller center-of-mass energy such as $\sqrt{s} = 350$ GeV, to allow better momentum resolution and to minimize the beamstrahlung. Under such conditions, one can precisely measure the recoil mass in $e^+e^- \to Zh$ events opposite to the reconstructed leptonic decay $Z \to e^+e^-$ or $\mu^+\mu^-$. This measurement is independent of the Higgs decay mode. Accuracy can be improved by reconstructing specific decay modes, leading, for example, to a four-jet topology where effective (5-C) kinematic constrained fits can be employed.

Figure 3.17 shows the distribution of the recoil mass,

$$M_{\text{recoil}} = \sqrt{s - 2\sqrt{s} \cdot E_{\ell^+\ell^-} + M^2_{\ell^+\ell^-}}\,, \tag{3.12}$$

in a simulation of the L linear collider detector [77] described in Chapter 15 for Higgs masses between 115 and 160 GeV [78]. Using Monte Carlo shape templates and an integrated luminosity of 500 fb^{-1}, precisions of $\Delta m_{h_{\text{SM}}} \simeq 80$ MeV at $\sqrt{s} = 350$ GeV and $\Delta m_{h_{\text{SM}}} \simeq 140$ MeV at $\sqrt{s} = 500$ GeV have been estimated for either the e^+e^- or $\mu^+\mu^-$ mode.

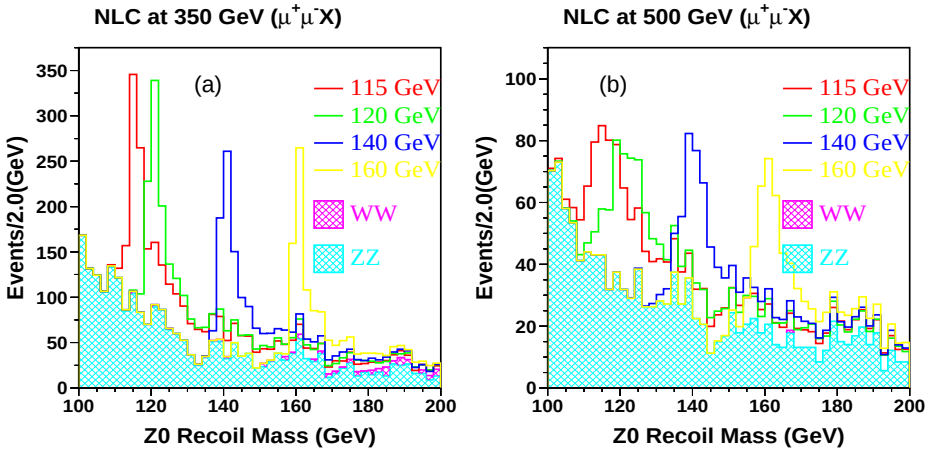

Figure 3.17: Recoil mass from a pair of leptons for different Higgs masses at (a) $\sqrt{s} =$ 350 GeV and (b) 500 GeV simulated in the L detector described in Chapter 15.

Realistic simulations have also been made with the L detector for the process $Zh \to q\bar{q}h$ resulting in four jets. Figure 3.18(a) shows the jet-jet invariant mass distribution for pairs of jets for Higgs with $m_{h_{\text{SM}}} = 115$ GeV recoiling against a Z reconstructed from its hadronic decay mode [79]. A clean Higgs signal with a mass resolution of approximately 2 GeV is observed. The central Higgs mass is shifted down by the loss of low-energy charged and neutral particles in the simulated event

reconstruction. A low-mass tail of the Higgs signal arises from missing neutrinos in semi-leptonic b and c quark decays. Using neural net tags and full kinematic fitting [80], the mass peak shown in Fig. 3.18(b) is obtained for $m_{h_{\rm SM}} = 120$ GeV, $\sqrt{s} = 500$ GeV, and 500 fb^{-1} resulting in $\Delta m_{h_{\rm SM}} \simeq 50$ MeV. If a second lower-energy IR is available, it might be attractive to perform a scan across the Zh threshold. With a total integrated luminosity of 100 fb^{-1}, $\Delta m_{h_{\rm SM}} \simeq 100$ MeV at $m_{h_{\rm SM}} = 150$ GeV is achievable [81], competitive with the methods above.

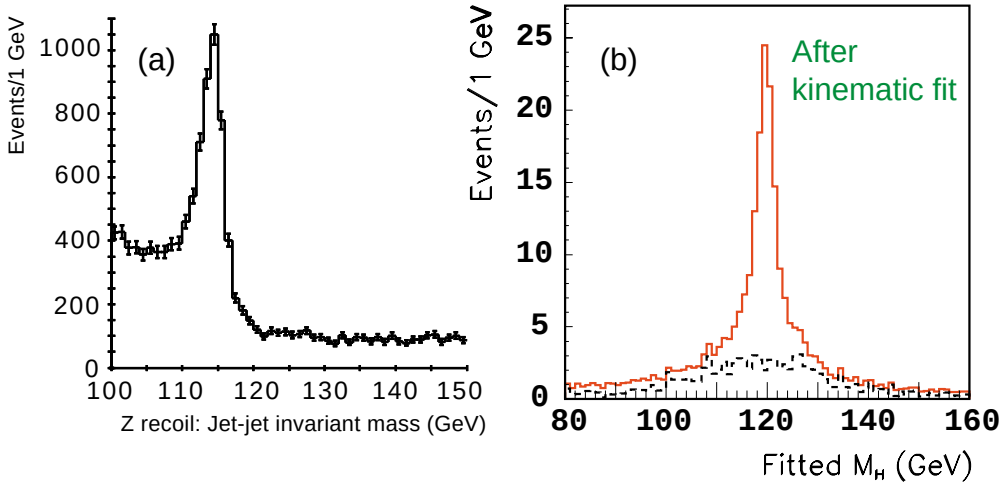

Figure 3.18: (a) Jet-jet invariant mass of the jets recoiling from a Z reconstructed hadronically simulated in the LCD Large detector, $m_{h_{\rm SM}} = 115$ GeV. (b) Direct reconstruction of the four-jet $q\overline{q}h_{\rm SM}$ state simulated in the L detector after fitting with full kinematic constraints, $m_{h_{\rm SM}} = 120$ GeV.

Further work is necessary to confirm analogous precisions for heavier Higgs bosons and MSSM Higgs bosons with different decay modes and possible close mass-degeneracies. The number of Zh events with $Z \to \ell^+\ell^-$ for an intermediate-mass ($m_h > 2m_W$) or heavy Higgs ($m_h > 2m_t$) with SM coupling falls quickly [82]. In this case, and for the decays $h \to ZZ$, hadronic decays of the Z would have to be considered to gain sufficient statistics. For the heavier MSSM Higgs boson states, European studies [83] have shown typical mass precisions of $\Delta m_{H^\pm}$ and $\Delta m_{A^0,H^0}$ of around 1 GeV for 500 fb^{-1}, but at $\sqrt{s} = 800$ GeV. The MSSM H^0 and A may be studied separately using $\gamma\gamma \to H/A$ with different states of γ linear polarization, thus helping to refine mass determinations in the nearly degenerate case.

8.2 Coupling determinations—light Higgs bosons

8.2.1 Cross sections

For Higgs masses below $2m_W$, the couplings g_{hZZ} and g_{hWW} are best measured through measurements of the Higgsstrahlung and WW fusion cross sections, respectively. These cross sections are also critical in the extraction of branching ratios since the experimental measurement will be a product of cross section and branching ratio.

Measurement of the cross section $\sigma(Z^* \to Zh)$ is best addressed via the recoil mass method outlined above [78]. Again, in this case, to reduce the contribution from the WW fusion process, it may be preferrable to run at a lower energy, *i.e.*, $\sqrt{s} =$ 350 GeV, and to examine recoil against $\mu^+\mu^-$ to avoid large Bhabha backgrounds. The study with the L detector described above finds $\Delta\sigma/\sigma \simeq 4\%$ at $\sqrt{s} = 350$ GeV and $\simeq$6.5% at 500 GeV with 500 fb^{-1} as shown in Fig. 3.19(a). These agree roughly with estimates from European studies [84].

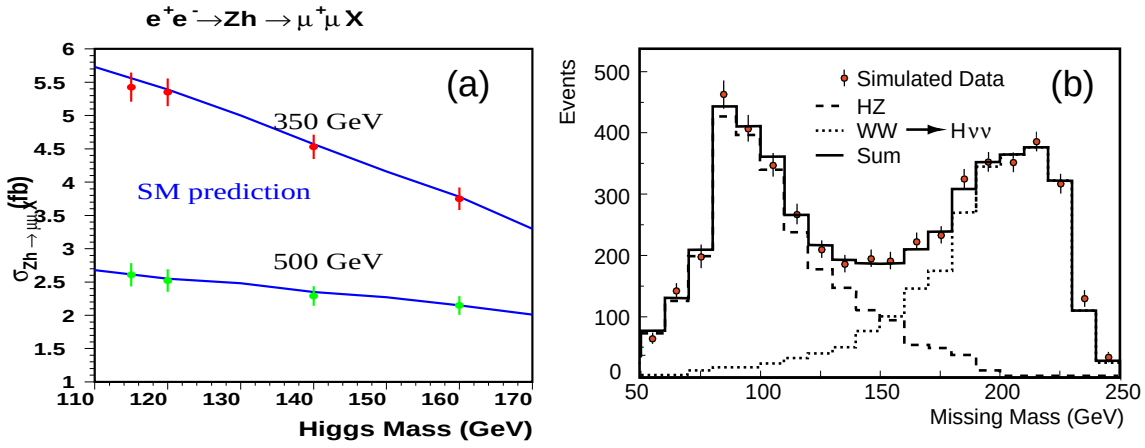

Figure 3.19: (a) Cross section measurement for 500 fb^{-1} and (b) separation of Higgsstrahlung and WW fusion ($\sqrt{s} = 350$ GeV) through a fit (after background subtraction), both simulated in the L detector.

With efficient and pure b-jet tagging, events due to $e^+e^- \to W^+W^-\nu\overline{\nu} \to \nu\overline{\nu}h \to \nu\overline{\nu}b\overline{b}$ can be separated from those due to Higgsstrahlung, $Zh \to \nu\overline{\nu}h \to \nu\overline{\nu}b\overline{b}$ by examining the missing mass distribution and fitting to the expected shapes of a peak at m_Z from Higgsstrahlung and the higher missing masses from WW fusion. This technique has been confirmed with simulations of the L detector as shown in Fig. 3.19(b) [85]. With 500 fb^{-1} and a precision BR($h_{\rm SM} \to b\overline{b}$) $\simeq 3\%$ (see below), the fusion-process cross section with this analysis can be found with a precision $\Delta\sigma/\sigma =$ 3.5% for $m_{h_{\rm SM}} = 120$ GeV.

	$m_{h_{\rm SM}} = 120$ GeV		$m_{h_{\rm SM}} = 140$ GeV	
	BR	δBR/BR	BR	δBR/BR
$h_{\rm SM} \to b\overline{b}$	$(69 \pm 2.0)\%$	2.9%	$(34 \pm 1.3)\%$	4.1%
$h_{\rm SM} \to WW^*$	$(14 \pm 1.3)\%$	9.3%	$(51 \pm 1.8)\%$	3.7%
$h_{\rm SM} \to c\overline{c}$	$(2.8 \pm 1.1)\%$	39%	$(1.4 \pm 0.64)\%$	45%
$h_{\rm SM} \to gg$	$(5.2 \pm 0.93)\%$	18%	$(3.5 \pm 0.79)\%$	23%
$h_{\rm SM} \to \tau^+\tau^-$	$(7.1 \pm 0.56)\%$	7.9%	$(3.6 \pm 0.38)\%$	10%

Table 3.1: Predicted branching ratio precisions in the L detector and typical vertex detector configuration for 500 fb^{-1} and $\sqrt{s} = 500$ GeV.

8.2.2 Branching ratios

A key advantage of the linear collider in Higgs studies is the identification of Higgsstrahlung Zh events through the tag of the Z decays. This selection is essentially independent of the decay mode of the h and simplifies the measurement of Higgs boson branching ratios.

Small beam sizes, the possibility of a first track measurement as close as 1 cm from the beam axis, and sophisticated pixel vertex detectors allow for efficient and clean separation of quark flavors. Separate tagging of b, c and g jets is possible.

In a study [86] of vertexing using a CCD vertex detector in a standard LC detector configuration (C1 in [87]), topological vertexing [88] with neural net selection was used for flavor (or anti-flavor, *i.e.*, WW^*) tagging. The separation of $b\overline{b}$ and $c\overline{c}$ events by this method is illustrated in Fig. 3.20(a). Assuming 500 fb^{-1} and 80% polarization, the results shown in Table 3.1 were obtained.

These results scale approximately as $(\sigma \int \mathcal{L}dt)^{-1/2}$ when taken together with other studies [89–91], but the results of [91] (shown in Fig. 3.20(b)) are noticeably more precise for the $c\overline{c}$ and gg modes. These branching ratio measurements can then be used to either distinguish a SM Higgs boson from an MSSM Higgs boson, or to probe higher-mass states and extract MSSM parameters such as m_{A^0} even if the CP-odd A^0 is not accessible. That analysis is described in more detail below.

An accessible decay mode for lighter Higgs bosons is $h \to \gamma\gamma$, which requires excellent electromagnetic calorimetry. As shown in Fig. 3.21, for a SM Higgs boson in a typical LC detector, this is a difficult measurement requiring a large luminosity, which is best optimized for masses around 120 GeV [92]. A higher-luminosity study [93] with 1000 fb^{-1} and $m_{h_{\rm SM}} = 120$ GeV for the TESLA detector finds δBR/BR = 14%. A $\gamma\gamma$ collider, discussed in Section 10, would be a more powerful tool for determining the Higgs coupling to photons.

For light Higgs bosons, the coupling to top quarks is still accessible via the radiative process $t\overline{t}h$ described below, or indirectly through BR($h \to gg$).

A set of difficult decay channels for the LHC is invisible decays of the Higgs boson

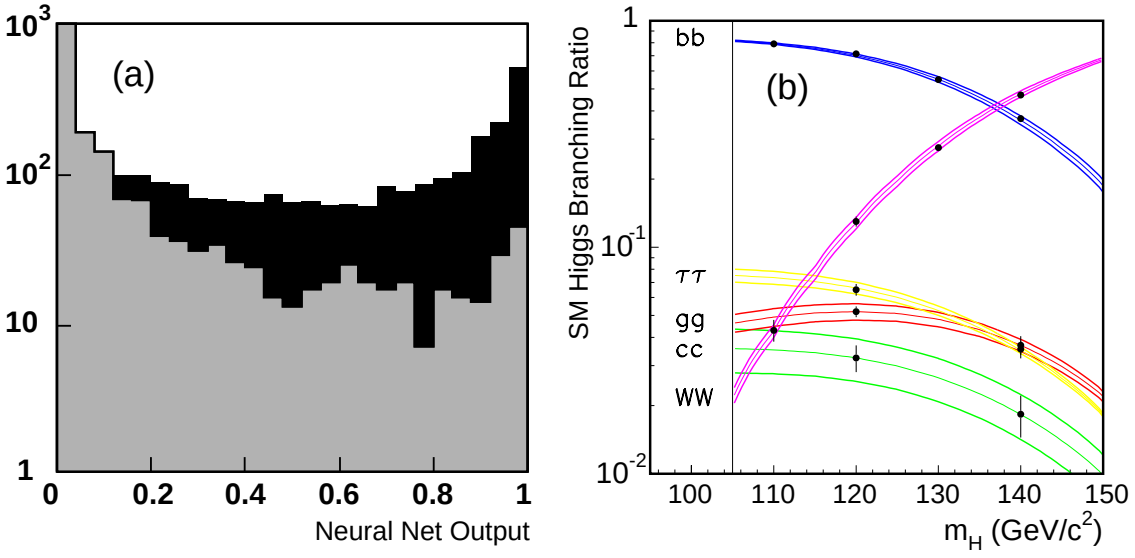

Figure 3.20: (a) For the simulated L detector with CCD vertex detector, neural net $h_{\rm SM} \to c\overline{c}$ output for $h_{\rm SM} \to c\overline{c}$ events (dark) compared to output for $h_{\rm SM} \to b\overline{b}$ events (gray). (b) Variation of branching ratios with SM Higgs mass (bands are 1σ uncertainties on the theoretical predictions) and measurement precisions in the TESLA detector (points with error bars).

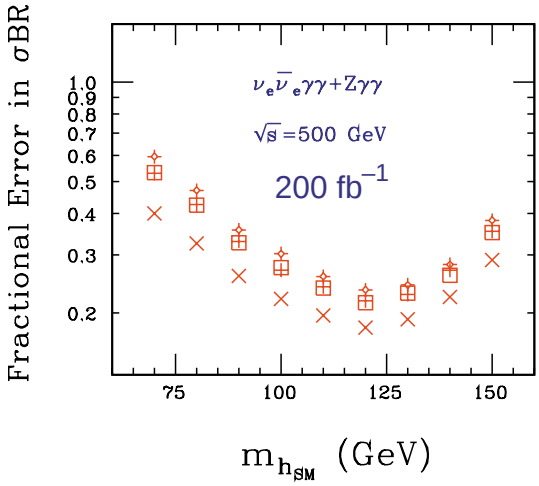

Figure 3.21: Fractional error on the branching ratio BR($h_{\rm SM} \to \gamma\gamma$). The open squares are for a typical LC detector electromagnetic energy resolution of $\Delta E/E = 10\%/\sqrt{E} \oplus 1.0\%$.

into, *e.g.*, neutralinos, majorans or heavy neutrinos. The LC can close this loophole and measure the branching ratio easily, even for branching ratios as small as 5% for a relatively narrow Higgs state, by using the recoil mass method and demanding no detector activity opposite the Z, or by comparing the number of events tagged with $Z \to \ell^+\ell^-$ with the total number of observed Higgs decays into known states.

8.2.3 Radiative production and $t\bar{t}h$ coupling

For a light Higgs boson, production through radiation off a top quark is feasible, resulting in a final state of $t\bar{t}h$. This allows a determination of the Yukawa top quark coupling g_{htt} [23,24]. For a SM-like Higgs boson with $m_h = 120$ GeV, the $t\bar{t}h$ cross section is roughly 10 times larger at $\sqrt{s} = 700$–800 GeV than at 500 GeV. At $\sqrt{s} =$ 800 GeV, a statistical error of $\delta g_{htt}/g_{htt} \sim 5\%$ was estimated [94] for $L = 500$ fb^{-1} on the basis of an optimal observable analysis. At $\sqrt{s} = 500$ GeV, a statistical error of $\delta g_{htt}/g_{htt} \simeq 21\%$ is estimated [95] using 1000 fb^{-1}. A more sophisticated analysis using neural net selections, full simulation, and the same integrated luminosity at $\sqrt{s} = 800$ GeV finds a total error of 6% on the coupling [96]. More details on this process can be found in Chapter 6, Section 3.1.

8.2.4 Higgs self-coupling

To delineate the Higgs sector fully, it is essential to measure the shape of the Higgs potential. The cross section for double Higgs production (*e.g.*, Zhh) is related to the triple Higgs coupling g_{hhh}, which in turn is related to the spontaneous symmetry breaking shape of the Higgs potential. The Higgs mass, $m_h^2 = 4\lambda v^2$, also measures the potential shape parameter λ, so independent determinations through hh production give a cross-check. In the MSSM, a variety of double Higgs production processes would be required to determine $g_{h^0h^0h^0}$, $g_{A^0h^0h^0}$, *etc.* [73].

These cross sections are low, and high integrated luminosity is needed, bolstered by polarization and neural net selections. Experimental studies [97,98] indicate that for a SM-like Higgs boson with $m_h = 120$ GeV at $\sqrt{s} = 500$ GeV and 1000 fb^{-1}, a precision of $\delta g_{hhh}/g_{hhh} = 23\%$ is possible. Regions of accessibility in MSSM parameters for MSSM Higgs self-couplings have also been determined [99,100].

The cross section for SM triple Higgs production is very low, $\sigma(Zhh) < 10^{-3}$ fb, so measurement of the quartic coupling g_{hhhh} is hopeless with currently envisioned luminosities.

8.2.5 Implications for the MSSM Higgs sector

The discussion of light Higgs coupling determinations has been based on the assumption that the actual Higgs couplings to fermions, vector bosons and scalars are close

to the corresponding Standard Model expectations. In Section 7.1, it was argued that such an expectation is rather generic, and applies to the decoupling limit of models of Higgs physics beyond the Standard Model. In particular, the decoupling limit of the MSSM Higgs sector sets in rather rapidly once $m_{A^0} \gtrsim 150$ GeV [see Section 5.1]. Since $m_{h^0} \lesssim 135$ GeV in the MSSM [Eq. (3.8)], the precision study of h^0 using the techniques discussed above can distinguish between h^0 and $h_{\rm SM}$ with a significance that depends on how close the model is to the decoupling limit. Said another way, the detection of deviations in the Higgs couplings from their Standard Model predictions would yield evidence for the existence of the non-minimal Higgs sector, and in the context of the MSSM would provide constraints on the value of m_{A^0} (with some dependence on $\tan\beta$ and other MSSM parameters that enter in the Higgs radiative corrections).

In [101], the potential impact of precision Higgs measurements at the LC on distinguishing h^0 from $h_{\rm SM}$ was examined. The fractional deviation of the h^0 branching ratios into a given final state from the corresponding result for $h_{\rm SM}$ (assuming the same Higgs mass in both cases) is defined as:

$$\delta{\rm BR} = \frac{{\rm BR}_{\rm MSSM} - {\rm BR}_{\rm SM}}{{\rm BR}_{\rm SM}}. \tag{3.13}$$

For the MSSM Higgs boson decay, both m_{h^0} and the corresponding branching ratios were computed including the radiative corrections due to the virtual exchange of Standard Model and supersymmetric particles, as described in Section 5.2. Thus, the h^0 branching ratios depend on m_{A^0} and $\tan\beta$ (which fix the tree-level MSSM Higgs sector properties) and a variety of MSSM parameters that govern the loop corrections. Four scenarios were considered: the minimal and maximal top-squark mixing cases [see Eq. (3.8) and surrounding text], and two additional cases with large $|\mu| = |A_t|$ (for $\mu A_t < 0$ and two possible sign choices of μ), where μ and A_t control the top-squark mixing. In the latter two scenarios, significant renormalization of the CP-even Higgs mixing angle α and Δ_b [see Eq. (3.9)] can arise.

In Fig. 3.22, contours of δBR are plotted for three h^0 decay modes: $b\overline{b}$, WW^* and gg. The contours shown correspond roughly to the 1σ and 2σ measurements claimed by [91], rescaled for the LC at $\sqrt{s} = 500$ GeV (see also the $b\overline{b}$ and WW^* branching ratio precisions given in Table 3.1). In the minimal and maximal scenarios, the dependence on m_{A^0} is nearly independent of $\tan\beta$, and demonstrates that one can achieve sensitivity to values of m_{A^0} that lie significantly beyond $\sqrt{s}/2$ where direct production at the LC via $e^+e^- \to H^0A^0$ is kinematically forbidden. However, the cases with large $|\mu| = |A_t|$ exhibit the possibility of "premature" decoupling, that is, relatively low values of m_{A^0} (at a particular large value of $\tan\beta$) at which the properties of h^0 and $h_{\rm SM}$ cannot be distinguished by the decay modes considered above.[7] Thus, a measured deviation of Higgs branching ratios that distinguishes h^0

[7]The premature decoupling is a consequence of the renormalization of the mixing angle α which

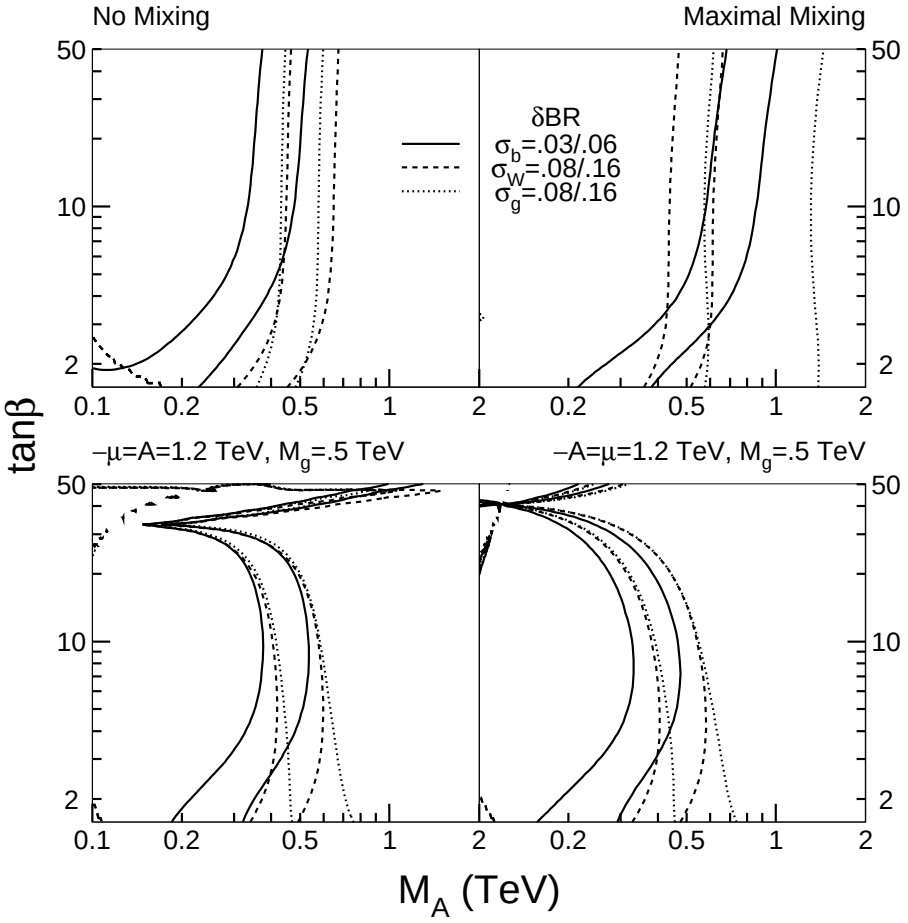

Figure 3.22: Contours of $\delta\mathrm{BR}(b\overline{b}) = 3$ and 6% (solid), $\delta\mathrm{BR}(WW^*) = 8$ and 16% (dashed) and $\delta\mathrm{BR}(gg) = 8$ and 16% (dotted) [BR deviations defined in Eq. (3.13)] in the no (*i.e.* minimal) mixing scenario (top left), the maximal mixing scenario (top right), and the large μ and A_t scenario with $\mu = -A_t = 1.2$ TeV (bottom left) and $\mu = -A_t = -1.2$ TeV (bottom right). Taken from [101].

from h_{SM} can place significant constraints on the heavier non-minimal Higgs states, although the resulting constraints can depend in a nontrivial way on the value of the MSSM parameters that control the Higgs radiative corrections.

8.3 Coupling determinations—intermediate mass Higgs bosons

For $m_h < 2m_W$, the measurement of branching ratios is extremely rich, yielding couplings to both many of the fermions and bosons. For larger masses, decays to $f\overline{f}$

just happens to yield $\cos(\beta-\alpha) = 0$, in which case the h^0 couplings reduce to those of h_{SM} as shown in Section 5.1.

become rarer until the threshold for decays into top is crossed. In this intermediate mass range, a LC can measure the W and Z couplings more precisely than the LHC both through Higgs production rates and via branching ratios for decays into these bosons. Whether the observed Higgs boson fully generates the W and Z mass can then be checked.

Precision electroweak measurements in the framework of the Standard Model indirectly predict [8,9] $m_{h_{\rm SM}} \lesssim$ 205–230 GeV at 95% CL, and a Higgs observed with mass much greater than this would imply new physics. At this point, measurements from a Giga-Z dataset would be particularly useful to probe this new sector.

8.3.1 Cross sections

Techniques described earlier [78,85] for cross section measurements of both the Higgsstrahlung and W-fusion processes, with subsequent Higgs decays into $b\overline{b}$, can still be used for the lower portion of the intermediate mass range, *i.e.*, $m_h \sim 160$ GeV. Even in this intermediate mass range, it is beneficial to run at the peak of the cross section at roughly $m_h + m_Z + 50$ GeV. The typical precisions that can be obtained are $\Delta\sigma(Zh_{\rm SM})/\sigma(Zh_{\rm SM}) \simeq 5\%$ and $\Delta\sigma(\nu\overline{\nu}h_{\rm SM})/\sigma(\nu\overline{\nu}h_{\rm SM}) \simeq 17\%$ for $m_{h_{\rm SM}} = 160$ GeV, at $\sqrt{s} = 350$ GeV with 500 fb^{-1}.

For heavier Higgs bosons in this mass range, cross sections for both Higgsstrahlung and W-fusion will need to be extracted from using the decay $h \to WW^*$, for example, as described in [90]. Couplings determined from $t\overline{t}h$ and Zhh production would clearly need higher $\sqrt{s}$.

8.3.2 Branching ratios

Using Higgsstrahlung events at an optimal $\sqrt{s}$, the statistical error on BR($h_{\rm SM} \to b\overline{b}$) is still only 6.5% at $m_{h_{\rm SM}} = 160$ GeV [91]. At $\sqrt{s} = 500\,\text{GeV}$, with leptonic decays of the Z only, the statistical error on this branching ratio reaches 25% at $m_{h_{\rm SM}} \simeq 165$ GeV with 250 fb^{-1} and remains below 30% for $m_{h_{\rm SM}} < 200$ GeV with 2000 fb^{-1} [82]. However, in addition to the leptonic decays of the Z, hadronic decays can also be used to tag the associated Z. Extrapolating from full LCD detector simulations, it is conservatively estimated that including the hadronic decays of the Z results in an increase in signal statistics above background by a factor of four. With these assumptions and 500 fb^{-1}, again with the optimal $\sqrt{s} \simeq 350$ GeV, the error on the $b\overline{b}$ branching ratio can then be estimated to reach 25% at $m_{h_{\rm SM}} \simeq 200$ GeV. Measurement of branching ratios to $c\overline{c}$, $\tau^+\tau^-$, gg, and $\gamma\gamma$ does not seem feasible in this mass range.

Branching ratios into vector bosons can be measured with good precision in the intermediate mass range. For $m_{h_{\rm SM}} = 160$ GeV and 500 fb^{-1}, a predicted excellent

precision of 2.1% on BR($h_{\rm SM} \to WW$), has been reported [90], with extrapolated estimated precision of better than 7% over the mass range of 150 to 200 GeV [82].

To measure BR($h \to ZZ$), it will be necessary to distinguish hadronic Z decays from hadronic W decays. This serves as an important benchmark for electromagnetic and hadronic calorimetry. With 500 fb^{-1}, and assuming that this separation allows one to identify one of the two Z's in the Higgs decays (through leptons or $b\bar{b}$) 40% of the time, the statistical uncertainty of this branching ratio would be approximately 8% for $m_{h_{\rm SM}} \simeq 210$ GeV [82], degrading to 17% for $m_{h_{\rm SM}} = 160$ GeV [76] where the branching ratio into Z's is still small.

8.4 Coupling determinations—heavy Higgs bosons

If the Higgs boson is heavy, *i.e.*, $m_h > 2m_t$, and if this Higgs boson possesses couplings close to those expected in the SM, then consistency with the precision electroweak data (which implies $m_{h_{\rm SM}} \lesssim 230$ GeV at 95% CL) would require the existence of new physics beyond the SM. A high statistics measurements at the Z peak could be useful to elucidate the non-SM effects. In addition, with high center of mass energy and large integrated luminosity, an experiment at the LC could directly observe heavy Higgs decay and make measurements of the Higgs couplings. These measurements could reveal departures from the SM Higgs properties and provide indirect evidence for the nature of the new physics, which would modify the SM Higgs couplings through loop effects.

8.4.1 Cross sections

As a specific case, for $m_h = 500$ GeV, a SM-like Higgs boson would have a width of 70 GeV and dominant decay modes into W^+W^- (55%), ZZ (25%), and $t\bar{t}$ (20%). The production cross section at $\sqrt{s} = 800$ GeV for Zh would be 6 fb, but Higgs production would be dominated by the W-fusion process, whose cross section would be 10 fb. With 1000 fb^{-1}, one would expect 400 Zh events where the Z decays to electrons or muons. With reasonable selection and acceptance cuts, a measurement of $\sigma(Zh)$ to better than 7% should be feasible.

8.4.2 Branching ratios

The LHC will have great difficulty distinguishing $h \to t\bar{t}$ decays from the huge QCD $t\bar{t}$ backgrounds. On the other hand, this mode should be observable at a LC. In the SM, the important coupling $g^2_{tth_{\rm SM}} \simeq 0.5$ can be compared to $g^2_{bbh_{\rm SM}} \simeq 4 \times 10^{-4}$. If the Higgs boson is heavier than 350 GeV, it will be possible obtain a good determination of the top-Higgs Yukawa coupling. Full simulations are needed for heavy Higgs decays into top, but with reasonable assumptions, one can expect a

statistical error of $\delta\mathrm{BR}/\mathrm{BR} \simeq 14\%$ with 500 fb^{-1} [82]. Simulations using the TESLA detector of the $W^+W^- \to h_{\mathrm{SM}} \to t\bar{t}$ process with 1000 fb^{-1} and 6-jet final states show impressive signal significance for $\sqrt{s} = 1000$ GeV and reasonably good significance at $\sqrt{s} = 800$ GeV [102]. These studies find that a relative error of better than 10% in the top quark Yukawa coupling measurement can be achieved for Higgs masses in the 350–500 GeV and 350–650 GeV ranges at $\sqrt{s} = 800$ GeV and 1000 GeV, respectively.

Assuming that detector performance allows separation of hadronic W and Z decays, and using production through W-fusion, the WW and ZZ coupling of the Higgs boson can be studied by using methods similar to those for $t\bar{t}$. This gives the estimates on $\mathrm{BR}(h_{\mathrm{SM}} \to W^+W^-)$ and $\mathrm{BR}(h_{\mathrm{SM}} \to ZZ)$ shown in Table 3.2.

8.5 Summary of couplings

The relative measurement errors for a SM Higgs at various masses are summarized in Table 3.2. As much as possible, the entries have been collected from simulations with the L detector described in Chapter 15. For uniformity, the entries have been scaled to 500 fb^{-1}, except where otherwise noted. The significant measurements of many branching ratios and couplings demonstrate the strength of the LC Higgs program.

Just as the computer program `ZFITTER` [103] is used with Z mass, widths, asymme-

Δm_h	$\simeq 140$ MeV (recoil against leptons from Z) $\simeq 50$ MeV (direct reconstruction)				
m_h (GeV)	120	140	160	200	400–500
$\sqrt{s}$ (GeV)	500				800
$\Delta\sigma(Zh)/\sigma(Zh)$	6.5%	6.5%	6%	7%	10%
$\Delta\sigma(\nu\overline{\nu}h)\mathrm{BR}(b\bar{b})/\sigma\mathrm{BR}$	3.5%	6%	17%	–	–
$\delta g_{hxx}/g_{hxx}$ (from BR's)					
$t\bar{t}$	7 – 20% †	–	–	–	10%
$b\bar{b}$	1.5%	2%	3.5%	12.5%	–
$c\bar{c}$	20%	22.5%	–	–	–
$\tau^+\tau^-$	4%	5%	–	–	–
$WW^{(*)}$	4.5%	2%	1.5%	3.5%	8.5%
$ZZ^{(*)}$	–	–	8.5%	4%	10%
gg	10%	12.5%	–	–	–
$\gamma\gamma$	7%	10%	–	–	–
g_{hhh}	23% §	–	–	–	–

Table 3.2: Summary of measurement precisions for the properties of a SM-like Higgs boson, h, and couplings for a range of Higgs boson masses for 500 fb^{-1}, unless otherwise indicated. † radiative $t\bar{t}h$ production, 1000 fb^{-1}, $\sqrt{s} = 800$ – 1000 GeV; § 1000 fb^{-1}.

tries and branching ratios to make global fits for Z couplings, a program HFITTER [104] is now available that performs a global fit taking into account correlations between measurements of Higgs boson properties. Individual couplings of the Higgs boson can then be extracted optimally, for example through the correct combination of cross section and branching ratio measurements for such couplings as g_{hWW} and g_{hZZ}. Such precision fits can be used to probe for indirect evidence of higher-mass states.

8.6 Total width

Determination that a Higgs boson total width is anomalously large would indicate new non-SM effects. For light Higgs bosons, the predicted SM width is too small to be measured directly, but a combination of branching ratios and coupling measurements allows the indirect and *model-independent* measurement of the total width through

$$\Gamma_{tot} = \Gamma(h \to X)/\mathrm{BR}(h \to X)\,. \tag{3.14}$$

For $m_{h_{\mathrm{SM}}} < 115$ GeV, the total width measurement would very likely require a $\gamma\gamma$ collider, an e^+e^- LC, and input from the LHC [2]. However, limits from LEP2 indicate $m_{h_{\mathrm{SM}}} \gtrsim 115$ GeV and therefore a significant branching ratio to WW^*. This gives the attractive prospect of a model-independent measurement of the total width using LC measurements alone.

First, measurements of $\sigma(h\nu\nu) \cdot \mathrm{BR}(h \to b\bar{b})$ and $\mathrm{BR}(h \to b\bar{b})$, through recoil Higgsstrahlung measurements, give $\Gamma(h \to WW^*)$. Then, a similar independent measurement of $\mathrm{BR}(h \to WW^*)$ gives the total width, through the relation $\Gamma_{tot} = \Gamma(h \to WW^*)/\mathrm{BR}(h \to WW^*)$. For example, from Table 3.2, even with as little as 200 fb^{-1}, Γ_{tot} can be found to approximately 10% for $m_{h_{\mathrm{SM}}} = 120$ GeV, improving to a few percent for $m_{h_{\mathrm{SM}}} = 150$ GeV. Even better precision can be attained with the introduction of some model assumptions in the value used for $\Gamma(h_{\mathrm{SM}} \to WW^*)$, *e.g.*, assuming the SU(2) relation between W and Z couplings along with $\sigma_{meas}(Zh_{\mathrm{SM}})$.

For $m_{h_{\mathrm{SM}}} \gtrsim 205$ GeV, $\Gamma_{tot}(h_{\mathrm{SM}})$ exceeds 2 GeV, and the physical width would be directly resolvable with typical LC detector resolutions. References [2,105] track these variations of precision for indirect and direct measurements for different values of $m_{h_{\mathrm{SM}}}$ and inputs from different machines. The jet-jet mass resolution assumed in [2] has been verified by full simulations [79] in the L detector with 200 fb^{-1} of data, resulting in estimated direct measurements of the total width whose accuracy reaches a minimum value of 6% in the mass range of 240–280 GeV. The indirect determination described above can also be pursued, and the combination would allow even better precision.

8.7 Quantum numbers

The spin, parity, and charge conjugation quantum numbers J^{PC} of a Higgs boson, generically denoted by ϕ in this subsection, can potentially be determined in a model-independent way. Useful ingredients include the following:

- A Higgs boson produced in $\gamma\gamma$ collisions cannot have $J = 1$ and must have positive C [106].
- The behavior of the $Z\phi$ Higgsstrahlung cross section at threshold constrains the possible values of J^{PC} of the state. If the spin of the ϕ is 2 or less, a cross section growing as β indicates a CP-even object, whereas a cross section growing as β^3 signals a CP-odd state [107], as shown in Fig. 3.23(a).

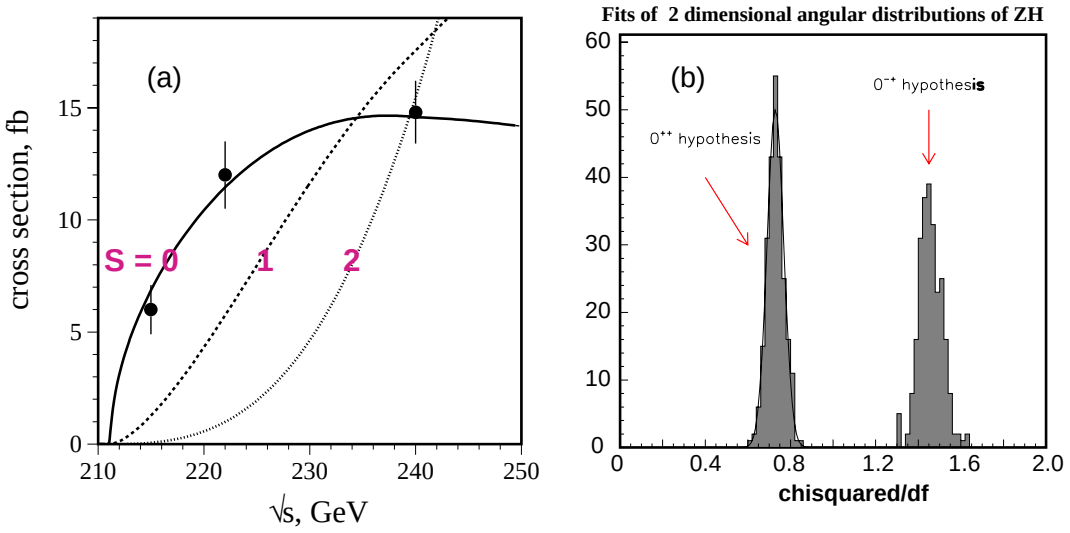

Figure 3.23: (a) Behavior of Higgsstrahlung threshold for various spin states along with typical measurement precisions on the cross section. (b) Fit to the double-differential angular distribution in $Z\phi$ events (see text) to distinguish CP-even and CP-odd states.

- The angular dependence of the $e^+e^- \to Z\phi$ cross section depends upon whether the ϕ is CP-even, CP-odd, or a mixture [107–110]. Following [110] we parameterize the $ZZ\phi$ vertex as

$$\Gamma_{\mu\nu}(k_1, k_2) = a g_{\mu\nu} + b\frac{k_{1\mu}k_{2\nu} - g_{\mu\nu}k_1 \cdot k_2}{m_Z^2} + \tilde{b}\frac{\epsilon_{\mu\nu\alpha\beta}k_1^\alpha k_2^\beta}{m_Z^2}\,, \tag{3.15}$$

where k_1 and k_2 are the momenta of the two Zs. The first term arises from a Standard-Model-like $ZZ\phi$ coupling, and the last two from effective interactions that could be induced by high-mass virtual particles. With this vertex the Higgsstrahlung cross section becomes

$$\frac{d\sigma}{d\cos\theta_Z} \propto 1+\frac{p_Z^2}{m_Z^2}\sin^2\theta_Z - 4\,\mathrm{Im}\left[\frac{\tilde{b}}{\tilde{a}}\right]\frac{v_e a_e}{v_e^2+a_e^2}\frac{p_z\sqrt{s}}{m_Z^2}\cos\theta_Z + \left|\frac{\tilde{b}}{\tilde{a}}\right|^2\frac{p_z^2 s}{2m_Z^4}(1+\cos^2\theta_Z)\,, \tag{3.16}$$

where θ_Z, p_Z, and E_Z are the scattering angle, momentum, and energy of the final-state Z boson; v_e and a_e are the vector and axial-vector couplings at the e^+e^-Z vertex; and $\tilde{a} \equiv a - bE_Z\sqrt{s}/m_Z^2$. The term in Eq. (3.16) proportional to $\cos\theta_Z$ arises from interference between the CP-even and CP-odd couplings in Eq. (3.15). If the CP-odd coupling $\tilde{b}$ is large enough, it can be extracted from the forward-backward asymmetry. Even upper limits on this asymmetry would be interesting. Note that the CP-even component of a Higgs boson will typically couple at tree-level whereas the CP-odd component will only couple via one-loop diagrams (typically dominated by the t quark loop). As a result the coupling strength $\tilde{b}$ is typically proportional to m_Z^2/s times a loop suppression factor. Thus, an asymmetry measurement may be able to provide a crude determination of the $\tilde{b}/a$ term. If ϕ is a purely CP-odd state with one-loop coupling, the resulting ZA^0 cross section will simply be too small to provide a useful measurement of the asymmetry.

- The angular distribution of the fermions in the $Z \to f\overline{f}$ decays in $Z\phi$ production also reflects the CP nature of the state ϕ [108,109]. For the decay $Z \to e^+e^-$ or $\mu^+\mu^-$, the following angles can be defined: the angle between the initial e^- and the Z; the angle between the final state e^- or μ^- and the direction of motion of the Z, in the rest frame of the Z; and the angle between the Z production plane and Z decay plane. Correlations between these angles can be exploited, *e.g.*, a fit to the double-differential angular distribution of the first two of these angles results in a 14σ separation between the 0^{++} (CP-even, scalar) and the 0^{-+} (CP-odd, pseudoscalar) [82], assuming that the $Z\phi$ cross section is independent of the CP nature of ϕ (see Fig. 3.23(b)). Even more powerful are fits to the triple-differential angular distribution, where sufficient luminosity can uncover non-standard $ZZ\phi$ couplings. However, this technique again suffers from the difficulty described in the previous item; namely, the CP-odd part of the state ϕ is typically so weakly coupled to ZZ that there is little sensitivity to the CP-odd component if there is any significant CP-even component in ϕ), or a very small cross section, if ϕ is almost purely CP-odd.

- If ϕ has significant branching ratios to either $\tau^+\tau^-$ or $t\overline{t}$, the polarization of the decay fermions can be measured. This can provide a direct determination of the ratio b_f/a_f in the $y_f\overline{f}(a_f + ib_f\gamma_5)f\phi$ ($f = \tau$ or t) Yukawa coupling structure of ϕ [111–113].

- The angular distributions in the $t\overline{t}\phi$ final state, which has adequate cross section for $\sqrt{s} \gtrsim 800\,\text{GeV}$ for modest values of $m_\phi \lesssim 200\,\text{GeV}$, assuming Yukawa coupling $y_t\overline{t}(a_t + ib_t\gamma_5)t\phi$ comparable to SM values, appear to provide an excellent means for determining the CP nature of ϕ by allowing one to probe the ratio b_t/a_t [114,94].

- It is likely that the CP properties of the ϕ can be well determined using photon polarization asymmetries in $\gamma\gamma \to \phi$ collisions [115,116,113]. This is discussed in Section 10.

- If the ϕ has substantial ZZ coupling, then $e^-e^- \to ZZe^-e^- \to \phi e^-e^-$ can be used to probe its CP nature [117] via the energy distributions of the ϕ and the final electrons, which are much harder in the case of a CP-odd state than for a CP-even state. Certain correlations are also useful probes of the CP properties of the ϕ. However, if the CP-odd portion of ϕ couples at one-loop (as expected for a Higgs boson), there will be either little sensitivity to this component or little cross section.

8.8 Precision studies of non-SM-like Higgs bosons

We confine our remarks to a two-doublet Higgs model (either the MSSM Higgs sector or a more general 2HDM). In the MSSM, we noted in Section 5.4 that for $m_{A^0} \lesssim \sqrt{s}/2$, as long as one is not too close to threshold, it is possible to observe all Higgs scalars of the non-minimal Higgs sector. In particular, in parameter regions away from the decoupling limit, none of the CP-even Higgs scalars may resemble the SM Higgs boson. Precision studies of all the Higgs bosons will provide a detailed profile of the non-minimal Higgs sector. Once $m_{A^0} \gtrsim \sqrt{s}/2$, only the h^0 will be visible at the LC. There may still be some possibilities for observing the heavier Higgs states produced singly, either in association with a $b\overline{b}$ pair at large $\tan\beta$ where the coupling to $b\overline{b}$ is enhanced, or by s-channel resonance production at a $\gamma\gamma$ collider.

Masses m_{A^0} and m_{H^0} in excess of 500 GeV to 1 TeV are certainly possible. In such cases, very substantial energy for the LC will be required to observe these states directly, either in association with $b\overline{b}$ (at large $\tan\beta$) or via H^0A^0 production. Measuring the former will provide a crucial determination of the $b\overline{b}$ couplings, which in the given model context will provide a determination of $\tan\beta$, with accuracy determined by the production rates. Moreover, if the H^0 and A^0 can be produced at a high rate (by whatever process), a detailed study of their branching ratios has the potential for providing very vital information regarding model parameters. In the supersymmetric context, the heavy H^0, A^0 and $H^\pm$ would generally decay to various pairs of supersymmetric particles as well as to b's and t's. A study of the relative branching ratios would provide powerful determinations of $\tan\beta$ and many of the soft-SUSY-breaking parameters [118–120].

9 The Giga-Z option—implications for the Higgs sector

Measurements of the effective leptonic mixing angle and the W boson mass to precisions of $\delta \sin^2\theta_w^{\rm eff} \simeq 10^{-5}$ and $\delta m_W \approx 6$ MeV at Giga-Z can be exploited in many

ways. The size of the Giga-Z 90% CL ellipses is illustrated in Fig. 3.15. Potential implications include the following.

- Within the SM context, the Higgs boson mass can be determined indirectly to a precision of about 7%. Deviation between the directly observed value and the value implied by Giga-Z data would require new physics beyond the SM.

- In the MSSM context it will be possible to obtain information about new high mass scales beyond the direct reach of the collider. This would be of particular importance if the heavier scalar top quark, $\tilde{t}_2$, and the heavy Higgs bosons A^0, H^0 and $H^\pm$ were beyond the kinematical reach of the LC and background problems precluded their observation at the LHC.

- In the context of a non-minimal Higgs sector, such as the general 2HDM extension of the minimal SM, constraints on the Higgs sector and/or new physics can be obtained. These would be particularly important in those cases where none of the Higgs bosons or new particles could be observed at the LC without higher $\sqrt{s}$ or at the LHC because of backgrounds.

9.1 The MSSM context

In the case of the MSSM, the relation between m_W and $\sin^2\theta_w^{\rm eff}$ is affected by the parameters of the supersymmetric sector, especially the $\tilde{t}$ sector. At a LC, the mass of the light $\tilde{t}$, $m_{\tilde{t}_1}$, and the $\tilde{t}$ mixing angle, $\theta_{\tilde{t}}$, should be measurable very well if the process $e^+e^- \to \tilde{t}_1\overline{\tilde{t}_1}$ is accessible [121].

In Fig. 3.24 (from [26]), it is demonstrated how *upper* bounds on m_{A^0} and $m_{\tilde{t}_2}$ can be derived from measurements of m_{h^0}, m_W and $\sin^2\theta_w^{\rm eff}$, supplemented by precise determinations of $m_{\tilde{t}_1}$ and $\theta_{\tilde{t}}$. The analysis assumes a lower bound, $\tan\beta \geq 10$, which can be expected from measurements in the gaugino sector (see, *e.g.*, [122]). The other parameters values are assumed to have the uncertainties as expected from LHC [123] and a LC [76].

For low $\tan\beta$ (where the prediction for m_{h^0} depends sensitively on $\tan\beta$) the heavier $\tilde{t}$ mass, $m_{\tilde{t}_2}$, can be restricted to $760\,\text{GeV} \lesssim m_{\tilde{t}_2} \lesssim 930\,\text{GeV}$ from the m_{h^0}, m_W and $\sin^2\theta_w^{\rm eff}$ precision measurements. The mass m_{A^0} varies between 200 GeV and 1600 GeV. If $\tan\beta \geq 10$ (where m_{h^0} has only a mild dependence on $\tan\beta$), the allowed region for the $\tilde{t}_2$ turns out to be much smaller, $660\,\text{GeV} \lesssim m_{\tilde{t}_2} \lesssim 680\,\text{GeV}$, and the mass m_{A^0} is restricted to $m_{A^0} \lesssim 800\,\text{GeV}$.

In deriving the bounds on the heavier $\tilde{t}$ mass, $m_{\tilde{t}_2}$, the constraints from m_{h^0} and from $\sin^2\theta_w^{\rm eff}$ and m_W play an important role. For the bounds on m_{A^0}, the main effect comes from $\sin^2\theta_w^{\rm eff}$. The assumed value of $\sin^2\theta_w^{\rm eff} = 0.23140$ differs slightly from the corresponding value obtained in the SM limit. For this value the (logarithmic) dependence on m_{A^0} is still large enough (see [124]) so that from the high precision

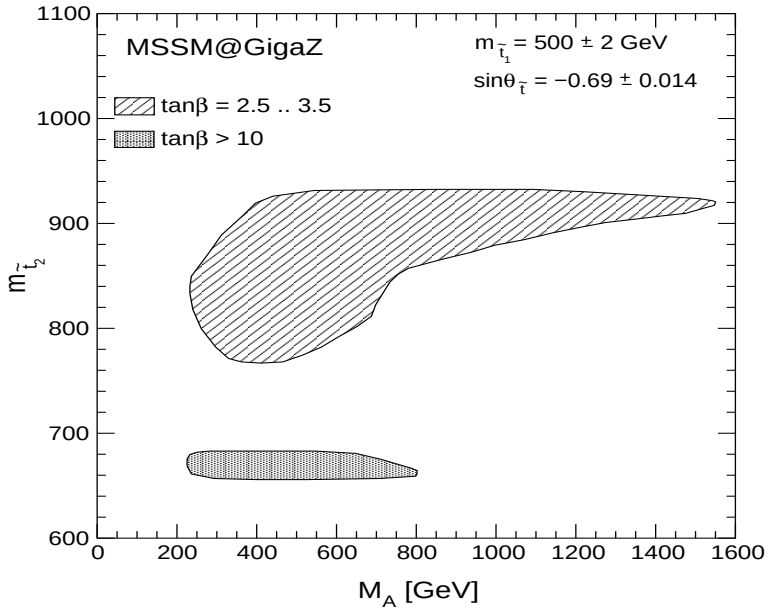

Figure 3.24: The region in the $m_{A^0} - m_{\tilde{t}_2}$ plane, allowed by $1\,\sigma$ errors obtained from the Giga-Z measurements of m_W and $\sin^2\theta_w^{\rm eff}$: $m_W = 80.400 \pm 0.006\,\text{GeV}$, $\sin^2\theta_w^{\rm eff} = 0.23140 \pm 0.00001$, and from the LC measurement of m_{h^0}: $m_{h^0} = 115 \pm 0.05\,\text{(exp.)} \pm 0.5\,\text{(theo.)}\,\text{GeV}$. $\tan\beta$ is assumed to be $\tan\beta = 3 \pm 0.5$ or $\tan\beta > 10$. The other parameters are given by $m_{\tilde{t}_1} = 500 \pm 2\,\text{GeV}$, $\sin\theta_{\tilde{t}} = -0.69 \pm 0.014$, $A_b = A_t \pm 10\%$, $m_{\tilde{g}} = 500 \pm 10\,\text{GeV}$, $\mu = -200 \pm 1\,\text{GeV}$ and $M_2 = 400 \pm 2\,\text{GeV}$.

in $\sin^2\theta_w^{\rm eff}$ at Giga-Z an *upper limit* on m_{A^0} can be set. For the error of $\sin^2\theta_w^{\rm eff}$ that could be obtained at an LC without the Giga-Z mode (which is at least ten times larger), no bound on m_{A^0} could be inferred.

9.2 Non-exotic extended Higgs sector context

Building on the discussion of the general 2HDM given earlier, one can imagine many situations for which the very small Giga-Z 90% CL ellipses illustrated in Fig. 3.15 would provide crucial (perhaps the only) constraints. For example, suppose the LHC observes a 1 TeV Higgs boson with very SM-like properties and no other new physics below the few-TeV scale. We have seen that this is possible in the 2HDM scenarios consistent with current precision electroweak constraints. Suppose further that it is not immediately possible to increase $\sqrt{s}$ sufficiently so that h^0A^0 production is allowed (typically requiring $\sqrt{s} > 1.5\,\text{TeV}$ in these models). Giga-Z measurements would provide strong guidance as to the probable masses of the non-SM-like Higgs bosons of any given non-minimal Higgs sector. However, it must be accepted that a particular Giga-Z result for S, T might have other non-Higgs interpretations as well.

10 The $\gamma\gamma$ collider option

Higgs production in $\gamma\gamma$ collisions offers a unique capability to measure the two-photon width of the Higgs and to determine its CP composition through control of the photon polarization. A brief discussion of photon collider technology can be found in Chapter 13.

The $\gamma\gamma$ coupling of a SM-like Higgs boson $h_{\rm SM}$ of relatively light mass receives contributions from loops containing any particle whose mass arises in whole or part from the vacuum expectation value of the corresponding neutral Higgs field. A measurement of $\Gamma(h_{\rm SM} \to \gamma\gamma)$ provides the possibility of revealing the presence of arbitrarily heavy particles that acquire mass via the Higgs mechanism.[8] However, since such masses are basically proportional to some coupling times v, if the coupling is perturbative the masses of these heavy particles are unlikely to be much larger than $0.5-1$ TeV. Since $B(h_{\rm SM} \to X)$ is entirely determined by the spectrum of light particles, and is thus not affected by heavy states, $N(\gamma\gamma \to h_{\rm SM} \to X) \propto \Gamma(h_{\rm SM} \to \gamma\gamma)B(h_{\rm SM} \to X)$ will provide an extraordinary probe for such heavy states. Even if there are no new particles that acquire mass via the Higgs mechanism, a precision measurement of $N(\gamma\gamma \to \widehat{h} \to X)$ for specific final states X ($X = b\overline{b}, WW^*, \ldots$) can allow one to distinguish between a $\widehat{h}$ that is part of a larger Higgs sector and the SM $h_{\rm SM}$. The deviations from the SM predictions typically exceed 5% if the other heavier Higgs bosons have masses below about 400 GeV.

The predicted rate for Higgs boson production followed by decay to final state X can be found in [56]. This rate depends strongly on $d\mathcal{L}_{\gamma\gamma}/dy$, the differential $\gamma\gamma$ collider luminosity, where $y = m_{\widehat{h}}/\sqrt{s}$ and $\sqrt{s}$ is the ee collider center-of-mass energy. An important parameter to maximize peak luminosity is $\langle\lambda\lambda'\rangle$, the average value of the product of the helicities of the two colliding photons after integration over their momentum fractions z and z'. Larger values of this parameter also suppress the dominant $J_z = \pm 2$, $\gamma\gamma \to b\overline{b}g$ background, which is proportional to $(1 - \langle\lambda\lambda'\rangle)$. The computation of $d\mathcal{L}_{\gamma\gamma}/dy$ was first considered in [125,126]. More realistic determinations [127] including beamstrahlung, secondary collisions between scattered electrons and photons from the laser beam, and other non-linear effects result in a substantial enhancement of the luminosity in the low-$E_{\gamma\gamma}$ region as shown in Fig. 3.25.

The choice of parameters that gives a peaked spectrum is well suited for light Higgs studies. Using the spectrum of Fig. 3.25 as an example, the di-jet invariant mass distributions for the Higgs signal and for the $b\overline{b}(g)$ background for $m_{h_{\rm SM}} = 120\,{\rm GeV}$ are shown in Fig. 3.26 [128]. After a year of operation, $\Gamma(h_{\rm SM} \to \gamma\gamma)B(h_{\rm SM} \to b\overline{b})$ could be measured with an accuracy of about 5%. (A much more optimistic error of close to 2% is quoted in [129] for $m_{h_{\rm SM}} = 120\,{\rm GeV}$, based upon a substantially higher peak luminosity.) The error for this measurement increases to about 20% for

[8] Loop contributions from particles that acquire a large mass from some other mechanism will decouple as $(\text{mass})^{-2}$ and $\Gamma(h_{\rm SM} \to \gamma\gamma)$ will not be sensitive to their presence.

$m_{h_{\rm SM}} = 160\,\text{GeV}$, primarily due to the decrease of the Higgs di-jet branching fraction by a factor of 18.

In many scenarios, it is possible that by combining this result with other types of precision measurements for the SM-like Higgs boson, small deviations can be observed indicating the possible presence of heavier Higgs bosons. For a 2HDM (either the MSSM or a two-Higgs-doublet model with partial decoupling), if $m_{H^0} \sim m_{A^0} > \sqrt{s}/2$ then $e^+e^- \to H^0A^0$ is not possible and $\gamma\gamma \to H^0, A^0$ may be the only option allowing their discovery (other than implementing higher $\sqrt{s}$). The alternatives of $b\overline{b}H$ and $b\overline{b}A$ production will only allow H and A detection if $\tan\beta$ is large [71]. A LC for which the maximum energy is $\sqrt{s} = 630\,\text{GeV}$ can potentially probe Higgs masses as high as 500 GeV. If m_{H^0} and m_{A^0} are known to within roughly 50 GeV on the basis of precision h^0 data, then there is an excellent chance of detecting them by scanning, *i.e.* stepping in $\sqrt{s}$, using a peaked $\gamma\gamma$ spectrum [57,128]. If no constraints have been placed on the H^0, A^0 masses (other than $m_{A^0} \sim m_{H^0} > \sqrt{s}/2$), it is best to employ a broad $\gamma\gamma$ spectrum, which would yield a visible signal for H^0, A^0 production for only some parameter choices of m_{A^0} and $\tan\beta$ [128].

In the non-decoupling 2HDM model with a light decoupled $\widehat{h}$ and all other Higgs bosons heavier than $\sqrt{s}$, $\gamma\gamma \to \widehat{h} \to b\overline{b}$ might allow detection of the $\widehat{h}$ for some of the $\tan\beta$ values in the wedge where the $b\overline{b}\widehat{h}$ and $t\overline{t}\widehat{h}$ production processes both yield fewer than 20 events for an integrated luminosity of 1000 fb^{-1} [128].

Once one or several Higgs bosons have been detected, precision studies can be performed including: determination of CP properties; a detailed scan to separate the H^0 and A^0 in the decoupling limit of a 2HDM; and branching ratios measurements. The branching ratios to supersymmetric final states are especially important for determining the basic supersymmetry breaking parameters [130,118,120,57].

The CP properties can be determined for any spin-0 Higgs $\widehat{h}$ produced in $\gamma\gamma$ collisions. Since $\gamma\gamma \to \widehat{h}$ is of one-loop order, whether $\widehat{h}$ is CP-even, CP-odd or a mixture, the CP-even and CP-odd parts of $\widehat{h}$ have $\gamma\gamma$ couplings of similar size. However, the structure of the couplings is very different:

$$\mathcal{A}_{\text{CP}=+} \propto \vec{\epsilon}_1 \cdot \vec{\epsilon}_2\,, \quad \mathcal{A}_{\text{CP}=-} \propto (\vec{\epsilon}_1 \times \vec{\epsilon}_2) \cdot \widehat{p}_{\text{beam}}\,. \tag{3.17}$$

By adjusting the orientation of the initial laser photon polarization vectors with respect to one another, it is possible to determine the relative amounts of CP-even and CP-odd content in the resonance $\widehat{h}$ [115]. If $\widehat{h}$ is a mixture, one can use helicity asymmetries for this purpose [115,113]. However, if $\widehat{h}$ is either purely CP-even or purely CP-odd, then one must employ transverse linear polarizations [116,113]. Substantial luminosity with transverse polarization can be obtained, although the spectrum is not peaked, as shown in Fig. 3.25.

One measure of the CP nature of a Higgs is the asymmetry for parallel *vs.* per-

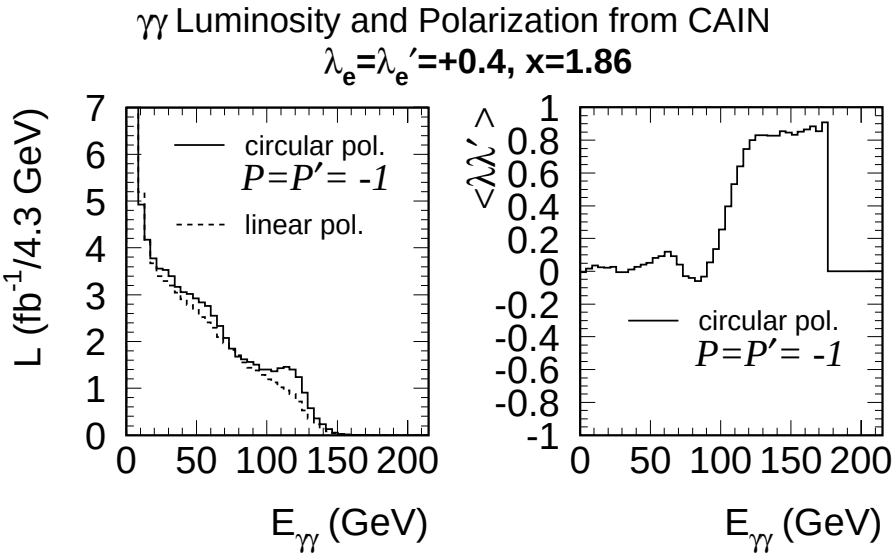

Figure 3.25: Left: CAIN [127] predictions for the $\gamma\gamma$ luminosity distribution for circularly polarized ($\lambda_e = \lambda'_e = 0.4$, $P = P' = -1$) and linearly polarized photons assuming 10^7 sec/year, $\sqrt{s} = 206\,\text{GeV}$, 80% electron beam polarization, and a 1.054 micron laser wavelength, after including beamstrahlung and other effects, from [128]. Right: The corresponding value of $\langle\lambda\lambda'\rangle$, for circular polarization.

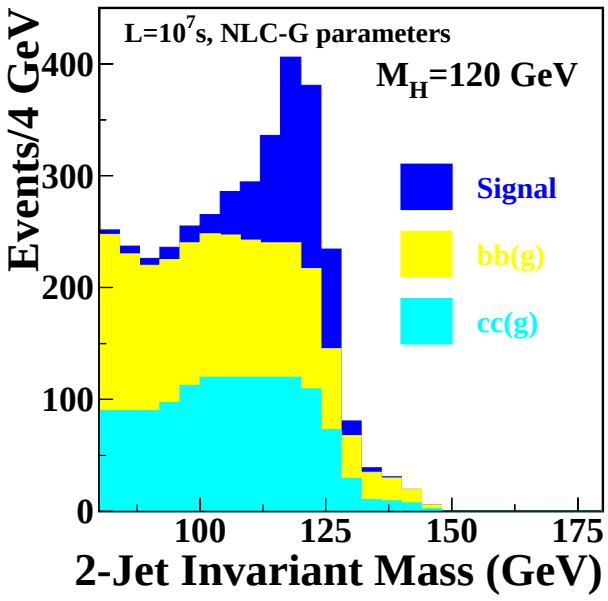

Figure 3.26: Higgs signal and heavy quark background in $\gamma\gamma \to h$ for a Higgs mass of 120 GeV [128].

pendicular orientation of the linear polarizations of the initial laser beams,

$$\mathcal{A} \equiv \frac{N_{\parallel} - N_{\perp}}{N_{\parallel} + N_{\perp}}\,, \tag{3.18}$$

which is positive (negative) for a CP-even (odd) state. Since 100% linear polarization for the laser beams translates into only partial linear polarization for the colliding photons, both $N_{\parallel}$ and $N_{\perp}$ will be non-zero for the signal. In addition, the heavy quark background contributes to both. The expected value of $\mathcal{A}$ must be carefully computed for a given model. For the SM Higgs with $m_{h_{\rm SM}} = 120\,\text{GeV}$, it is estimated [128] that $\mathcal{A}$ can be measured with an accuracy of about 20% in one year of operation, assuming the linear polarization spectrum of Fig. 3.25, 60% linear polarization of the colliding photons, and S/B comparable to that shown in Fig. 3.26. This measurement would thus provide a moderately strong test of the CP=+ nature of the $h_{\rm SM}$.

We end by noting that the $e^-\gamma$ and e^-e^- collider options are most relevant to exotic Higgs scenarios, as discussed in Section 11.

11 Exotic Higgs sectors and other possibilities

As we have seen, there are many scenarios and models in which the Higgs sector is more complicated than the one-Higgs-doublet of the minimal SM. Supersymmetry requires at least two Higgs doublets. Even in the absence of supersymmetry, a two-doublet Higgs sector allows for CP-violating phenomena. Singlets can also be added without altering the tree-level prediction of $\rho = 1$. However, the possibility of Higgs representations with still higher weak (left handed, denoted L) isospin should not be ignored. The primary negative is that, for triplets and most higher representations, if the vacuum expectation value of the neutral Higgs field member of the representation is non-zero ($v_L \neq 0$) then ρ becomes infinitely renormalized and can no longer be computed [131]; instead it becomes a parameter that must be input as part of the renormalization program. Triplets have received the most attention, as they arise naturally in left-right symmetric extensions of the Standard Model gauge group [132]. (These and other models that utilize Higgs triplets are reviewed in [1].) In this section we will also briefly consider the Higgs-like pseudo-Nambu-Goldstone bosons that arise in generic technicolor theories.

11.1 A triplet Higgs sector

Including a single complex SU(2)-triplet Higgs representation, in addition to some number of doublets and singlets, results in six additional physical Higgs eigenstates: $H^{--,++}$, $H^{-,+}$, H^0 and $H^{0\prime}$. All but the doubly-charged states can mix with the doublet/singlet Higgs states under some circumstances. Even if $v_L \neq 0$ for the neutral field, $\rho = 1$ can be preserved at tree-level if, in addition, a real triplet field is

also included [133,134]. However, ρ will still be infinitely renormalized at one-loop unless $v_L = 0$ is chosen. Left-right symmetric models capable of yielding the see-saw mechanism for neutrino mass generation *require* two triplet Higgs representations (an L-triplet and an R-triplet). The large see-saw mass entry, M, arises from a lepton-number-violating Majorana coupling (which L-R symmetry requires to be present for both the L-triplet and R-triplet representations). Again, ρ will not be altered if $v_L = 0$, but v_R must be non-zero and large for large M. We will briefly discuss the phenomenology of an L-triplet. That for the R-triplet of the L-R symmetric model is quite different. (See [1] for a review.)

The resulting Higgs sector phenomenology can be very complex. We focus on the most unequivocal signal for a triplet representation, namely observation of a doubly-charged Higgs boson. Pair production, $Z^* \to H^{++}H^{--}$, has limited mass reach, $m_{H^{++}} < \sqrt{s}/2$. Fortunately, single production is also generally possible. Most interestingly, the generically-allowed lepton-number-violating Majorana coupling leads to an $e^-e^- \to H^{--}$ coupling and the possibility of s-channel resonance production of the H^{--} in e^-e^- collisions. Observation of this process would provide a dramatic confirmation of the presence of the Majorana coupling and, in many cases, the ability to actually measure its magnitude. For a discussion and review, see [135] (and also [136,137]). If the H^{--} is heavy *and* has significant W^-W^- coupling (requiring $v_L \neq 0$), then it can become broad and the s-channel resonant production cross section is suppressed (see, *e.g.*, [138]) and might not be observable. Another production mechanism sensitive to the $e^-e^- \to H^{--}$ coupling that might be useful in such an instance is $e^-e^- \to H^{--}Z$, and $e^-e^- \to H^-W^-$ will be sensitive to the $e^-\nu_e \to H^-$ coupling that would be present for the H^- member of the triplet representation [139]. Using just the Majorana coupling, doubly-charged Higgs bosons can also be produced via $e^-\gamma \to e^+H^{--}$ and $e^+e^- \to e^+e^+H^{--}$ [140] and the singly-charged members of the same representation can be produced in $e^-e^- \to H^-W^-$ [139].

Despite loss of ρ predictivity, it could be that non-zero v_L is Nature's choice. In this case, the e^-e^- collider option again has some unique advantages. The neutral, singly-charged and doubly-charged Higgs bosons of the triplet representation can *all* be produced (via ZZ fusion, W^-Z fusion and W^-W^- fusion, respectively). For example, [141] studies $W^-W^- \to H^{--}$ fusion.

11.2 Pseudo Nambu Goldstone bosons

In the context of technicolor and related theories, the lowest-mass states are typically a collection of pseudo-Nambu-Goldstone bosons, of which the lightest is very possibly a state P^0 which can have mass below 200 GeV and couplings and other properties not unlike those of a light SM-like Higgs boson. Typically, its WW, ZZ coupling is very small (arising via loops or anomalies), while its $b\overline{b}$ coupling can be larger. The phenomenology of such a P^0 was studied in [142]. The best modes for detection of the P^0 at an LC are $e^+e^- \to \gamma P^0 \to \gamma b\overline{b}$ and $\gamma\gamma \to P^0 \to b\overline{b}$. Since the

P^0 is likely to be discovered at the LHC in the $\gamma\gamma$ final state, we will know ahead of time of its existence, and precision measurements of its properties would be a primary goal of the LC.

References

[1] J. F. Gunion, H. E. Haber, G. Kane and S. Dawson, *The Higgs Hunter's Guide* (Perseus Publishing, Reading, MA, 2000).

[2] J. F. Gunion, L. Poggioli, R. Van Kooten, C. Kao, P. Rowson *et al.*, "Higgs boson discovery and properties," in *New Directions for High Energy Physics*, Proceedings of the 1996 DPF/DPB Summer Study on High Energy Physics, Snowmass '96, edited by D. G. Cassel, L. T. Gennari and R. H. Siemann (Stanford Linear Accelerator Center, Stanford, CA, 1997) pp. 541–587 [hep-ph/9703330].

[3] H. E. Haber, T. Han, F. S. Merritt, J. Womersley *et al.*, "Weakly coupled Higgs bosons and precision electroweak physics," in *New Directions for High Energy Physics*, Proceedings of the 1996 DPF/DPB Summer Study on High Energy Physics, Snowmass '96, edited by D. G. Cassel, L. T. Gennari and R. H. Siemann (Stanford Linear Accelerator Center, Stanford, CA, 1997) pp. 482–498 [hep-ph/9703391].

[4] H. Murayama and M. E. Peskin, Ann. Rev. Nucl. Part. Sci. **46**, 533 (1996) [hep-ex/9606003].

[5] E. Accomando *et al.* [ECFA/DESY LC Physics Working Group], Phys. Rep. **299**, 1 (1998) [hep-ph/9705442].

[6] For a recent review, see R. N. Mohapatra, "Supersymmetric grand unification: An update," in *Supersymmetry, Supersymmetry and Supercolliders*, edited by J. Bagger (World Scientific, 1998) [hep-ph/9911272].

[7] D. Abbaneo *et al.* [ALEPH, DELPHI, L3 and OPAL Collaborations, LEP Electroweak Working Group, and SLD Heavy Flavor and Electroweak Groups], CERN-EP-2000-016.

[8] J. Erler, hep-ph/0102143.

[9] G. Degrassi, hep-ph/0102137.

[10] R. Barate *et al.* [ALEPH Collaboration], Phys. Lett. **B495**, 1 (2000) [hep-ex/0011045]; P. Abreu *et al.* [DELPHI Collaboration], Phys. Lett. **B499**, 23 (2001) [hep-ex/0102036]; M. Acciarri *et al.* [L3 Collaboration], hep-ex/0012019; G. Abbiendi *et al.* [OPAL Collaboration], Phys. Lett. **B499**, 38 (2001) [hep-ex/0101014].

[11] E. Farhi and L. Susskind, Phys. Rep. **74**, 277 (1981); R.K. Kaul, Rev. Mod. Phys. **55**, 449 (1983); K. Lane, in *The Building Blocks of Creation—From Microfermis to Megaparsecs*, Proceedings of the Theoretical Advanced Study Institute (TASI 93) in Elementary Particle Physics, Boulder, CO, 6 June—2 July 1993, edited by S. Raby and T. Walker (World Scientific, Singapore, 1994) [hep-ph/9401324].

[12] M. E. Peskin and T. Takeuchi, Phys. Rev. Lett. **65**, 964 (1990); Phys. Rev. **D46**, 381 (1992).

[13] M. E. Peskin and J. D. Wells, hep-ph/0101342.

[14] A. G. Cohen, in *The Building Blocks of Creation—From Microfermis to Megaparsecs*, Proceedings of the Theoretical Advanced Study Institute (TASI 93) in Elementary Particle Physics, Boulder, CO, 6 June—2 July 1993, edited by S. Raby and T. Walker (World Scientific, Singapore, 1994).

[15] The most recent analysis of this type can be found in: T. Hambye and K. Riesselmann, Phys. Rev. **D55**, 7255 (1997) [hep-ph/9610272].

[16] The most recent analyses of this type can be found in: G. Altarelli and G. Isidori, Phys. Lett. **B337**, 141 (1994); J. A. Casas, J. R. Espinosa and M. Quirós, Phys. Lett. **B342**, 171 (1995) [hep-ph/9409458]; **B382**, 374 (1996) [hep-ph/9603227].

[17] R. Dashen and H. Neuberger, Phys. Rev. Lett. **50**, 1897 (1983); M. Lüscher and P. Weisz, Phys. Lett. **B212**, 472 (1988), Nucl. Phys. **B318**, 705 (1989); U. M. Heller, M. Klomfass, H. Neuberger and P. Vranas, Nucl. Phys. **B405**, 555 (1993).

[18] K. Riesselmann, hep-ph/9711456.

[19] G. 't Hooft, in *Recent Developments in Gauge Theories,* Proceedings of the NATO Advanced Summer Institute, Cargese, 1979, edited by G. 't Hooft *et al.* (Plenum, New York, 1980) p. 135; E. Witten, Nucl. Phys. **B188**, 513 (1981); L. Susskind, Phys. Rep. **104**, 181 (1984).

[20] H. P. Nilles, Phys. Rep. **110**, 1 (1984).

[21] H. E. Haber and G. L. Kane, Phys. Rep. **117**, 75 (1985); S. P. Martin, hep-ph/9709356.

[22] A. Djouadi, J. Kalinowski and M. Spira, Comput. Phys. Commun. **108**, 56 (1998) [hep-ph/9704448]. The HDECAY program is available at `http://home.cern.ch/~mspira/proglist.html`.

[23] A. Djouadi, J. Kalinowski and P. M. Zerwas, Z. Phys. **C54**, 155 (1992).

[24] S. Dittmaier, M. Kramer, Y. Liao, M. Spira and P. M. Zerwas, Phys. Lett. **B441**, 383 (1998) [hep-ph/9808433].

[25] A. Freitas, W. Hollik, W. Walter and G. Weiglein, Phys. Lett. **B495**, 338 (2000) [hep-ph/0007091]; A. Freitas, S. Heinemeyer, W. Hollik, W. Walter and

G. Weiglein, Nucl. Phys. Proc. Suppl. **89**, 82 (2000) [hep-ph/0007129]; hep-ph/0101260.

[26] J. Erler, S. Heinemeyer, W. Hollik, G. Weiglein and P. M. Zerwas, Phys. Lett. **B486**, 125 (2000) [hep-ph/0005024].

[27] M. Carena, J. S. Conway, H. E. Haber and J. D. Hobbs *et al.*, FERMILAB-CONF-00/270-T [hep-ph/0010338].

[28] M. Dittmar, "LHC luminosity requirements to observe H0 and measure its couplings," presented at Workshop on the Future of Higgs Physics, Fermilab, Chicago, May 3–5 2001.

[29] For a recent review, see V. A. Mitsou, ATLAS-CONF-2000-002.

[30] K. Lassila-Perini, ETH Dissertation thesis No. 12961 (1998).

[31] D. Zeppenfeld, R. Kinnunen, A. Nikitenko and E. Richter-Wąs, Phys. Rev. **D62**, 013009 (2000) [hep-ph/0002036].

[32] O. J. Eboli and D. Zeppenfeld, Phys. Lett. **B495**, 147 (2000) [hep-ph/0009158].

[33] K. Inoue, A. Kakuto, H. Komatsu, and S. Takeshita, Prog. Theor. Phys. **68**, 927 (1982) [E: **70**, 330 (1983)]; **71**, 413 (1984); R. Flores and M. Sher, Ann. Phys. (NY) **148**, 95 (1983).

[34] J. F. Gunion and H. E. Haber, Nucl. Phys. **B272**, 1 (1986); **B278**, 449 (1986) [E: **B402**, 567 (1993)].

[35] For a review of the two-Higgs-doublet model (both non-supersymmetric and supersymmetric), see Chapter 4 of [1].

[36] H. E. Haber and Y. Nir, Phys. Lett. **B306**, 327 (1993) [hep-ph/9302228]; H. E. Haber, in *Physics From the Planck Scale to the Electroweak Scale*, Proceedings of the US–Polish Workshop, Warsaw, Poland, September 21–24, 1994, edited by P. Nath, T. Taylor, and S. Pokorski (World Scientific, Singapore, 1995) pp. 49–63 [hep-ph/9501320].

[37] L. J. Hall and M. B. Wise, Nucl. Phys. **B187**, 397 (1981).

[38] H. E. Haber and R. Hempfling, Phys. Rev. Lett. **66**, 1815 (1991); Y. Okada, M. Yamaguchi and T. Yanagida, Prog. Theor. Phys. **85**, 1 (1991); J. Ellis, G. Ridolfi and F. Zwirner, Phys. Lett. **B257**, 83 (1991).

[39] S. Heinemeyer, W. Hollik and G. Weiglein, Phys. Rev. **D58**, 091701 (1998) [hep-ph/9803277]; Phys. Lett. **B440**, 296 (1998) [hep-ph/9807423]; Eur. Phys. J. **C9**, 343 (1999) [hep-ph/9812472]; M. Carena, H. E. Haber, S. Heinemeyer, W. Hollik, C. E. M. Wagner and G. Weiglein, Nucl. Phys. **B580**, 29 (2000) [hep-ph/0001002]; R.-J. Zhang, Phys. Lett. **B447**, 89 (1999) [hep-ph/9808299]; J. R. Espinosa and R.-J. Zhang, JHEP **0003**, 026 (2000) [hep-ph/9912236]; Nucl. Phys. **B586**, 3 (2000) [hep-ph/0003246]. The computer programs FeynHiggs and FeynHiggsFast are described respectively in S. Heinemeyer, W. Hollik and G. Weiglein, Comput. Phys. Commun. **124**, 76 (2000) [hep-ph/9812320]; CERN-TH-2000-055 [hep-ph/0002213].

[40] J. Ellis, J. F. Gunion, H. E. Haber, L. Roszkowski and F. Zwirner, Phys. Rev. **D39**, 844 (1989). For a recent treatment and guide to the literature see: C. Panagiotakopoulos and A. Pilaftsis, Phys. Rev. D **63**, 055003 (2001) [hep-ph/0008268]. A detailed discussion of NMSSM phenomenology can be found in U. Ellwanger, M. Rausch de Traubenberg and C. A. Savoy, Nucl. Phys. **B492**, 21 (1997) [hep-ph/9611251].

[41] J. R. Espinosa and M. Quirós, Phys. Rev. Lett. **81**, 516 (1998) [hep-ph/9804235].

[42] J. A. Coarasa, R. A. Jiménez and J. Solà, Phys. Lett. **B389**, 312 (1996) [hep-ph/9511402]; R. A. Jiménez and J. Solà, Phys. Lett. **B389**, 53 (1996) [hep-ph/9511292]; A. Bartl *et al.*, Phys. Lett. **B378**, 167 (1996) [hep-ph/9511385].

[43] L. Hall, R. Rattazzi and U. Sarid, Phys. Rev. **D50**, 7048 (1994) [hep-ph/9306309]; R. Hempfling, Phys. Rev. **D49**, 6168 (1994).

[44] M. Carena, M. Olechowski, S. Pokorski and C. E. M. Wagner, Nucl. Phys. **B426**, 269 (1994) [hep-ph/9402253].

[45] D. Pierce, J. Bagger, K. Matchev, and R. Zhang, Nucl. Phys. **B491**, 3 (1997) [hep-ph/9606211].

[46] S. Heinemeyer, W. Hollik and G. Weiglein, Eur. Phys. J. **C16**, 139 (2000) [hep-ph/0003022].

[47] M. Carena, D. Garcia, U. Nierste and C. E. M. Wagner, Nucl. Phys. **B577**, 88 (2000) [hep-ph/9912516].

[48] H. Eberl, K. Hidaka, S. Kraml, W. Majerotto and Y. Yamada, Phys. Rev. **D62**, 055006 (2000) [hep-ph/9912463].

[49] M. Carena, S. Mrenna and C.E.M. Wagner, Phys. Rev. **D60**, 075010 (1999) [hep-ph/9808312]; Phys. Rev. **D62**, 055008 (2000) [hep-ph/9907422].

[50] H. Baer and J. D. Wells, Phys. Rev. **D57**, 4446 (1998) [hep-ph/9710368]; W. Loinaz and J. D. Wells, Phys. Lett. **B445**, 178 (1998) [hep-ph/9808287].

[51] J. L. Diaz-Cruz, H.-J. He, T. Tait and C. P. Yuan, Phys. Rev. Lett. **80**, 4641 (1998) [hep-ph/9802294]; C. Balázs, J. L. Diaz-Cruz, H.-J. He, T. Tait and C. P. Yuan, Phys. Rev. **D59**, 055016 (1999) [hep-ph/9807349].

[52] H. E. Haber *et al.*, Phys. Rev. **D63**, 055004 (2001) [hep-ph/0007006].

[53] P. H. Chankowski, S. Pokorski and J. Rosiek, Nucl. Phys. **B423**, 497 (1994).

[54] A. Djouadi, P. Janot, J. Kalinowski and P. M. Zerwas, Phys. Lett. **B376**, 220 (1996) [hep-ph/9603368]; A. Djouadi, J. Kalinowski, P. Ohmann and P. M. Zerwas, Z. Phys. **C74**, 93 (1997) [hep-ph/9605339].

[55] S. Heinemeyer, W. Hollik, J. Rosiek and G. Weiglein, Eur. Phys. J. **C19**, 535 (2001) [hep-ph/0102081].

[56] J. F. Gunion and H. E. Haber, Phys. Rev. **D48**, 5109 (1993).

[57] M. M. Mühlleitner, M. Krämer, M. Spira and P. M. Zerwas, hep-ph/0101083.

[58] The LEP working group for Higgs boson searches, LHWG note 2001-1 (3 April 2001).

[59] The ALEPH, DELPHI, L3 and OPAL Collaborations and the LEP Higgs Working Group, LHWG note 2001-2 (26 March 2001).

[60] The results of Fig. 3.14 were provided by F. Gianotti on behalf of the ATLAS collaboration. They are the preliminary results available as of March 3, 2001.

[61] See, for example, J. F. Gunion, hep-ph/9705282.

[62] S. L. Glashow and S. Weinberg, Phys. Rev. **D15**, 1958 (1977); E. A. Paschos, Phys. Rev. **D15**, 1966 (1977).

[63] B. A. Dobrescu, hep-ph/9903407 and hep-ph/0103038.

[64] M. Cvetic, H. Lu, C. N. Pope, A. Sadrzadeh and T. A. Tran, Nucl. Phys. **B586**, 275 (2000) [hep-th/0003103].

[65] P. Chankowski *et al.*, Phys. Lett. **B496**, 195 (2000) [hep-ph/0009271].

[66] J. F. Gunion and H. E. Haber, in preparation.

[67] U. Ellwanger and C. Hugonie, hep-ph/9909260.

[68] J. F. Gunion, H. E. Haber and T. Moroi, "Will at least one of the Higgs bosons of the next-to-minimal supersymmetric extension of the Standard Model be observable at LEP2 or the LHC?" in *New Directions for High Energy Physics*, Proceedings of the 1996 DPF/DPB Summer Study on High Energy Physics, Snowmass '96, edited by D. G. Cassel, L. T. Gennari and R. H. Siemann (Stanford Linear Accelerator Center, Stanford, CA, 1997) [hep-ph/9610337].

[69] J. F. Gunion and B. Grzadkowski, work in progress.

[70] J. R. Espinosa and J. F. Gunion, Phys. Rev. Lett. **82**, 1084 (1999) [hep-ph/9807275].

[71] B. Grzadkowski, J. F. Gunion and J. Kalinowski, Phys. Lett. **B480**, 287 (2000) [hep-ph/0001093].

[72] H. E. Haber and Y. Nir, Phys. Lett. **B306**, 327 (1993) [hep-ph/9302228].

[73] A. Djouadi, P. M. Zerwas and H. E. Haber, Phys. Lett. **B375**, 203 (1996) [hep-ph/9602234].

[74] J. F. Gunion and T. Farris, LC note in preparation.

[75] M. Battaglia and K. Desch, hep-ph/0101165.

[76] TESLA Technical Design Report, R. Heuer, D. Miller, F. Richard, A. Wagner and P. M. Zerwas (editors), obtainable from `www.desy.de/~lcnotes/tdr/` .

[77] See also `http://www-sldnt.slac.stanford.edu/nld/`.

[78] H. Yang and K. Riles, "Measurement of Higgs Mass and Cross Section at NLC", presented at Workshop on Physics and Detectors for Future e^+e^- Linear Colliders, Johns Hopkins University, Baltimore, 19–21 March 2001.

[79] M. Ronan, "Jet-Jet Reconstruction in Full Detector Simulations", presented at Workshop on Physics and Detectors for Future e^+e^- Linear Colliders, Johns Hopkins University, Baltimore, 19–21 March 2001.

[80] A. Juste, hep-ex/9912041.

[81] V. Barger, M. S. Berger, J. F. Gunion and T. Han, Phys. Rev. Lett. **78**, 3991 (1997) [hep-ph/9612279].

[82] P. F. Derwent *et al.*, FERMILAB-FN-701, report in preparation.

[83] A. Küskinen, M. Battaglia, P. Pöyhoönen, "Study of $e^+e^- \to H^+H^-$ at a 800 GeV Linear Collider", to appear in the Proc. of the Fifth Int. Workshop on Linear Colliders - LCSW2000, Fermilab, October 2000, LC-PHSM-2001-041; A. Andreazza, C. Troncon, "Study of HA Production in e^+e- Collisions at $\sqrt{s} = 800$ GeV, DESY-123-E, p. 417.

[84] P. Garcia-Abia and W. Lohmann, hep-ex/9908065.

[85] R. Van Kooten, "Separation of the Higgsstrahlung and WW-fusion process", presented at Workshop on Physics and Detectors for Future e^+e^- Linear Colliders, Johns Hopkins University, Baltimore, 19–21 March 2001.

[86] J. Brau, C. Potter, and M. Iwasaki, "Higgs Branching Ratio Measurements at a Future Linear Collider", presented at Workshop on Physics and Detectors for Future e^+e^- Linear Colliders, Johns Hopkins University, Baltimore, 19–21 March 2001.

[87] J. Brau, C. Potter, and M. Iwasaki, "Linear Collider Vertex Detector Optimization for Higgs Branching Ratio Measurements", LCWS 2000 Proceedings, session D3.

[88] D. J. Jackson, Nucl. Instrum. Meth. **A388**, 247 (1997).

[89] M. D. Hildreth, T. L. Barklow, and D. L. Burke, Phys. Rev. **D49**, 3441 (1994); K. Kawagoe, UT-ICEPP-93-10, contributed to the *2nd International Workshop on Physics and Experiments with Linear e^+e^- Colliders*, Waikoloa, HI, 26–30 April 1993.

[90] G. Borisov and F. Richard, hep-ph/9905413.

[91] M. Battaglia, hep-ex/0012021; hep-ph/9910271.

[92] J. F. Gunion and P. C. Martin, hep-ph/9610417; J. F. Gunion and P. C. Martin, Phys. Rev. Lett. **78**, 4541 (1997) [hep-ph/9607360].

[93] E. Boos, J. C. Brient, D. W. Reid, H. J. Schreiber and R. Shanidze, hep-ph/0011366.

[94] J. F. Gunion, B. Grzadkowski and X. He, Phys. Rev. Lett. **77**, 5172 (1996) [hep-ph/9605326].

[95] S. Dawson and L. Reina, Phys. Rev. **D57**, 5851 (1998); **D59**, 054012 (1999); **D60**, 015003 (1999); H. Baer, S. Dawson, and L. Reina, Phys. Rev. **D61**, 0113002 (2000).

[96] A. Juste and G. Merino, hep-ph/9910301.

[97] D. J. Miller and S. Moretti, hep-ph/0001194.

[98] C. Castanier, P. Gay, P. Lutz and J. Orloff, hep-ex/0101028.

[99] R. Lafaye, D. J. Miller, M. Mühlleitner and S. Moretti, hep-ph/0002238.

[100] A. Djouadi, W. Kilian, M. Mühlleitner and P. M. Zerwas, hep-ph/0001169.

[101] M. Carena, H. E. Haber, H. E. Logan and S. Mrenna, FERMILAB-Pub-00/334-T, in preparation.

[102] J. Alcaraz and E. Ruiz Morales, hep-ph/0012109.

[103] D. Bardin, P. Christova, M. Jack, L. Kalinovskaya, A. Olchevski, S. Riemann and T. Riemann, Comput. Phys. Commun. **133**, 229 (2001) [hep-ph/9908433].

[104] M. Battaglia and K. Desch, hep-ph/0101165.

[105] V. Drollinger and A. Sopczak, hep-ph/0102342.

[106] L. D. Landau, Dokl. Akad. Nauk Ser. Fiz. **60**, 207 (1948); C. N. Yang, Phys. Rev. **77**, 242 (1950); J.J. Sakurai, *Invariance Principles and Elementary Particles* (Princeton University Press, 1964).

[107] D. J. Miller, S. Y. Choi, B. Eberle, M. M. Muhlleitner and P. M. Zerwas, Phys. Lett. B **505**, 149 (2001) [hep-ph/0102023].

[108] K. Hagiwara and M. L. Stong, Z. Phys. **C62**, 99 (1994) [hep-ph/9309248].

[109] V. Barger, K. Cheung, A. Djouadi, B. A. Kniehl and P. M. Zerwas, Phys. Rev. **D49**, 79 (1994) [hep-ph/9306270].

[110] T. Han and J. Jiang, Phys. Rev. **D63**, 096007 (2001) [hep-ph/0011271].

[111] B. Grzadkowski and J. F. Gunion, Phys. Lett. **B350**, 218 (1995) [hep-ph/9501339].

[112] B. Grzadkowski and J. F. Gunion, hep-ph/9503409.

[113] M. Krämer, J. Kühn, M. L. Stong and P. M. Zerwas, Z. Phys. **C64**, 21 (1994) [hep-ph/9404280].

[114] J. F. Gunion and X. G. He, hep-ph/9609453.

[115] B. Grzadkowski and J. F. Gunion, Phys. Lett. **B294**, 361 (1992) [hep-ph/9206262].

[116] J. F. Gunion and J. G. Kelly, Phys. Lett. **B333**, 110 (1994) [hep-ph/9404343].

[117] C. A. Boe, O. M. Ogreid, P. Osland and J. Zhang, Eur. Phys. J. **C9**, 413 (1999) [hep-ph/9811505].

[118] J. F. Gunion and J. Kelly, Phys. Rev. **D56**, 1730 (1997) [hep-ph/9610495].

[119] J. F. Gunion and J. Kelly, hep-ph/9610421.

[120] J. L. Feng and T. Moroi, Phys. Rev. **D56**, 5962 (1997) [hep-ph/9612333].

[121] A. Bartl *et al.*, Z. Phys. **C76**, 549 (1997) [hep-ph/9701336]; hep-ph/9909378; M. Berggren, R. Keränen, H. Nowak and A. Sopczak, hep-ph/9911345.

[122] S. Y. Choi, A. Djouadi, M. Guchait, J. Kalinowski and P. M. Zerwas, Eur. Phys. J. **C14**, 535 (2000) [hep-ph/0002033].

[123] ATLAS Collaboration, "Detector and Physics Performance Technical Design Report", CERN/LHCC/99-15 (1999); CMS Collaboration, Technical Design Reports, CMS TDR 1-5 (1997/98).

[124] J. Erler and S. Heinemeyer, hep-ph/0102083.

[125] I. F. Ginzburg, G. L. Kotkin, V. G. Serbo and V. I. Telnov, Nucl. Instrum. Meth. **A205**, 47 (1983).

[126] I. F. Ginzburg, G. L. Kotkin, S. L. Panfil, V. G. Serbo and V. I. Telnov, Nucl. Instrum. Meth. **A219**, 5 (1984).

[127] P. Chen, G. Horton-Smith, T Ohgaki, A. W. Weidemann and K. Yokoya, Nucl. Instrum. Meth. **A355**, 107 (1995). See `http://www-acc-theory.kek.jp/members/cain/cain21b.manual/main.html`.

[128] D. Asner, J. Gronberg, J. Gunion and T. Hill, UCRL–ID–143967.

[129] S. Söldner-Rembold and G. Jikia, hep-ex/0101056.

[130] J. F. Gunion, J. G. Kelly and J. Ohnemus, Phys. Rev. **D51**, 2101 (1995) [hep-ph/9409357].

[131] J. F. Gunion, R. Vega and J. Wudka, Phys. Rev. **D43**, 2322 (1991).

[132] R. N. Mohapatra, Fortsch. Phys. **31**, 185 (1983); J. F. Gunion, J. Grifols, A. Mendez, B. Kayser and F. Olness, Phys. Rev. **D40**, 1546 (1989); N. G. Deshpande, J. F. Gunion, B. Kayser and F. Olness, Phys. Rev. **D44**, 837 (1991).

[133] H. Georgi and M. Machacek, Nucl. Phys. **B262**, 463 (1985).

[134] M. S. Chanowitz and M. Golden, Phys. Lett. **B165**, 105 (1985).

[135] J. F. Gunion, Int. J. Mod. Phys. **A11**, 1551 (1996) [hep-ph/9510350]; **A13**, 2277 (1998) [hep-ph/9803222].

[136] P. H. Frampton, Int. J. Mod. Phys. **A15**, 2455 (2000) [hep-ph/0002017].

[137] F. Cuypers and M. Raidal, Nucl. Phys. **B501**, 3 (1997) [hep-ph/9704224].

[138] J. Gluza, Phys. Lett. **B403**, 304 (1997) [hep-ph/9704202].

[139] R. A. Alanakian, Phys. Lett. **B436**, 139 (1998) [hep-ph/9706383].

[140] G. Barenboim, K. Huitu, J. Maalampi and M. Raidal, Phys. Lett. **B394**, 132 (1997) [hep-ph/9611362].

[141] V. Barger, J. F. Beacom, K. Cheung and T. Han, Phys. Rev. **D50**, 6704 (1994) [hep-ph/9404335].

[142] R. Casalbuoni, A. Deandrea, S. De Curtis, D. Dominici, R. Gatto and J. F. Gunion, Nucl. Phys. **B555**, 3 (1999) [hep-ph/9809523].